AD-776-586

HANDBOOK OF BLUNT-BODY AERODYNAMICS VOL. I

J. A. Darling

Naval Ordinance Laboratory
Silver Spring, MD

DEC 73

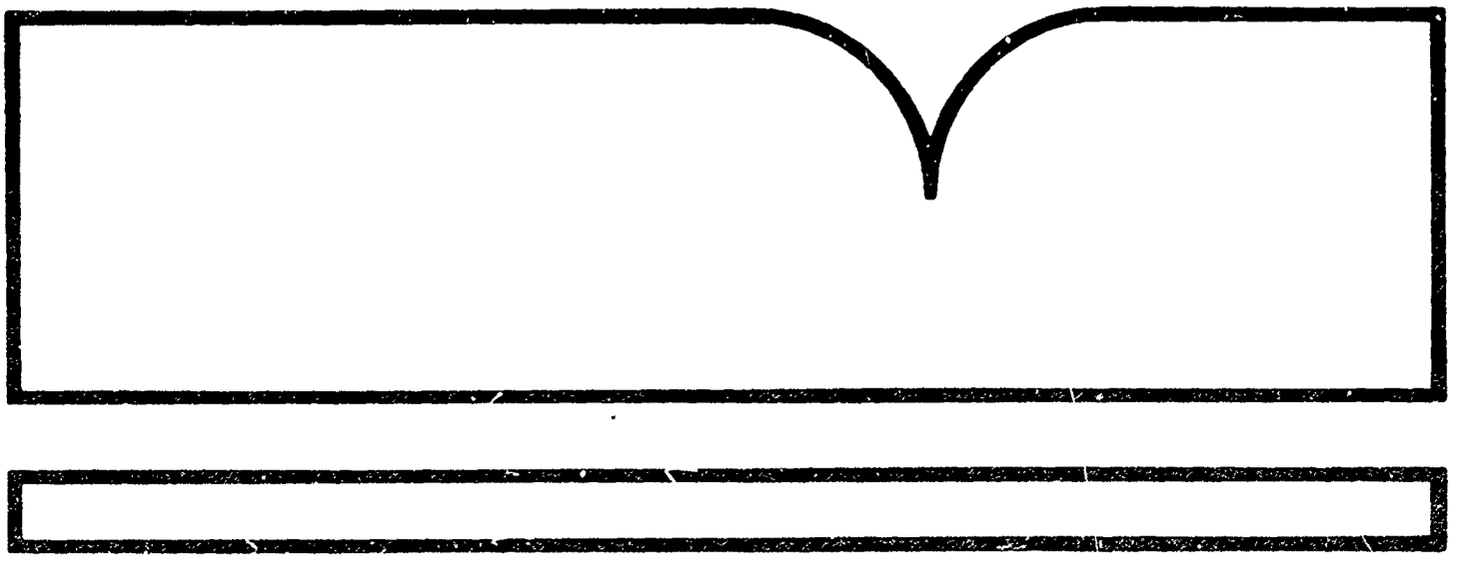

REPORT DOCUMENTATION PAGE

READ INSTRUCTIONS BEFORE COMPLETING FORM

1. REPORT NUMBER: NOLTR 73-225	2. GOVT ACCESSION NO.
3. RECIPIENT'S CATALOG NUMBER: AD 776586	
4. TITLE (and Subtitle): HANDBOOK OF BLUNT-BODY AERODYNAMICS VOLUME 1 STATIC STABILITY	5. TYPE OF REPORT & PERIOD COVERED
	6. PERFORMING ORG. REPORT NUMBER: NOLTR 73-225
7. AUTHOR(s): John A. Darling	8. CONTRACT OR GRANT NUMBER(s)
9. PERFORMING ORGANIZATION NAME AND ADDRESS: Naval Ordnance Laboratory, White Oak, Silver Spring, Maryland 20910	10. PROGRAM ELEMENT, PROJECT, TASK AREA & WORK UNIT NUMBERS: Task No. NOL-533/AF
11. CONTROLLING OFFICE NAME AND ADDRESS: Air Force Armament Test Laboratory, Eglin Air Force Base, Florida 32542	12. REPORT DATE: 1 December 1973
	13. NUMBER OF PAGES: 151
14. MONITORING AGENCY NAME & ADDRESS(if different from Controlling Office)	15. SECURITY CLASS. (of this report): UNCLASSIFIED
	15a. DECLASSIFICATION/DOWNGRADING SCHEDULE

16. DISTRIBUTION STATEMENT (of this Report)

Approved for public release; distribution unlimited.

17. DISTRIBUTION STATEMENT (of the abstract entered in Block 20, if different from Report)

18. SUPPLEMENTARY NOTES

19. KEY WORDS (Continue on reverse side if necessary and identify by block number)

Blunt Body
Static Stability
Normal Force
Center of Pressure
Aerodynamics
Mach Number

20. ABSTRACT (Continue on reverse side if necessary and identify by block number)

This report describes methods for quickly estimating the normal force and center of pressure of blunt free-fall shapes of ℓ/d = 0.5 to 10 over a Mach number range of 0.4 to 2.5 and up to α = 90 degrees. Charts and equations presented in this report are from cited reference material and original sources. Methods based on slender-body theory were tested on blunt shapes and modifying factors were developed where needed.

DD FORM 1 JAN 73 1473 EDITION OF 1 NOV 65 IS OBSOLETE
S/N 0102-014-6601 |

UNCLASSIFIED
SECURITY CLASSIFICATION OF THIS PAGE (When Data Entered)

NOLTR 73-225 1 December 1973

HANDBOOK OF BLUNT-BODY AERODYNAMICS
VOLUME 1 - STATIC STABILITY

This report contains the results of a study of handbook methods for predicting normal force and center of pressure of blunt free-fall shapes. The work was sponsored by the Air Force at the request of C. B. Butler, Air Force Armament Test Laboratory (AFATL), Eglin Air Force Base, Florida. Existing handbook methods apply to slender bodies and break down when applied to blunt free-fall shapes. Reference material on blunt shapes and systematic blunt-body wind-tunnel test results obtained by C. B. Butler were the source of information used to test and modify the existing handbook prediction methods to apply to blunt shapes. This project was performed under Task Number NOL-533/AF.

Acknowledgments are due C. B. Butler of AFATL and S. M. Hastings of NOL, for seeing the need for a handbook on blunt-body aerodynamics, also to K. D. Thomson of Weapons Research Establishment, Australia, and J. E. Fidler of Martin Marietta, for contributions which make possible estimating coefficients at high angles of attack.

Illustrations were prepared by M. T. Faile of NOL, and typing and editorial corrections by A. T. McLearen and L. L. Lord, both of NOL.

ROBERT WILLIAMSON, II
Captain, USN
Commander

Leon H. Schindel

LEON H. SCHINDEL
By direction

CONTENTS

CONTENTS (Cont'd)

ILLUSTRATIONS

ILLUSTRATIONS (Cont'd)

ILLUSTRATIONS (Cont'd)

ILLUSTRATIONS (Cont'd)

TABLES

SYMBOLS

A - function used in Equation (9) and shown on Figure 23 $\left[4/\pi \int_0^x (C_{D_c}/F)dx\right]$ (Ref. (10))

A_p - area of body as seen in crossflow when $\alpha = 90°$ (dxl)

AR - aspect ratio of fin panel (b_e^2/S_{f_e})

B - function used in Equations (9) and (11) and shown on Figure 24 $\left[4/\pi \int_0^x (C_{D_c}/F)xdx\right]$ (Ref. (10))

b_e - span of lifting surface

C - function shown on Figure 23a, $C = \left[4/\pi \int_0^x (C_{D_c}/F)x^2dx\right]$

c or c_r - root chord of fin panel (Fig. 41)

C_A - axial force coefficient

C_{D_c} - drag coefficient of an infinite cylinder in crossflow (Fig. 5)

C_m - pitching moment coefficient $\left[C_N(\bar{x}_{cp})\right]$

ΔC_{m_v} - viscous contribution to total pitching moment coefficient (Eq. (10))

C_N - normal force coefficient

C_{N_c} - fin normal force at $\alpha = 90°$ (Fig. 59)

C_{N_α} - slope of normal force coefficient per radian near $\alpha = 0°$

SYMBOLS (Cont'd)

ΔC_{N_v} - viscous contribution to total normal force coefficient (Eq. (8))

$C_{N_{\alpha fb}}$ - fin normal force slope referred to the body cross section area

$C_{N_{\alpha fe}}$ - fin normal force slope coefficient per radian referred to the exposed fin area (S_{f_e})

$C_{N_{\alpha fw}}$ - fin normal force slope coefficient per radian referred to the wetted area (S_{f_e} + cd)

ΔC_N - dimensionless C_N increment above α' (Fig. 57)

ΔC_{N_m} - maximum increment of normal force above α' (Fig. 58)

d - body diameter also referred to as caliber, used as reference length for all body and fin dimensions (inches)

D_1 - viscous component of Equation (6) for finding x_{cp} of a body

d_{BT} - diameter at small end of boattail (inches)

d_c - diameter of cylinder at large end of boattail (Eq. (11)) or small end of flare (Eq. (17)) (inches)

d_f - diameter of the flare (Eq. (17)) (inches)

E - base influence factor (Fig. 27)

e - reduction factor for cylinder planform area acted on by crossflow drag for subsonic speeds (Fig. 8)

F - vortex strength parameter (Fig. 28)

F(MACH) - variation factor of $\Delta x_{cp}/cr$ (Fig. 64)

F_z - normal force (pounds)

F_x - axial force (pounds)

SYMBOLS (Cont'd)

$f\left(\frac{\pi}{2}\right)$ - fin crossflow drag coefficient at $\alpha' = \left(\frac{\pi}{2}\right)$ (Fig. 55)

$f(30)$ - fin normal force at $\alpha = 30°$ (Fig. 60a, b, c)

$f'(0)$ - fin normal force slope at $\alpha = 0°$ (Fig. 40, 44, 47, 48a - c)

$f'(30)$ - fin normal force slope at $\alpha = 30°$ (Fig. 61)

G - crossflow drag correction factor due to axial pressure gradient (Fig. 34)

H - reduction factor to allow for effect of base influence on viscous normal force and pitching moment (Fig. 29)

J - reduction factor to allow for effect of nose on viscous normal force and pitching moment (Fig. 30)

K - effect of incidence on ratio of $\frac{C_{D_c} \text{ (turbulent separation)}}{C_{D_c} \text{ (laminar separation)}}$ (Fig. 31)

$K_{1,2}$ - Munk's apparent mass factors (Fig. 2)

K_{BT} - boattail factor (Fig. 36)

$K_{b(f)}$, $K_{f(b)}$ - fin-body interference factors (Fig. 42)

K_c - fin-cap effectiveness factor (Fig. 69)

$K_{f(n)}$ - nose bluntness fin effectiveness factor (Fig. 67a, b, 68a, b)

$K_{f(sc)}$ - subcaliber fin effectiveness factor (Fig. 54)

ℓ - total body length ($\ell_N + \ell_B$) (calibers)

ℓ_B - body length (calibers)

ℓ_N - nose length (calibers)

SYMBOLS (Cont'd)

ℓ_{BT} - length of boattail (calibers)

ℓ_f - length of flare (calibers)

M - Mach number

M_c - crossflow Mach number (M sin α)

M_y - pitching moment (inch-pounds)

M_{FB} - force break Mach number (Fig. 45a)

N or n - ratio of drag of finite cylinder to drag of infinite cylinder (Fig. 32 same as Fig. 6)

N - sign factor for delta fins (Fig. 65)

q - dynamic pressure at M (psia)

r_c - radius of corner of blunt nose (inches)

S - Strouhal number (S = 2 Eqs. (9), (11))

S_B or S_{ref} - cross-sectional area of body (square inches)

S_{bt} - projected area of boattail (square inches)

S_{eff} - effective fin area (Fig. 53)

S_f - projected area of flare (square inches)

S_{f_e} - exposed area of fin panels in horizontal plane (Fig. 41) (square inches)

S_w - wetted area of fins (S_{f_e} + cd) (square inches)

t - fin thickness (inches)

x_{cp} - location of center of pressure of normal force (calibers)

X_L, X_N - nose and body lengths as expressed on Figure 26

$\frac{x_{cp}}{cr}$ - center of pressure of fin panel as percent of root chord (Fig. 62, 63)

SYMBOLS (Cont'd)

y - vertical distance between two horizontal planes as on Figures 69, 70

α - angle of attack (degrees or radians)

α' - see Figure 56

β - Mach number parameter $\sqrt{M^2-1}$ where $M<1$, $\beta = \sqrt{|M^2-1|}$

ε - angle between fin leading edge and body on clipped delta fin (Fig. 52a - f)

λ - fin taper ratio (c_t/c)

ω - angle between fin leading edge and body on delta fin (Fig. 52a - f)

INTRODUCTION

The design of blunt free-fall shapes requires a source of aerodynamic performance characteristics for use in predicting the free-fall trajectory. The blunt shape may be described as a body symmetrical in both planes with a characteristic blunt-nose shape and a low-aspect ratio tail configuration. In calculating the aerodynamic characteristics of the shape, the order of procedure is to find: (1) drag, (2) static stability and (3) dynamic stability, magnus, and roll damping. The drag is dependent primarily on the nose shape and usually may be quickly fixed because of fuzing requirements.

The procedure used by handbooks such as the "USAF Stability and Control Handbook" sometimes referred to as DATCOM (Ref. (1)) and the AMCP 706-280 "Design of Aerodynamically Stabilized Free Rockets" (Ref. (2)) is to calculate the drag and lift of the component parts of a body and then add them up, with appropriate influence factors, to arrive at total aerodynamic coefficients. The two handbooks mentioned are comprehensive and are good guides to this procedure. For use in blunt body design, some of the charts in the handbook are not applicable since both handbooks start with the premise that every aerodynamic shape is first of all a slender streamlined body.

The purpose of this report was originally to collect available blunt-body aerodynamic data from test reports on shapes already

designed. This collection of data was to form the foundation for a handbook for blunt-body design.

After collecting the available data, the author attempted to use the AMCP handbook to calculate the normal force and center of pressure for various blunt shapes and compare the calculated values with the experimental values taken from the collected reference data. This started the basis for putting together a modified version of the Static Stability section of the AMCP handbook.

ESTIMATING STATIC-STABILITY COEFFICIENTS OF NONROLLING BLUNT SHAPES

A body in flight experiences two primary static forces: lift and drag. The total of the pressures distributed over the body surface are resolved into these two static force components. Lift and drag are aircraft forces related to the ground as a reference plane. In the free-fall shape, the pressures over the body are referred to the body axis system which coincides with the ballistic path during fall. The forces are given in dimensionless coefficient form to ease scaling of the forces to body size and operating altitude. Instead of lift and drag, we have normal force (F_z) and axial force (F_x) which in coefficient form are $C_N = F_z/qS_{ref}$ and $C_A = F_x/qS_{ref}$. For a body in flight to be statically stable, the center of pressure of the normal force (x_{cp}) must be behind the body center of gravity. Generally on bodies, it is necessary to add a tail configuration to move the center of pressure back of the center of gravity.

The procedure in finding the normal force coefficient and the center of pressure of a blunt shape is to start by estimating the normal force and center of pressure for the nose-body combination alone and then select a tail configuration and calculate normal force

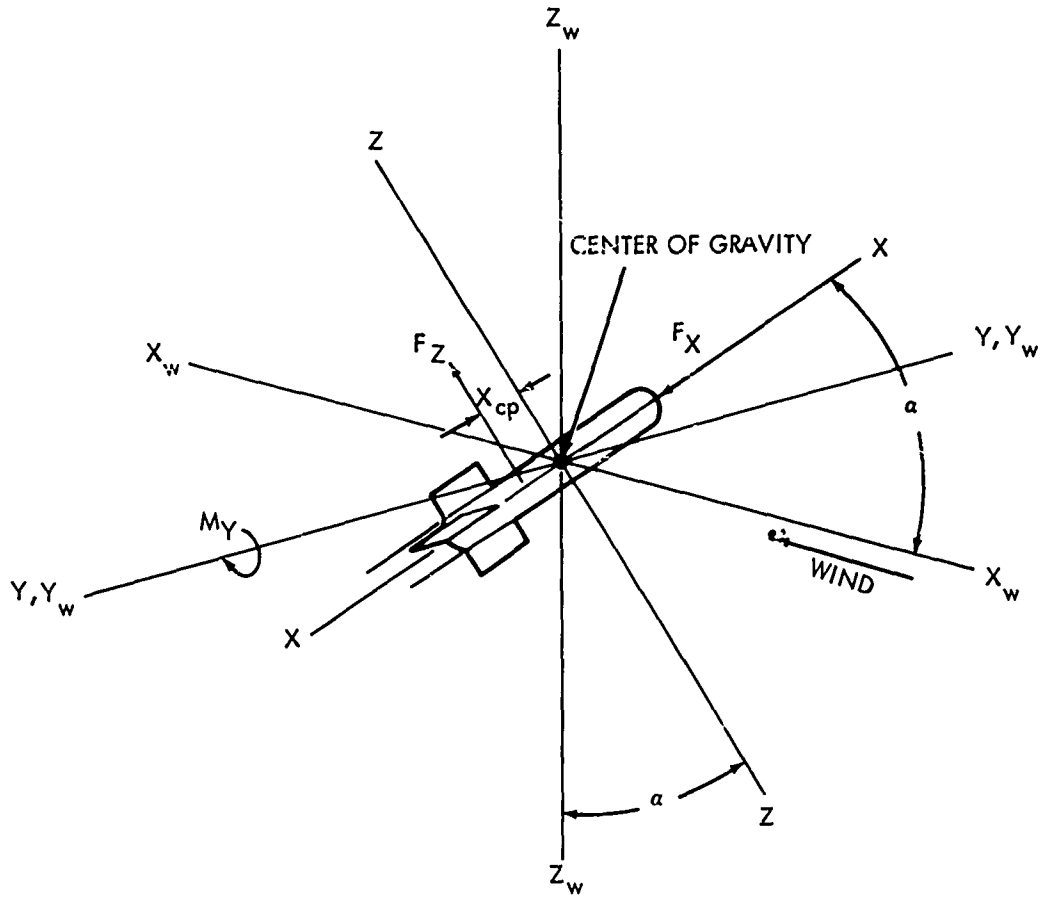

FIG. 1 STATIC STABILITY AXIS SYSTEM FOR BLUNT FREE FALL BODIES

and center of pressure for the tail. The two component forces are added together and the overturning moments they cause, acting about the center of gravity, determine the location of the resultant center of pressure. The resultant normal force acting at the resultant center of pressure causes a resultant moment about the center of gravity which is referred to as the pitching moment (M_y). Generally the aerodynamic coefficients are functions of the Mach number (speed) and angle of attack to the wind (α). Figure 1 shows the static force axis system with the normal force caused by the body being at angle of attack, α.

Following are methods with accompanying figures for use in estimating the normal force coefficients (C_N) and the center of pressure (x_{cp}) for blunt-shaped bodies and typical stabilizing configurations. The handbook first tells how to find C_N and x_{cp} near $\alpha = 0°$. Up to α = 4 to 8 degrees, the values are linear with angle of attack. The nonlinearity begins when the body crossflow drag force comes into play. So to construct a curve of C_N and C_m or (x_{cp}) versus α up to high angles of attack, the curves must be built up in sections. Another point that will be noted is that there are separate curves and charts for subsonic and supersonic speeds. The handbook starts with the nose-body at subsonic speeds, goes through supersonic speeds and then does the same with the stabilizing tails. On the figures and illustrations, nose and body lengths are given as ℓ_N and ℓ_B with the total length as ℓ. When shown this way, it is understood that all lengths have been divided by the body diameter, d, such that the dimensions are said to be in calibers.

C_{N_α} NORMAL FORCE SLOPE COEFFICIENT OF BLUNT-NOSE CYLINDER AT SUBSONIC SPEEDS

The slender-body theory provides a basis for obtaining C_{N_α} at subsonic speeds at low angles of attack where viscous crossflow forces are small. The theory states that:

$$\left(\frac{dC_N}{dx}\right) = \frac{(K_2 - K_1)}{S_{ref}} \left(\frac{ds}{dx}\right) \sin 2\alpha \quad \text{(Ref. (2))} \qquad (1)$$

which when integrated from x = 0 to x = ℓ gives

$$C_{N_\alpha}\Big|_{\alpha=0} = 2(K_2 - K_1) \frac{S_B}{S_{ref}} \qquad (2)$$

$(K_2 - K_1)$ is the apparent mass factor defined by Munk in Reference (3). The theory does not apply very well at low-fineness ratios ($\ell/d < 4.0$) because the nose bluntness begins to overpower the body effects.

For fineness ratios less than 1.0, normal force is very sensitive to nose radius for flat-face noses. As the nose shape approaches a hemisphere, the sensitivity to nose shape disappears. C_{N_α} for blunt-nosed bodies may be obtained from Figure 2 which includes experimental data from References (4), (5), and (6) and a plot of C_{N_α} using the slender-body theory, as presented in Reference (2).

For blunt-face cylinders where $\ell/d < 2.0$, C_{N_α} can be negative at angles of attack from 2 to 20 degrees.

The cause is explained in Reference (7) as a separation bubble along the top surface of the cylinder starting at the corner of the

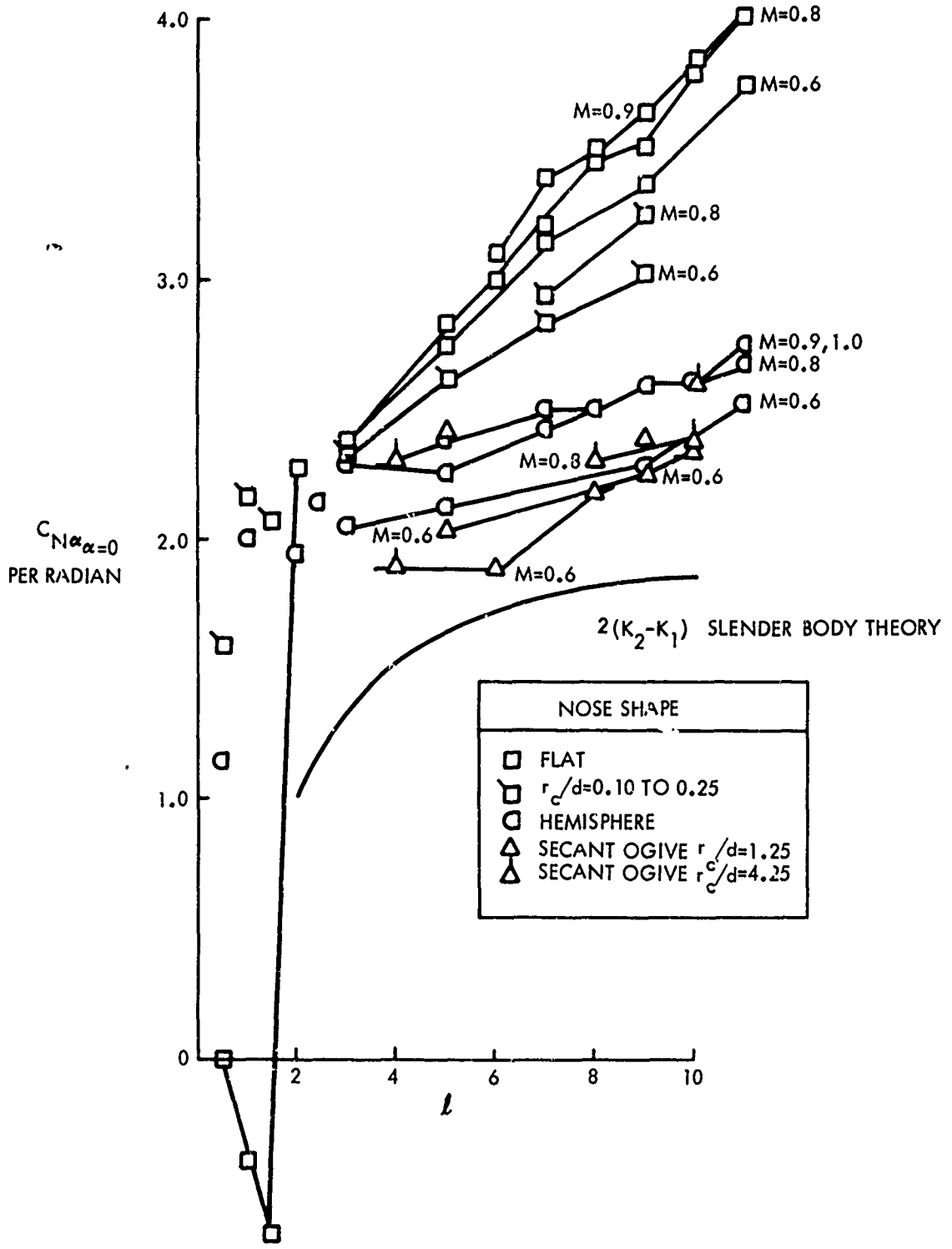

FIG. 2 C_N NORMAL FORCE SLOPE COEFFICIENT NEAR 0= DEGREES ANGLE OF ATTACK FOR BLUNT CYLINDRICAL BODIES, M=0.6 TO 0.9 (REF 4,5, AND 6)

flat face and body juncture which gives a negative normal force. As the cylinder becomes longer, the flow reattaches and past the point of reattachment the flow is normal and gives a positive normal force. Figure 3 shows the effect of nose shape on C_N versus α for $\ell/d = 0.5$ cylindrical body. Figure 4 shows C_N versus α for flat-faced cylindrical bodies of $\ell/d = 1.0$, 1.5, and 2.0.

EFFECT OF VISCOUS FORCES ON NORMAL FORCE

At low angles of attack, generally only the nose shape affects the normal force on a cylindrical body. For blunt bodies where $r_c/d < 0.5$, the length of the body also affects normal force. As the angle of attack increases, the body is exposed to the wind; and a crossflow drag component is added to the normal force.

$$\Delta C_{N_\alpha} = \eta C_{D_c} \frac{A_p}{S_{ref}} \sin^2\alpha \qquad (3)$$

This normal force component is the Allen-Perkins Viscous Crossflow component (Ref. (8)). Values of C_{D_c} and η may be found on Figures 5 and 6.

In testing Equation (3) with the existing blunt-body data, two things were found: (1) that the onset of viscous crossflow was affected by the body length and (2) that the crossflow component so predicted was too high. Figure 7 shows the angle of attack (α), where the crossflow component becomes part of the normal force plotted as a function of body length. Figure 8 shows a reduction factor (e) which reduces the effective cylindrical planform area A_p of the cylindrical body.

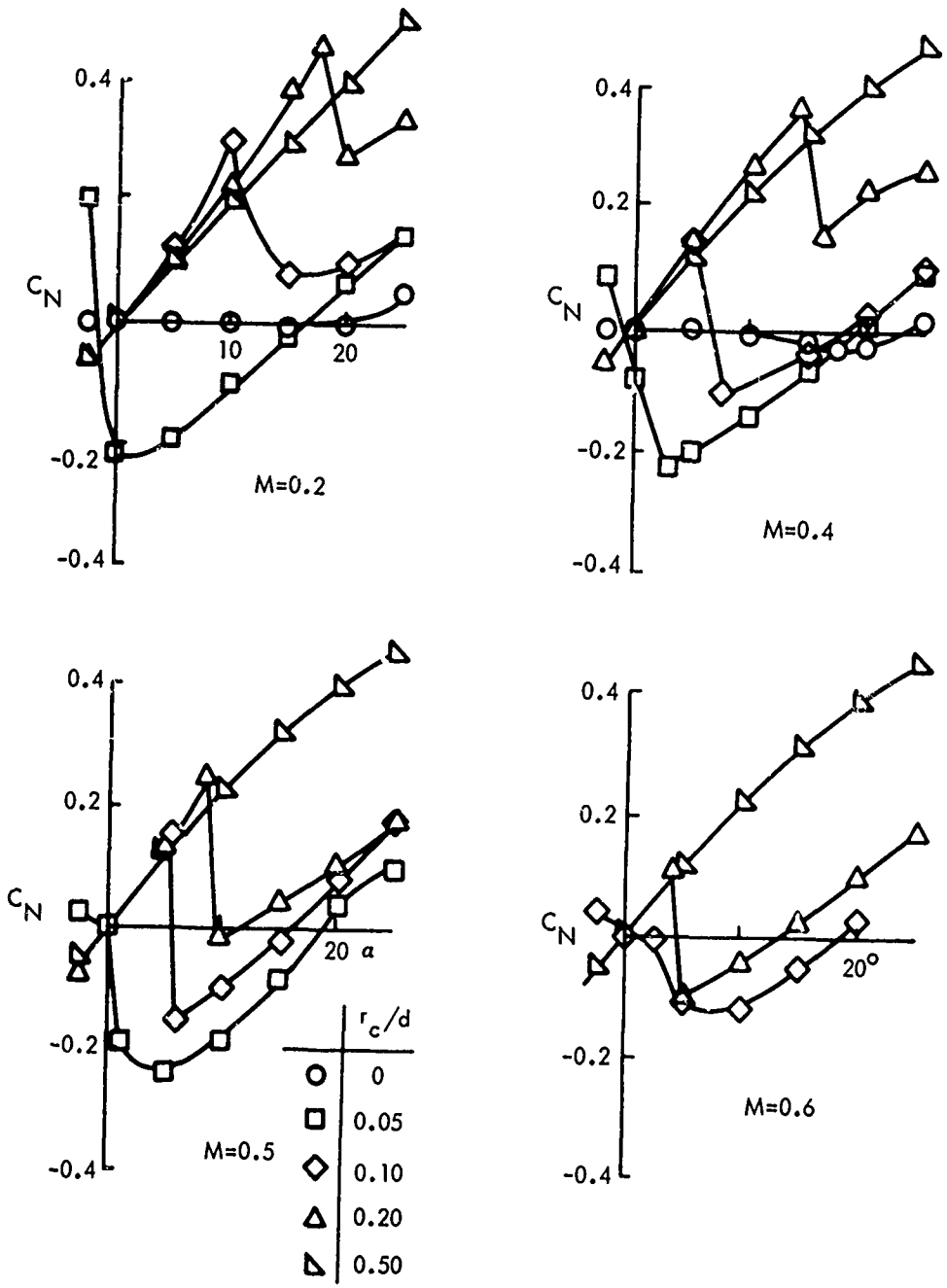

FIG. 3 EFFECT OF NOSE CORNER RADIUS ON C_N FOR ℓ =0.5 CYLINDER AT SUBSONIC SPEEDS (REF 4)

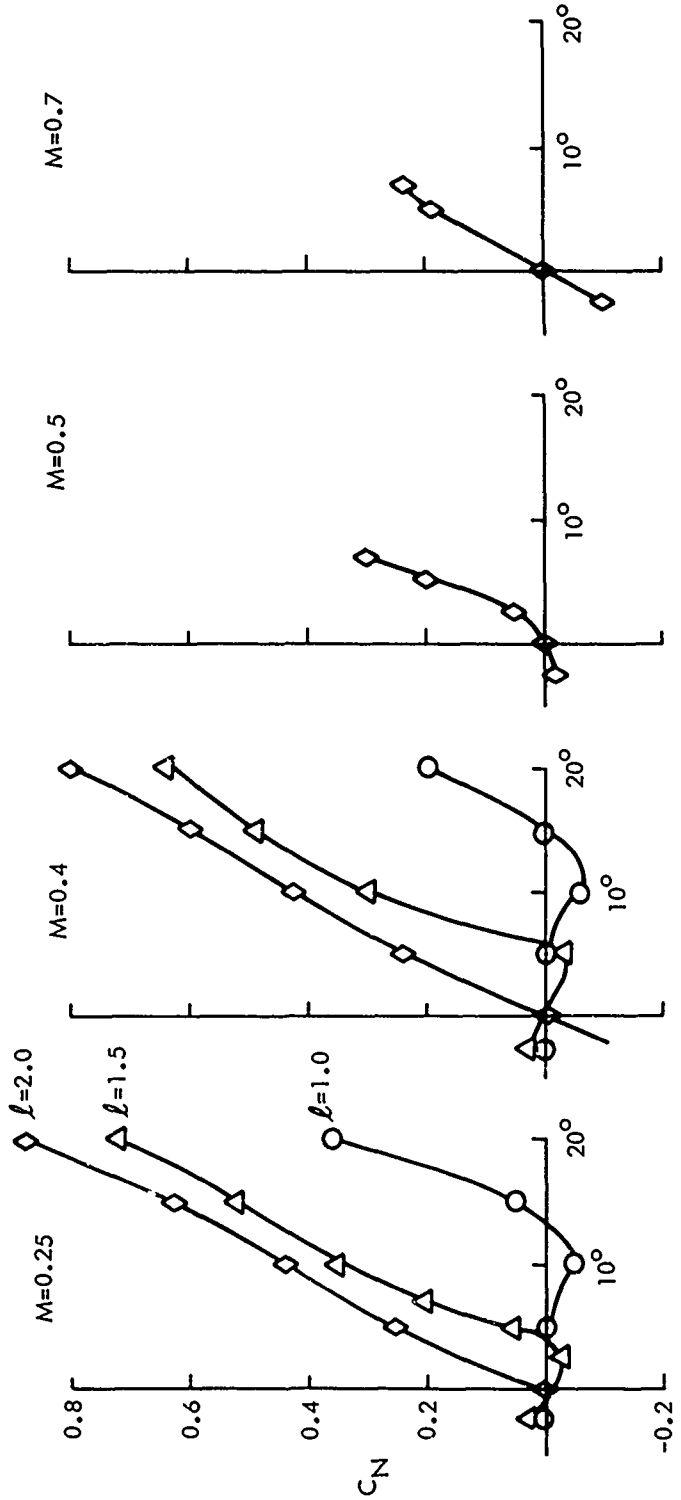

FIG. 4 NORMAL FORCE COEFFICIENT AT SUBSONIC SPEEDS FOR FLAT FACED CYLINDRICAL BODIES ℓ=1.0, 1.5, AND 2.0 (REF 4)

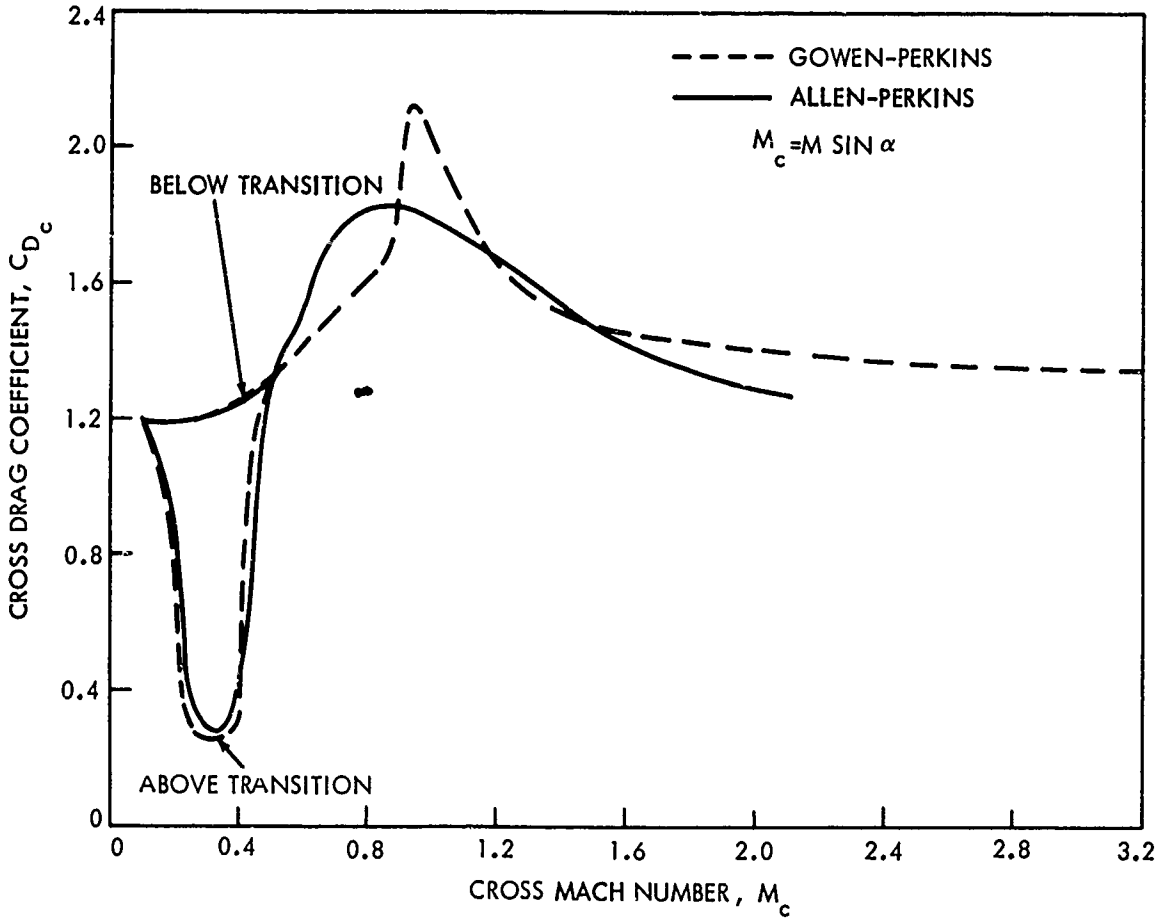

FIG. 5 CROSS-DRAG COEFFICIENT FOR CIRCULAR CYLINDER AS A FUNCTION OF CROSS FLOW MACH NUMBER (REF 8)

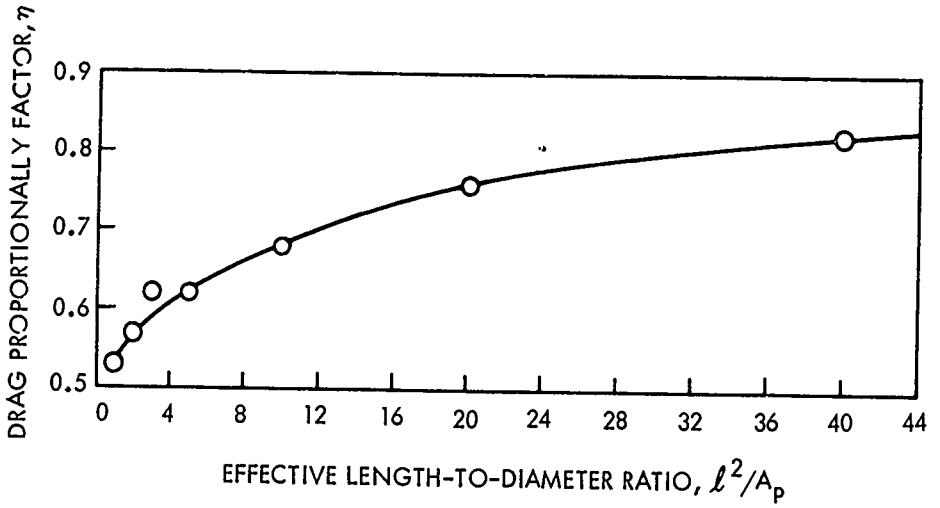

FIG. 6 RATIO OF THE DRAG OF A FINITE CYLINDER TO THAT OF AN INFINITE CYLINDER AS A FUNCTION OF THE FINENESS RATIO OF THE FINITE CYLINDER. (REF 8)

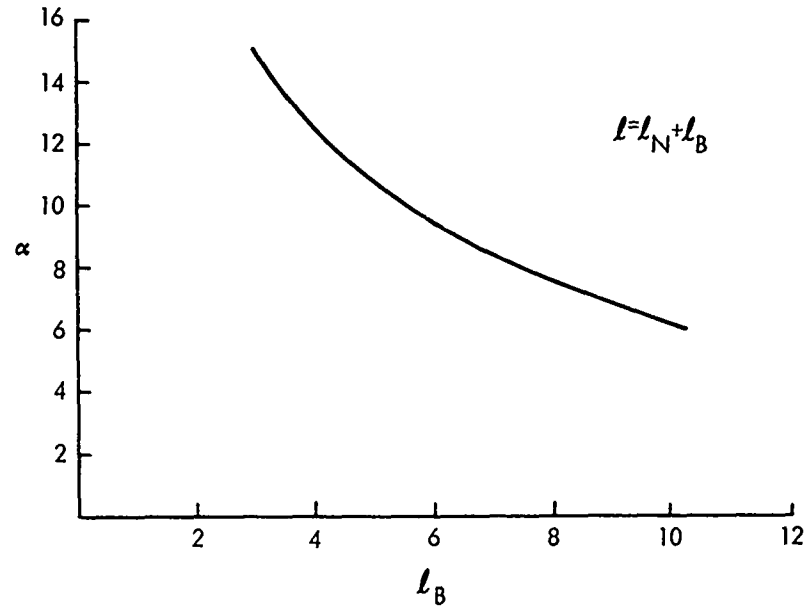

FIG. 7 ANGLE OF ATTACK OF CYLINDRICAL BODIES WHERE CROSS-FLOW DRAG BEGINS TO AFFECT NORMAL FORCE AS A FUNCTION OF CYLINDER LENGTH FOR SUBSONIC SPEEDS (REF. 6)

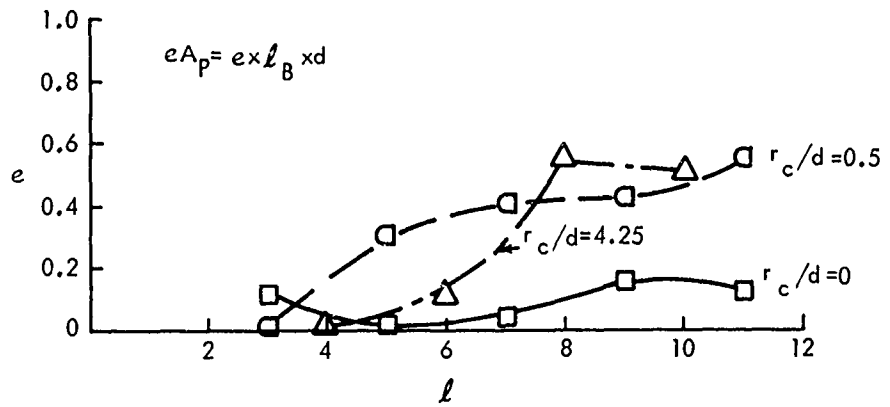

FIG. 8 REDUCTION FACTOR (e) FOR CYLINDER PLANFORM AREA ACTED ON BY CROSS-FLOW DRAG FOR SUBSONIC SPEEDS (REF 6)

The complete expression for normal force of a blunt body for α between end of linearity and 15° is:

$$C_N = C_{N_\alpha}{}_{\alpha=0}(\alpha) + \eta C_{D_c} e(Ap/S_{ref})\sin^2\alpha \qquad (4)$$

x_{cp} CENTER OF PRESSURE OF BLUNT NOSE CYLINDERS AT α NEAR 0 DEGREE FOR SUBSONIC SPEEDS

At low angles of attack, the center of pressure of the normal force (x_{cp}) for a flat-faced cylinder has an apparent shift in location from ahead of the flat face for $\ell/d < 1.0$ to aft of the flat face between $\ell/d = 1.0$ to 3.0. This shift in location is caused by the separation bubble over the upper surface of the cylinder. Figure 9 shows x_{cp} for blunt-faced cylinders up to $\ell/d = 11.0$ for subsonic speeds.

Generally increasing nose bluntness increases the static stability of a body. Figure 10 shows the effect of nose corner radius (r_c/d) on the location of x_{cp} for a 7-caliber cylindrical body. Summarizing for Figures 9 and 10, static stability decreases with increasing r_c/d, increases with the addition of an oversized ring, and is not much affected by concaving the flat face. Figure 11 shows x_{cp} for blunt bodies M = 1.0. Here again, stability is improved by bluntness of the nose.

C_N AND x_{cp} FOR BLUNT AND SLENDER-NOSED CYLINDERS OF ℓ/d = 6 TO 15 FOR α = 0 TO 10 DEGREES, FOR M = 0.8 TO 1.2

A method, developed by H. Barth (Ref. (9)), gives charts for calculating C_N and x_{cp} from α = 0 to 10 degrees angle of attack. The charts are good over a range of M = 0.8 to 1.2 and body length ℓ/d = 6 to 15. Nose bluntness varies

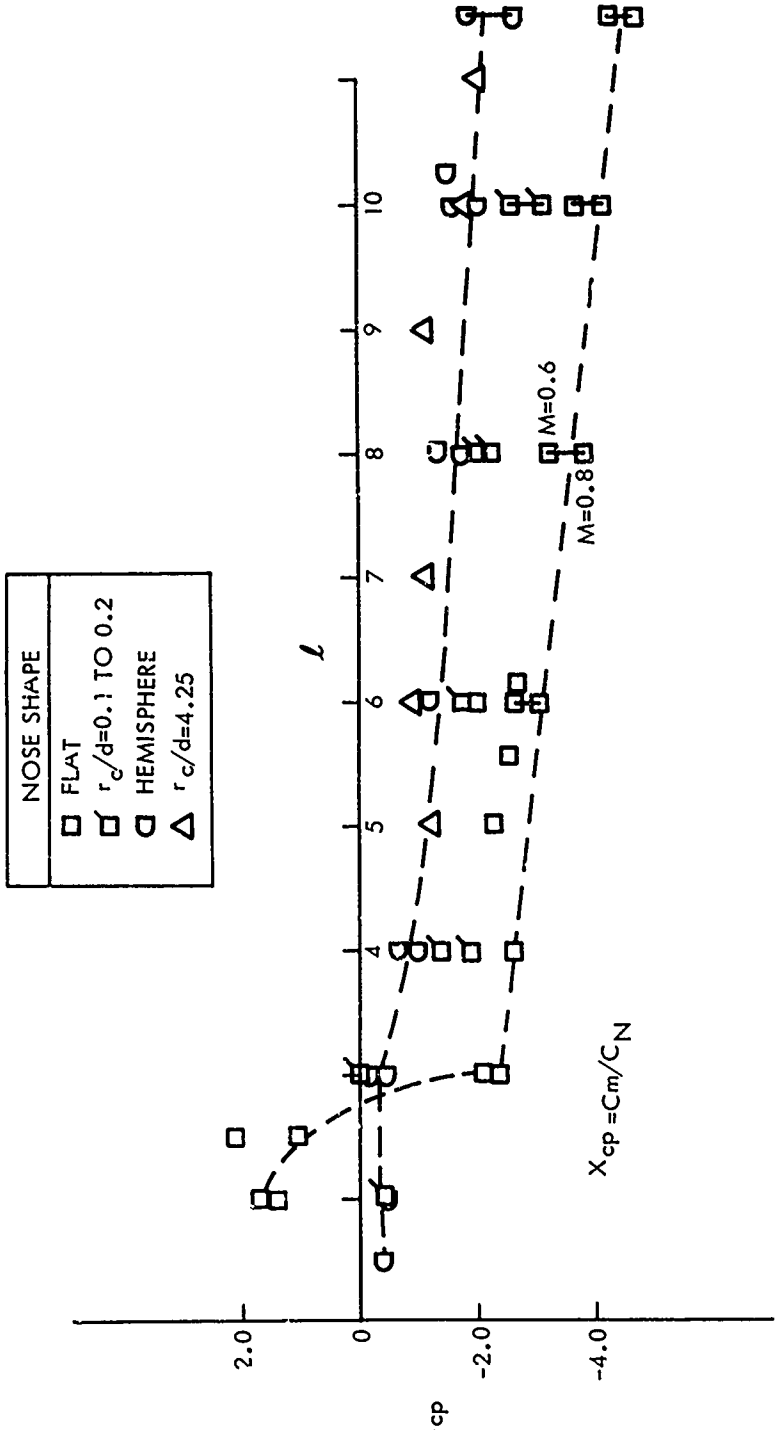

FIG. 9 X_{cp} CENTER OF PRESSURE OF NORMAL FORCE IN CALIBERS FROM NOSE FOR BLUNT CYLINDRICAL BODIES AT SUBSONIC SPEEDS α =0-DEGREES (REF 4,5, AND 6)

NOSE SHAPE	r_c/d
	0
	0.125
	0.250
	0.500

NOSE SHAPE	r_c/d	MODIFICATION	LOCATION FROM TIP
	0	1.1-D RING	0
	0	1.1-D RING	-0.58D
	0	1.0-D PLATE	+0.25D
	0	0.8-D CAVITY	-0.2D(WITH 12-0.05D BLEEDS) DEEP
	0 125	1.1-D RING	-0.58D

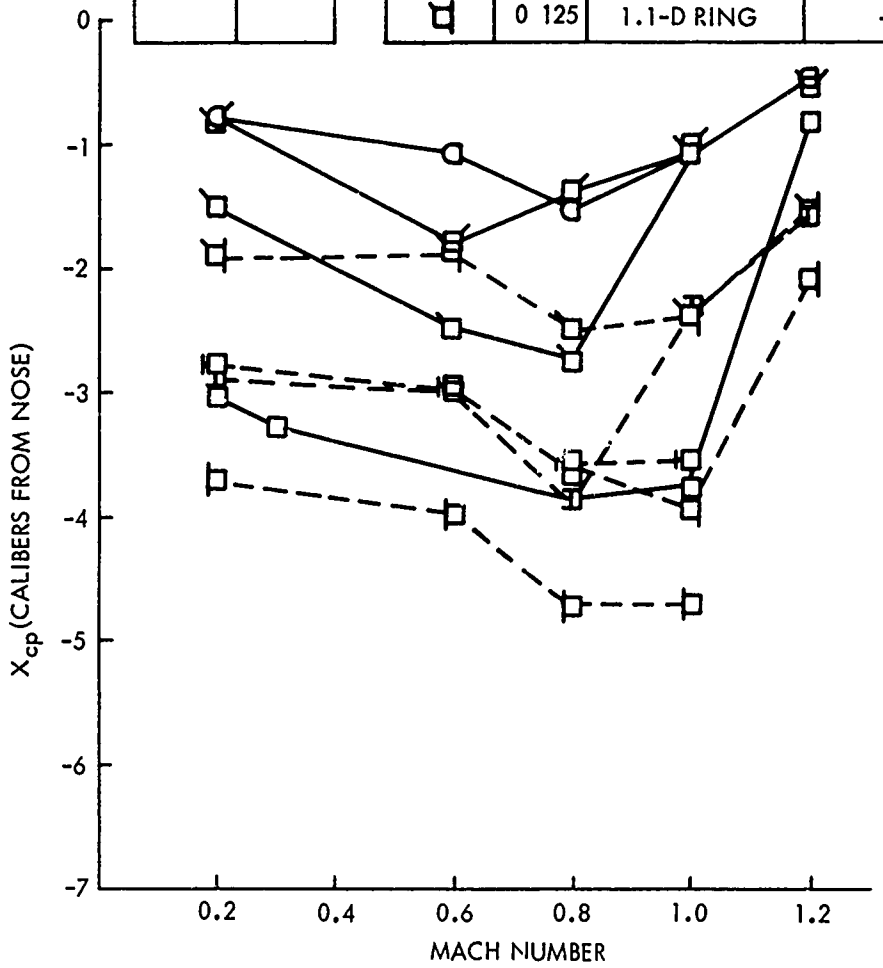

FIG. 10 EFFECT OF VARIOUS BLUNT NOSE SHAPES ON NORMAL FORCE CENTER OF PRESSURE (X_{cp}) WHEN α =0 DEGREES FOR A 7-CALIBER CYLINDRICAL BODY (REF 6)

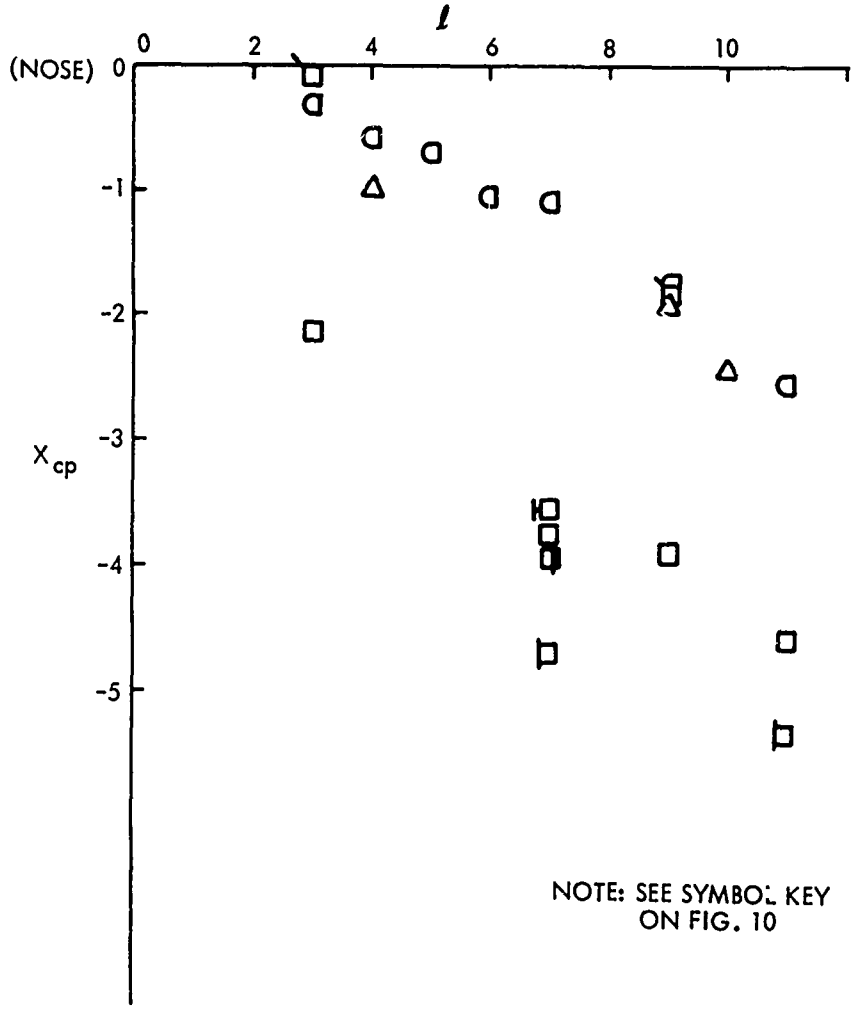

FIG. 11 X_{cp}-CENTER OF PRESSURE FOR BLUNT CYLINDRICAL BODIES, M=1.0 (CALIBERS FROM NOSE) (REF 6)

from flat to a 2.5-caliber ogive and cone. By this method which is based on experimental data:

$$C_N = C_{N_\alpha}{}_{\alpha=0^\circ}(\alpha) + C_{N_{\alpha_2}}(\alpha)^2 \tag{5}$$

$$x_{cp} = (x_{cp})_{\alpha=0^\circ} + D_1\alpha \tag{6}$$

Figures 12, 13, 14, and 15, a through g, are carpet plots of C_{N_α}, $C_{N_{\alpha_2}}$, x_{cp}, and D_1 as a function of M and ℓ_B/d. The ordinates of the plots do not give the desired values directly. As an example for Figure 12a, the ordinate gives $C_{N_\alpha} + 0.4\ \ell_B/d = A$ so that $C_{N_\alpha} = A - 0.4\ \ell_B/d$.

C_{N_α} AND x_{cp} FOR BLUFF CYLINDERS ℓ/d = 1 TO 11, α NEAR 0 DEGREE. $\alpha=0$ AND α = 10 DEGREES FOR SUPERSONIC SPEEDS

Figures 16 and 17 give $C_{N_\alpha}{}_{\alpha=0}$ and x_{cp} for short bluff cylinders over the Mach number range of 1.2 to 2.5. These figures are based on the AEDC data (Ref. (6)). As a companion to these, Figures 18a and b give the center of pressure of C_N when $\alpha = 10^\circ$. This accounts for the nonlinearity above α = 4 to 8 degrees. Here C_N is found with Equation (4) and:

$$C_{m_{\alpha=10^\circ}} = C_{N_{\alpha=10^\circ}}\ x_{cp_{\alpha=10^\circ}} \tag{7}$$

C_{N_α} AND x_{cp} FOR SLENDER CYLINDRICAL BODIES, α NEAR 0 DEGREE FOR SUPERSONIC SPEEDS

Carpet plots from Reference (2) are reproduced on Figures 19 through 22. These plots based on experimental data are for ogives and cone-nosed cylinders where ℓ_n/d = 3 to 7 and M = 1.4 to 7.0.

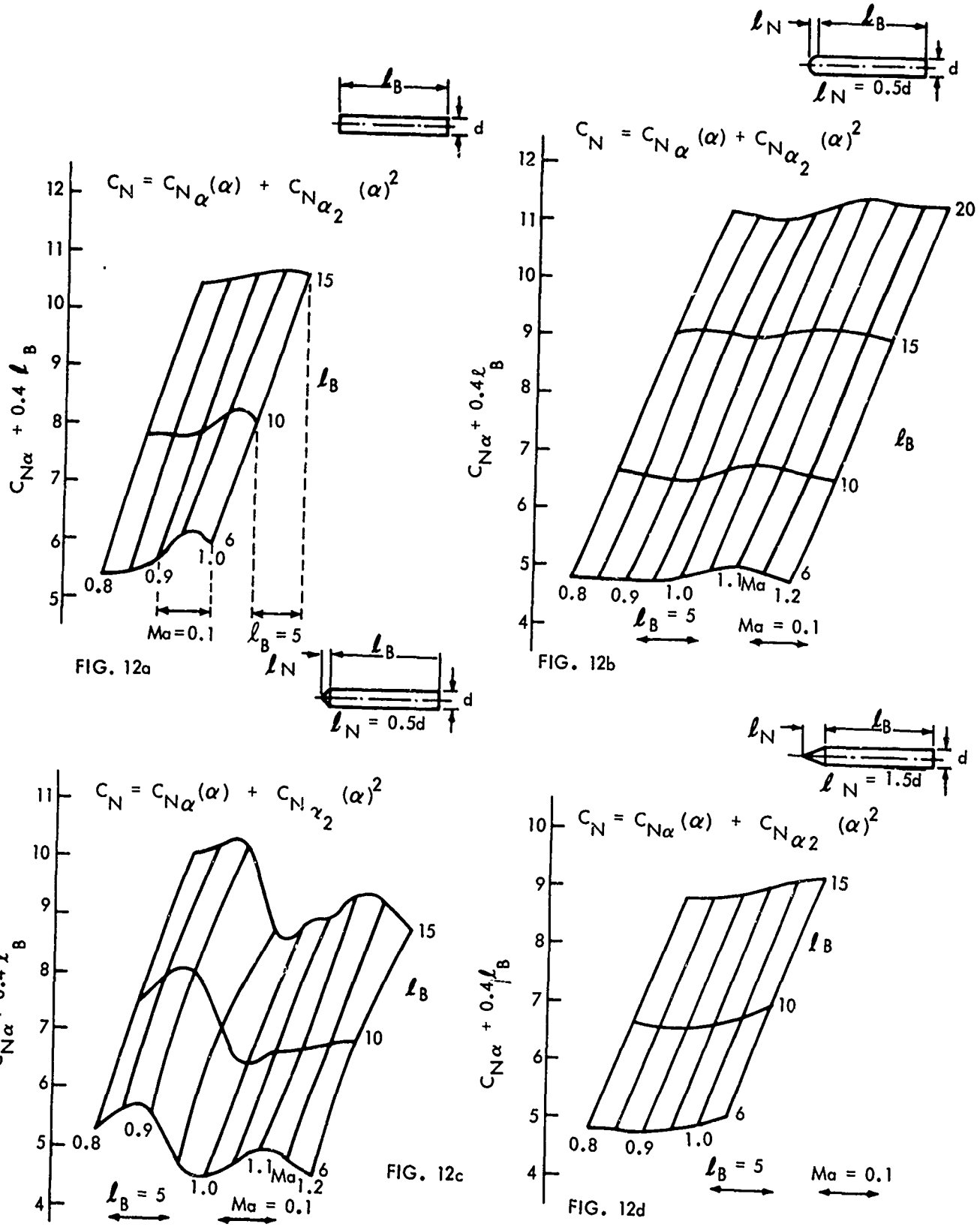

FIG. 12 C_{N_α} AS FUNCTION OF MACH NUMBER FOR CYLINDRICAL BODIES ℓ_B = 6 TO 15 (REF 9)

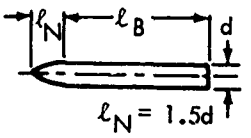

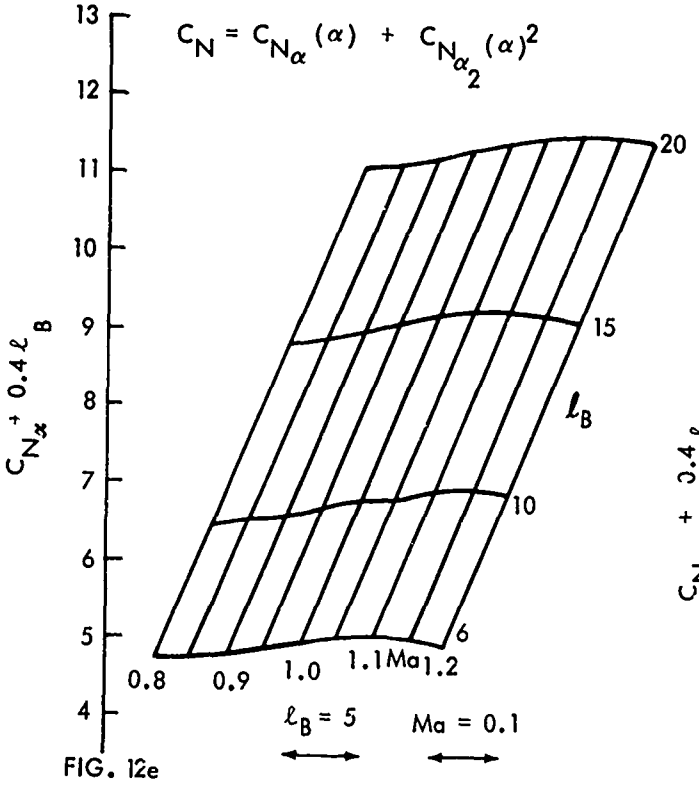

FIG. 12e

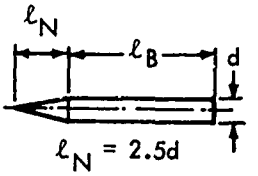

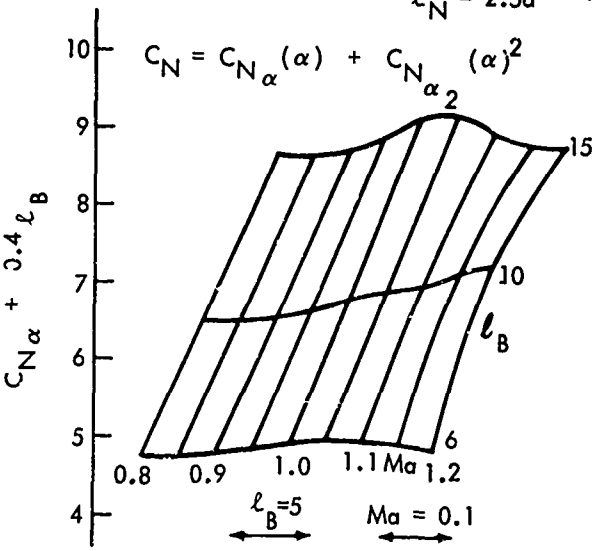

FIG. 12f

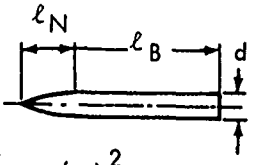

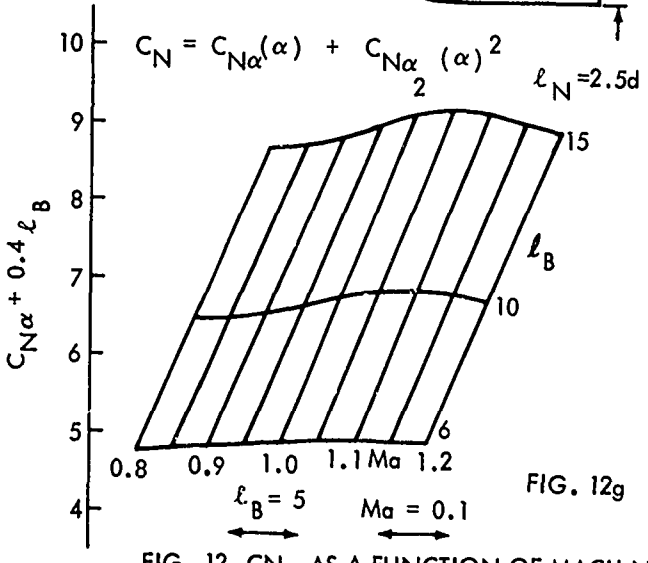

FIG. 12g

FIG. 12 CN_α AS A FUNCTION OF MACH NUMBER FOR CYLINDRICAL BODIES ℓ_B= 6 TO 15 (REF 9)

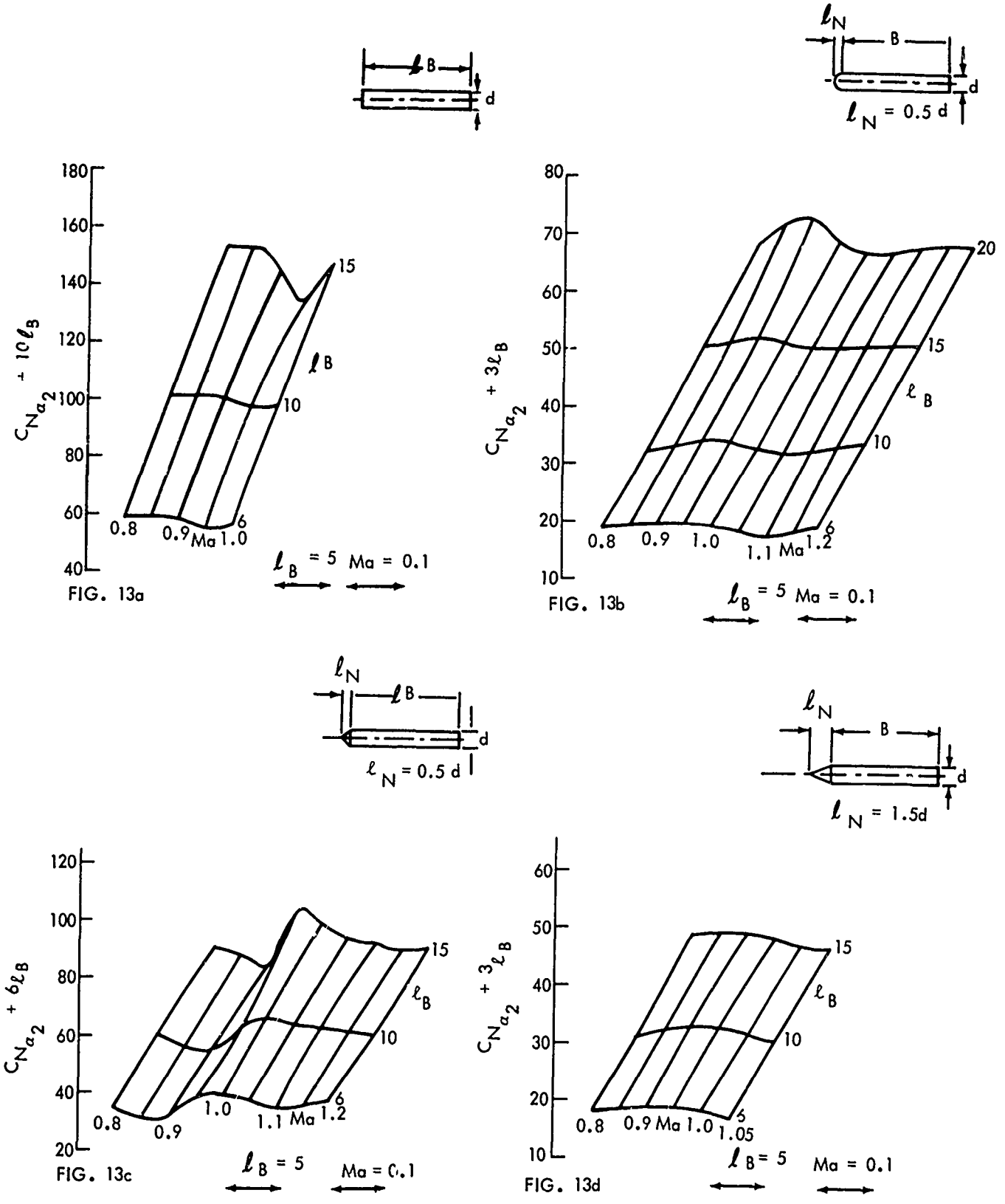

FIG. 13 $C_{N_{\alpha_2}}$ AS A FUNCTION OF MACH NUMBER FOR CYLINDRICAL BODIES ℓ_B = 6 TO 15 (REF 9)

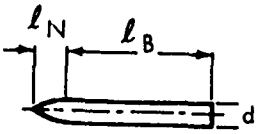

$\ell_N = 1.5d$

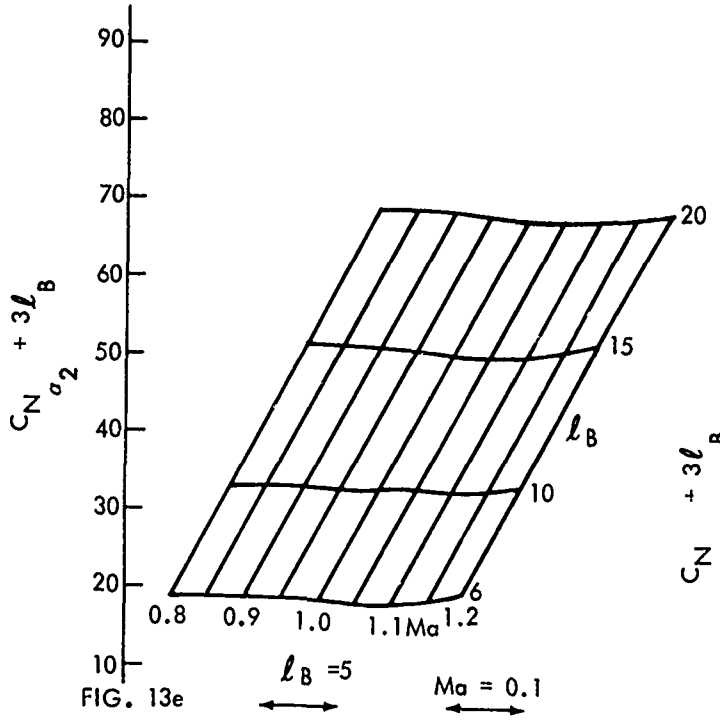

FIG. 13e

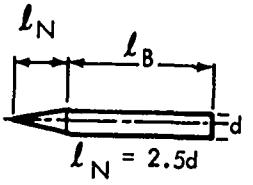

$\ell_N = 2.5d$

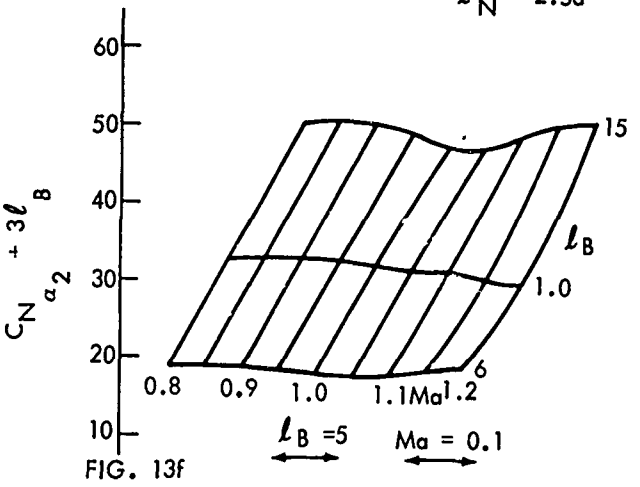

FIG. 13f

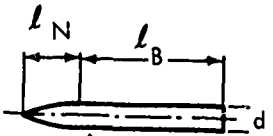

$\ell_N = 2.5d$

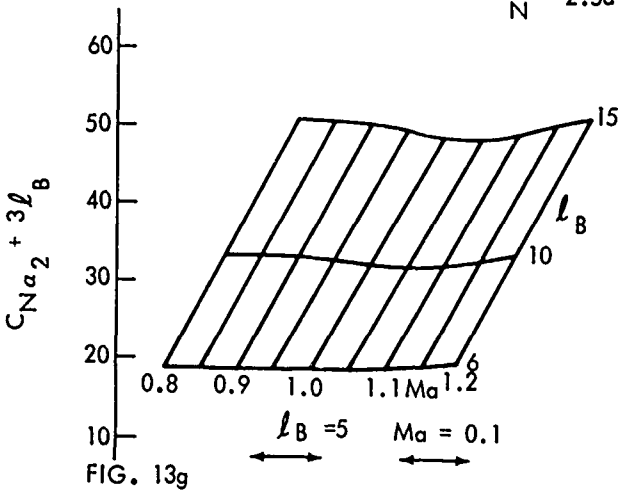

FIG. 13g

FIG. 13 $C_{N\alpha_2}$ AS A FUNCTION OF MACH NUMBER FOR CYLINDRICAL BODIES ℓ_B= 6 TO 15 (REF 9)

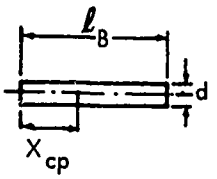

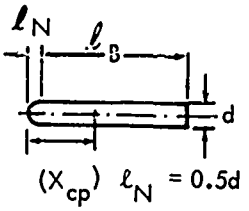

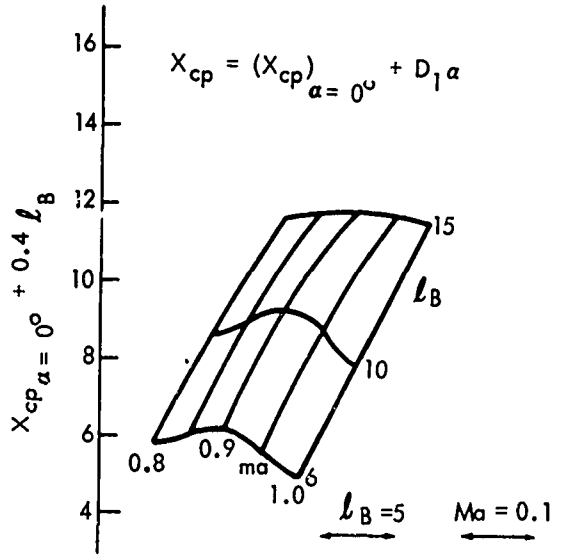

FIG. 14a

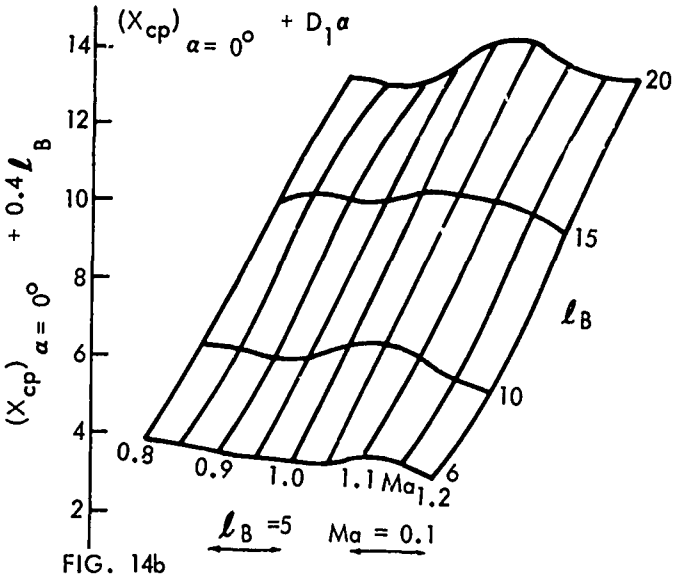

FIG. 14b

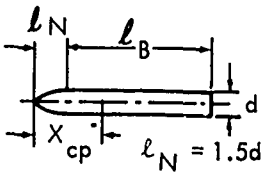

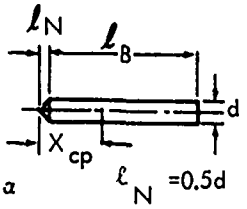

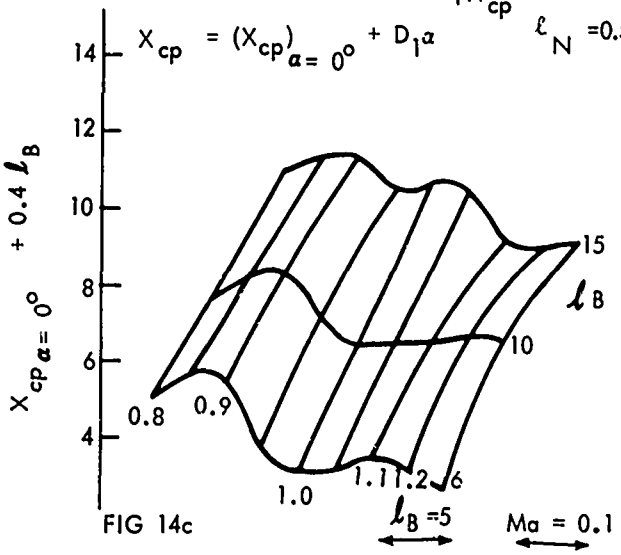

FIG 14c

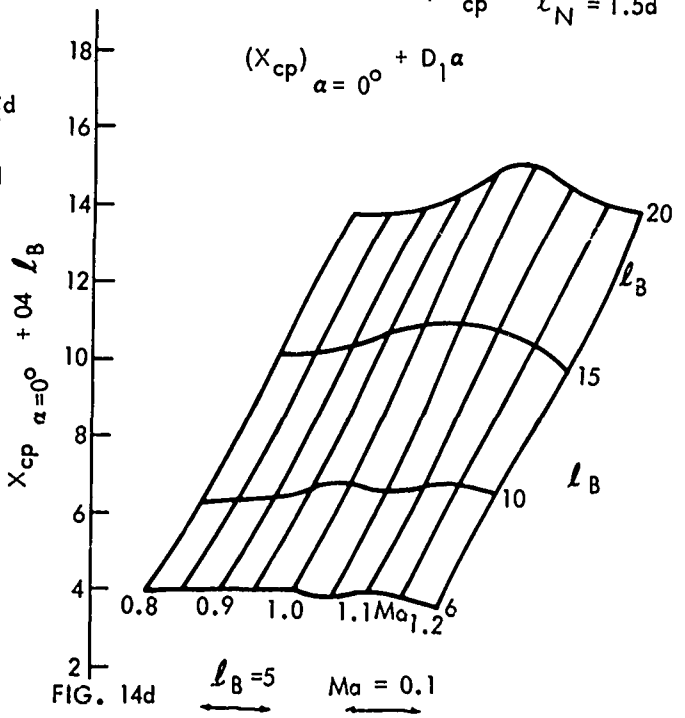

FIG. 14d

FIG. 14 $(X_{cp})_{\alpha = 0^o}$ AS FUNCTION OF MACH NUMBER FOR CYLINDRICAL BODIES, ℓ_B = 6 TO 15 (REF 9)

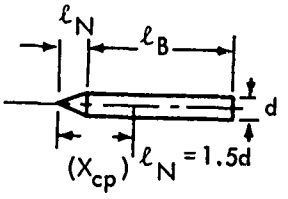

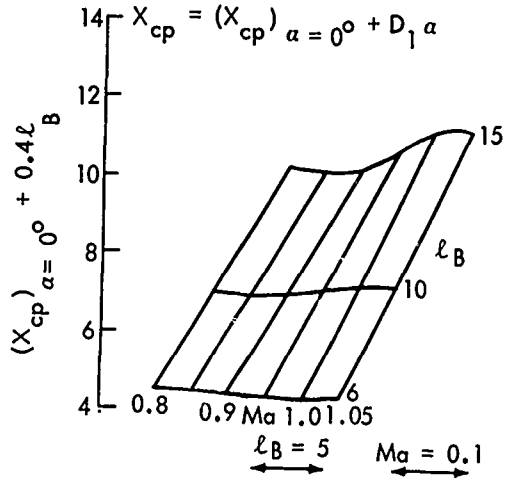

FIG. 14e

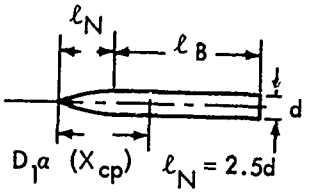

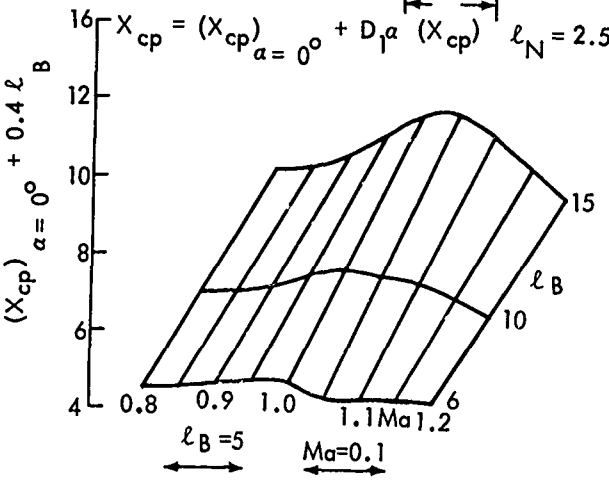

FIG. 14f

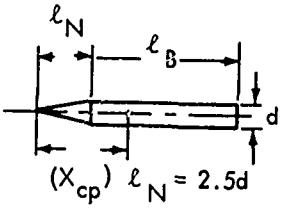

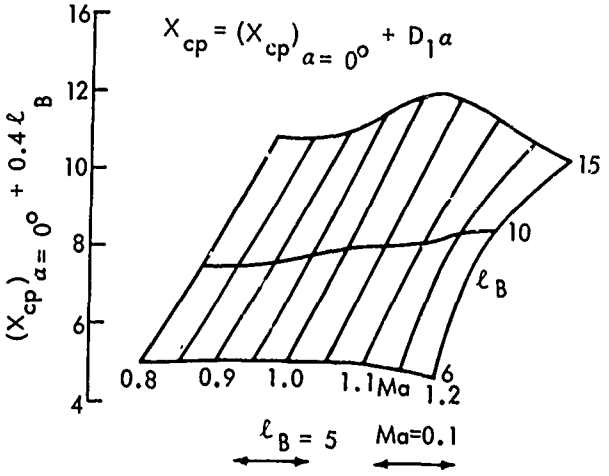

FIG. 14g

FIG. 14 $(X_{cp})_{\alpha = 0^o}$ AS A FUNCTION OF MACH NUMBER FOR CYLINDRICAL BODIES, ℓ_B = 6 TO 15 (REF 9)

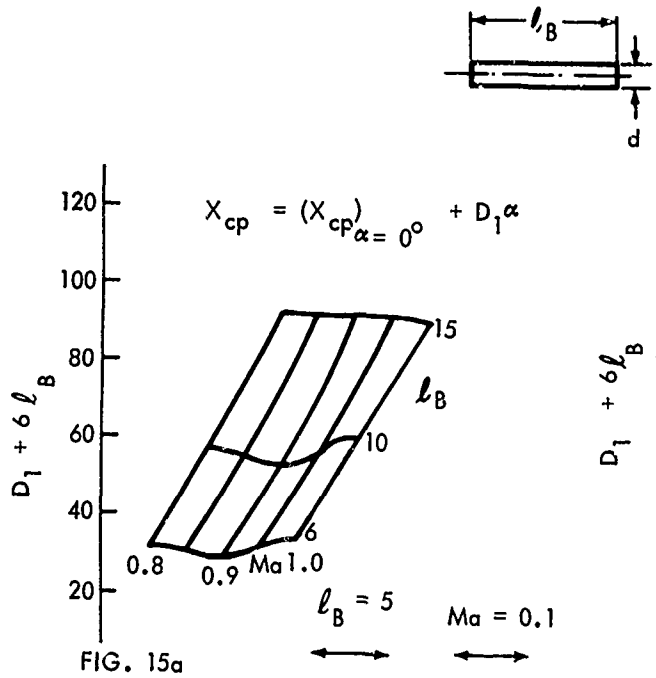

FIG. 15a

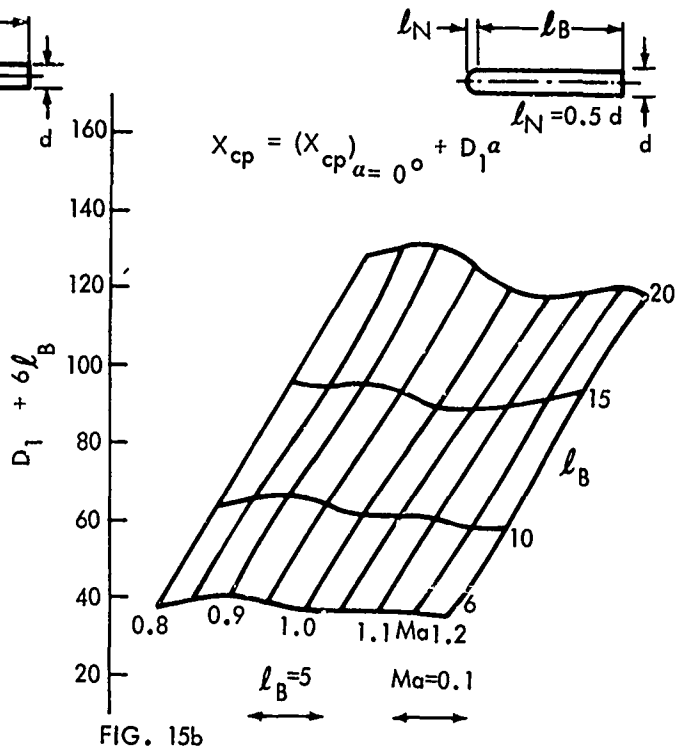

FIG. 15b

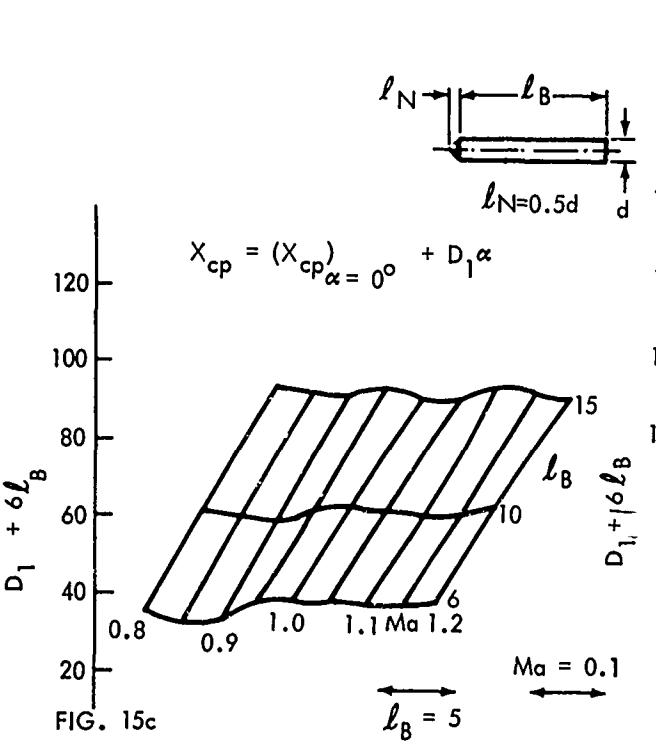

FIG. 15c

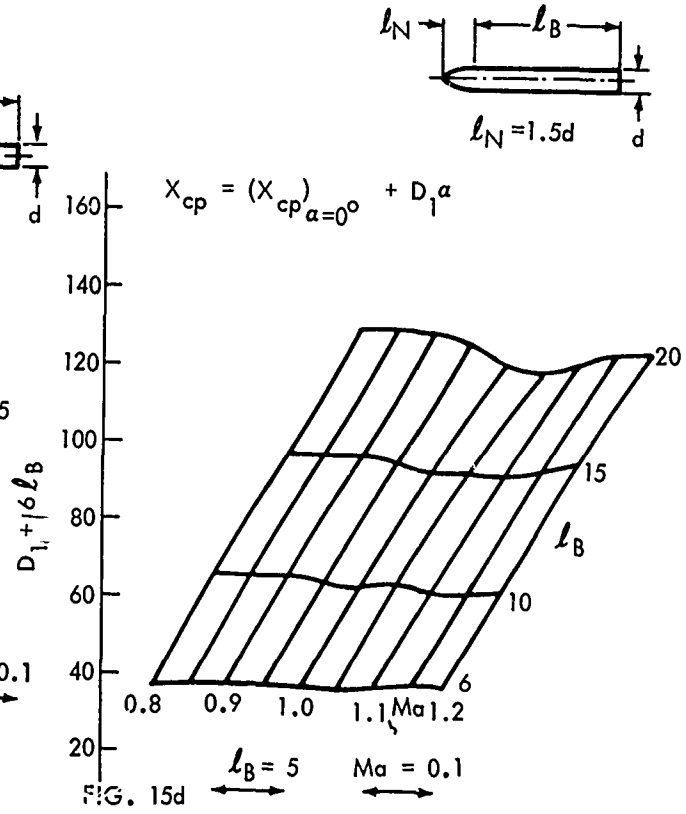

FIG. 15d

FIG. 15 D_1 AS A FUNCTION OF MACH NUMBER FOR CYLINDRICAL BODIES, ℓ_B = 6 TO 15 (REF 9)

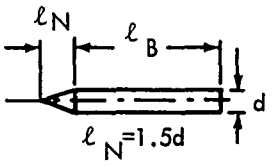

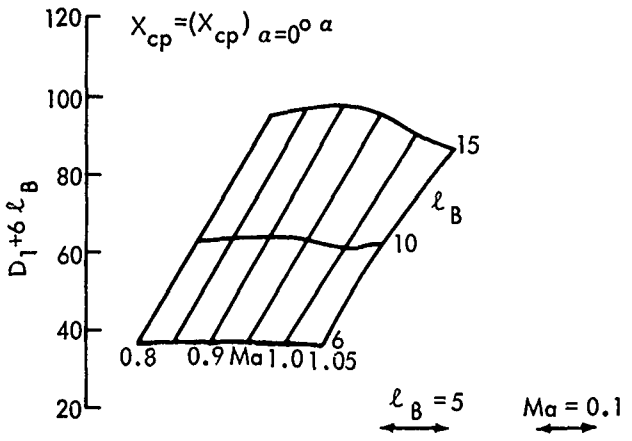

FIG. 15e

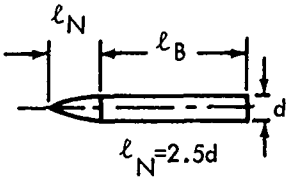

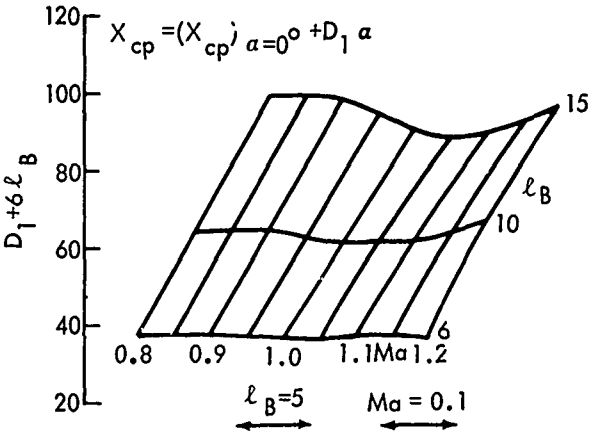

FIG. 15f

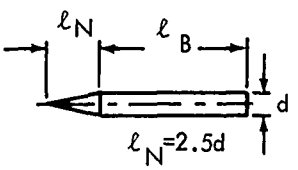

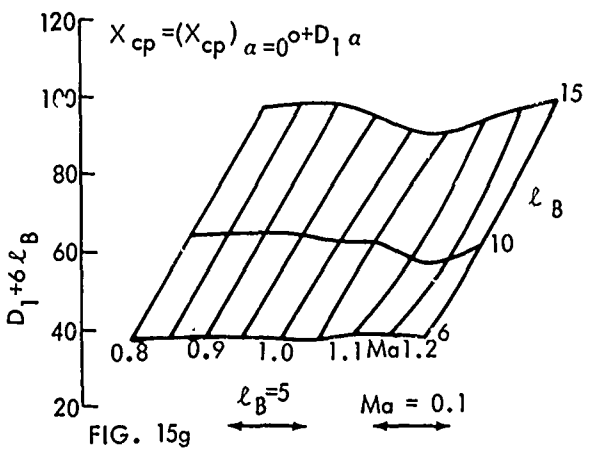

FIG. 15g

FIG. 15 D_1 AS A FUNCTION OF MACH NUMBER FOR CYLINDRICAL BODIES, ℓ_B=6 TO 15 (REF 9)

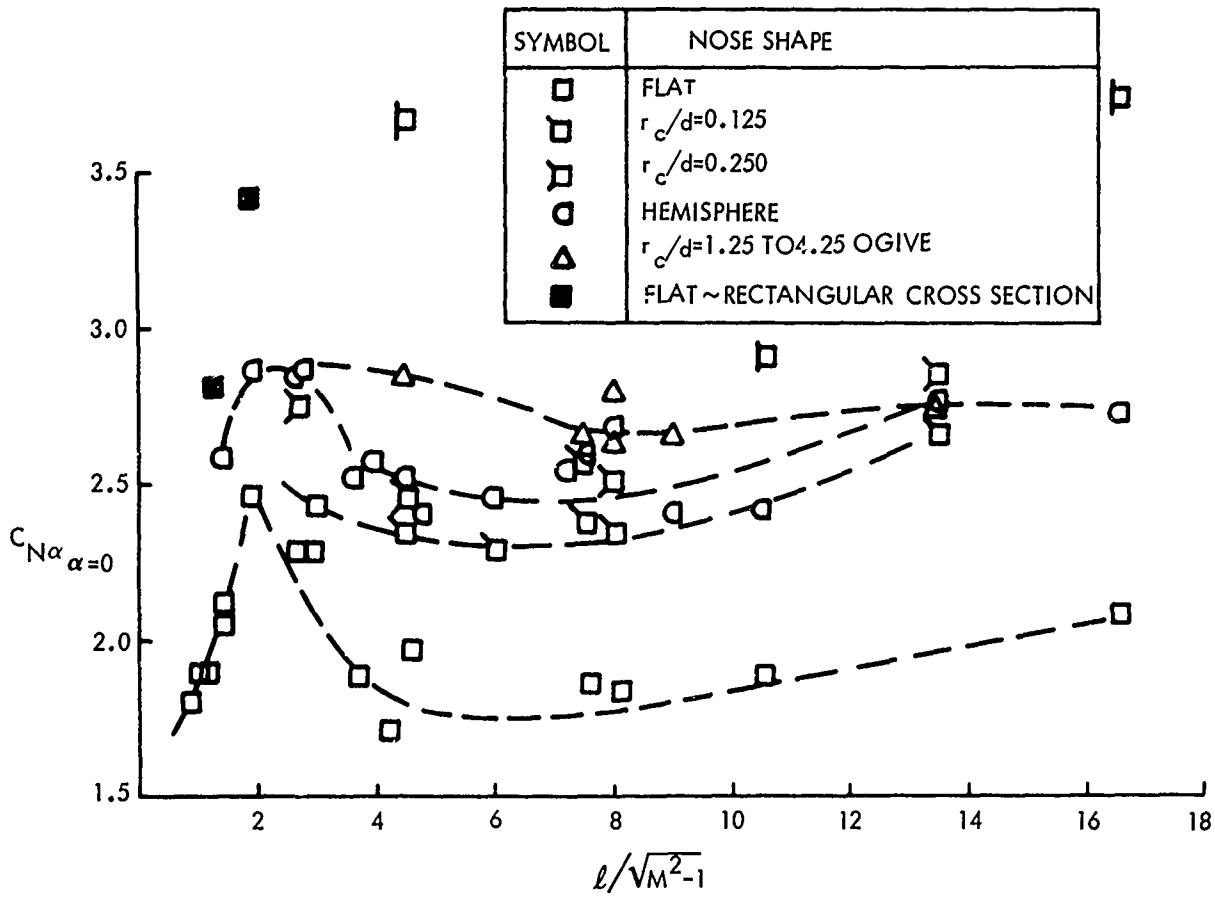

FIG. 16 $C_{N\alpha}$ BLUNT CYLINDRICAL BODIES M=1.2 TO 2.5 (REF 6,7)

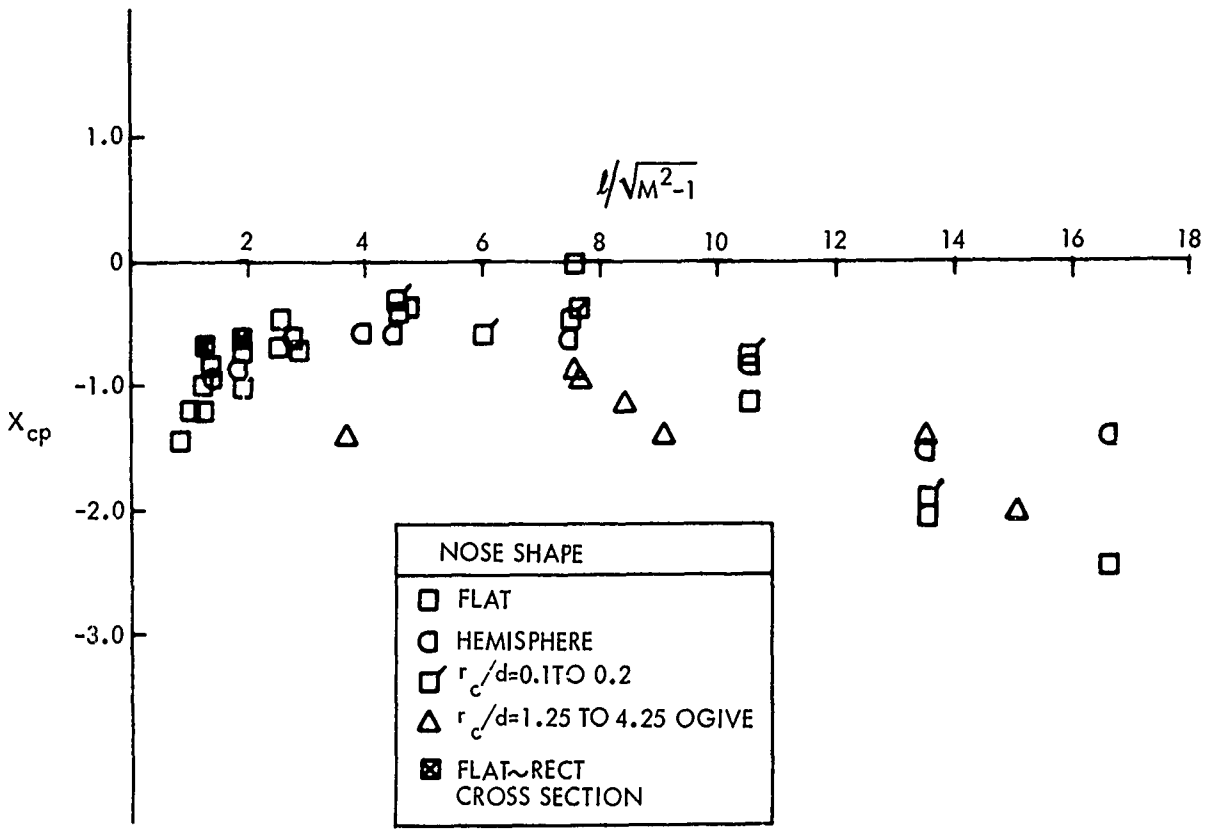

FIG. 17 X_{cp} CALIBERS FROM NOSE FOR BLUNT CYLINDRICAL BODIES $\ell < 10$, M=1.2 TO 2.6 (REF 6,7)

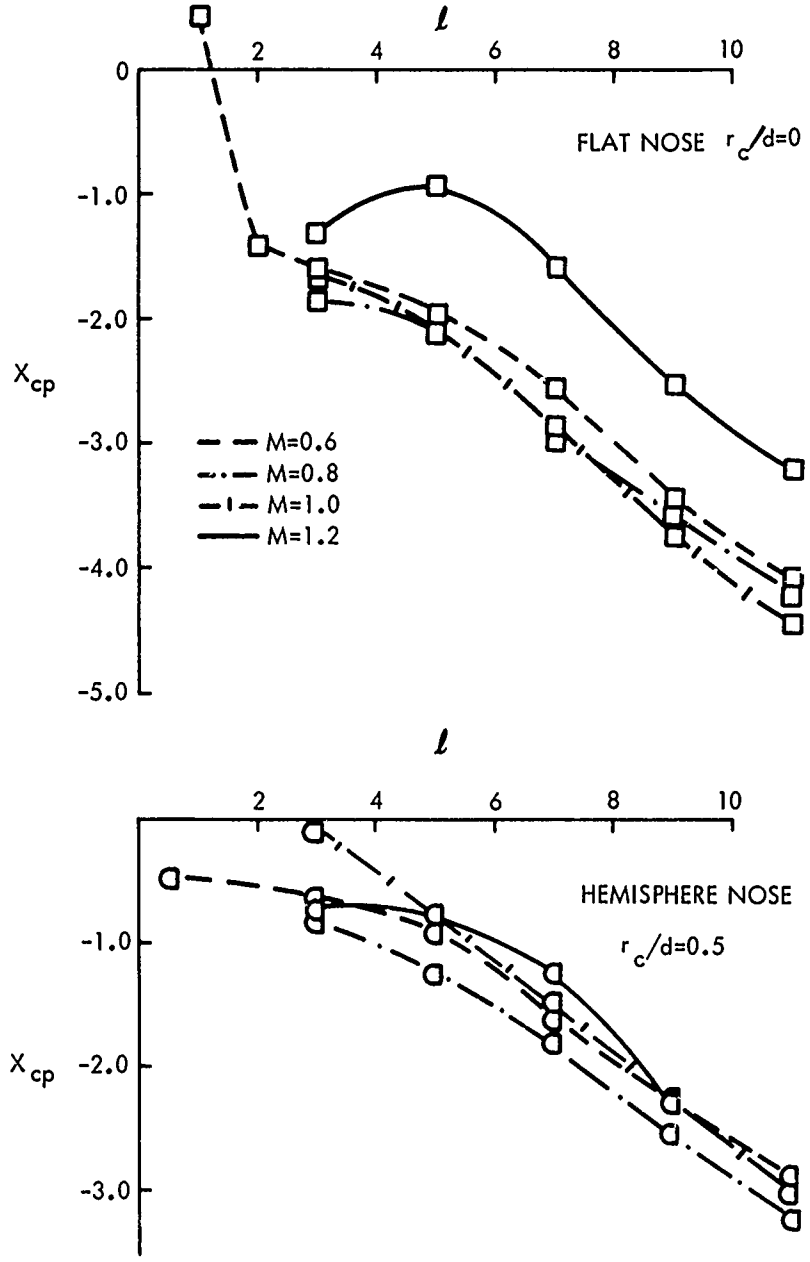

FIG. 18a CENTER OF PRESSURE (X_{cp}) AT α=10 DEGREES FOR CYLINDRICAL BODIES AT TRANSONIC SPEEDS (REF 6)

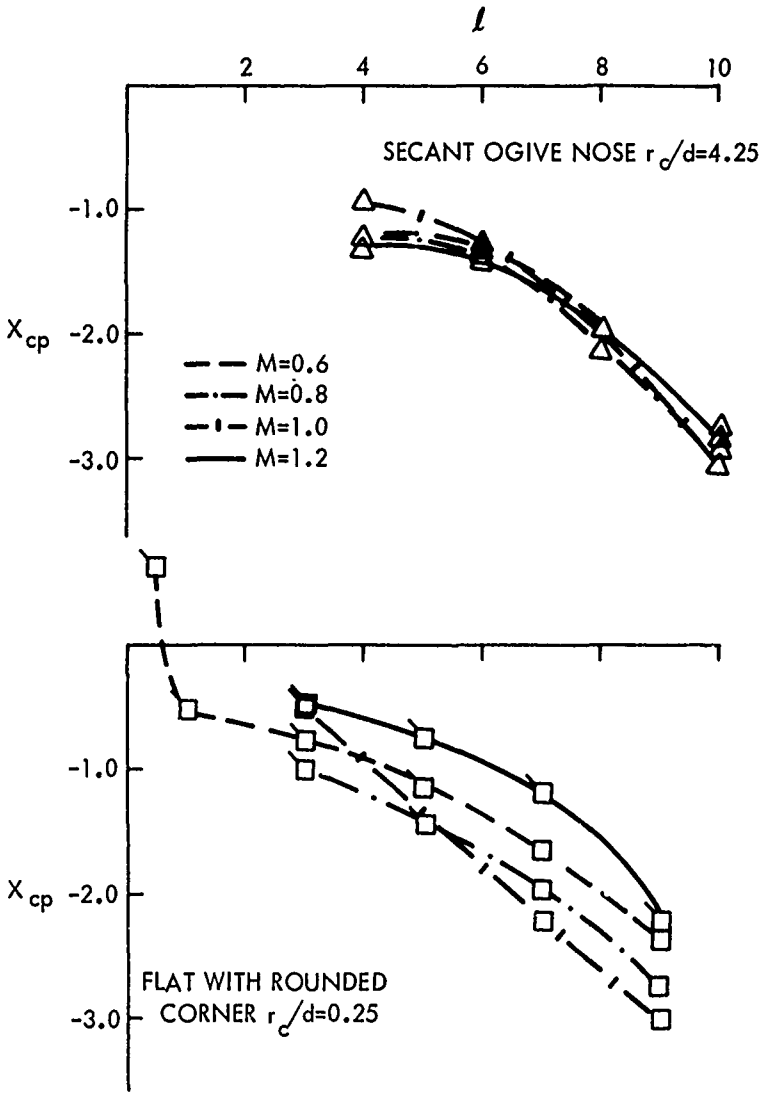

FIG. 18b CENTER OF PRESSURE (X_{cp}) AT α=10 DEGREES FOR CYLINDRICAL BODIES AT TRANSONIC SPEEDS (REF 6)

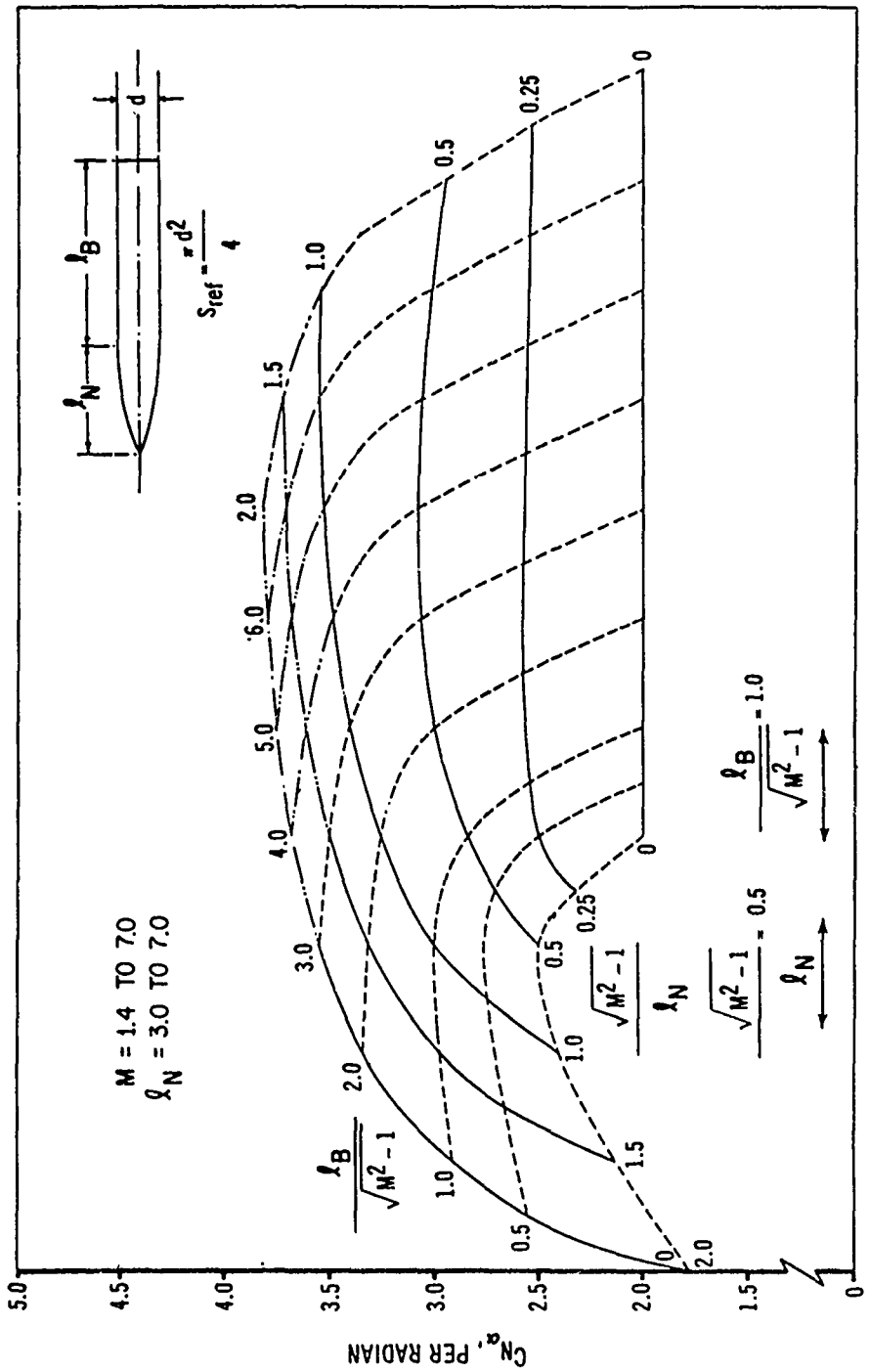

FIG. 19 NORMAL FORCE COEFFICIENT GRADIENT FOR TANGENT OGIVE CYLINDER CONFIGURATIONS (REF 2)

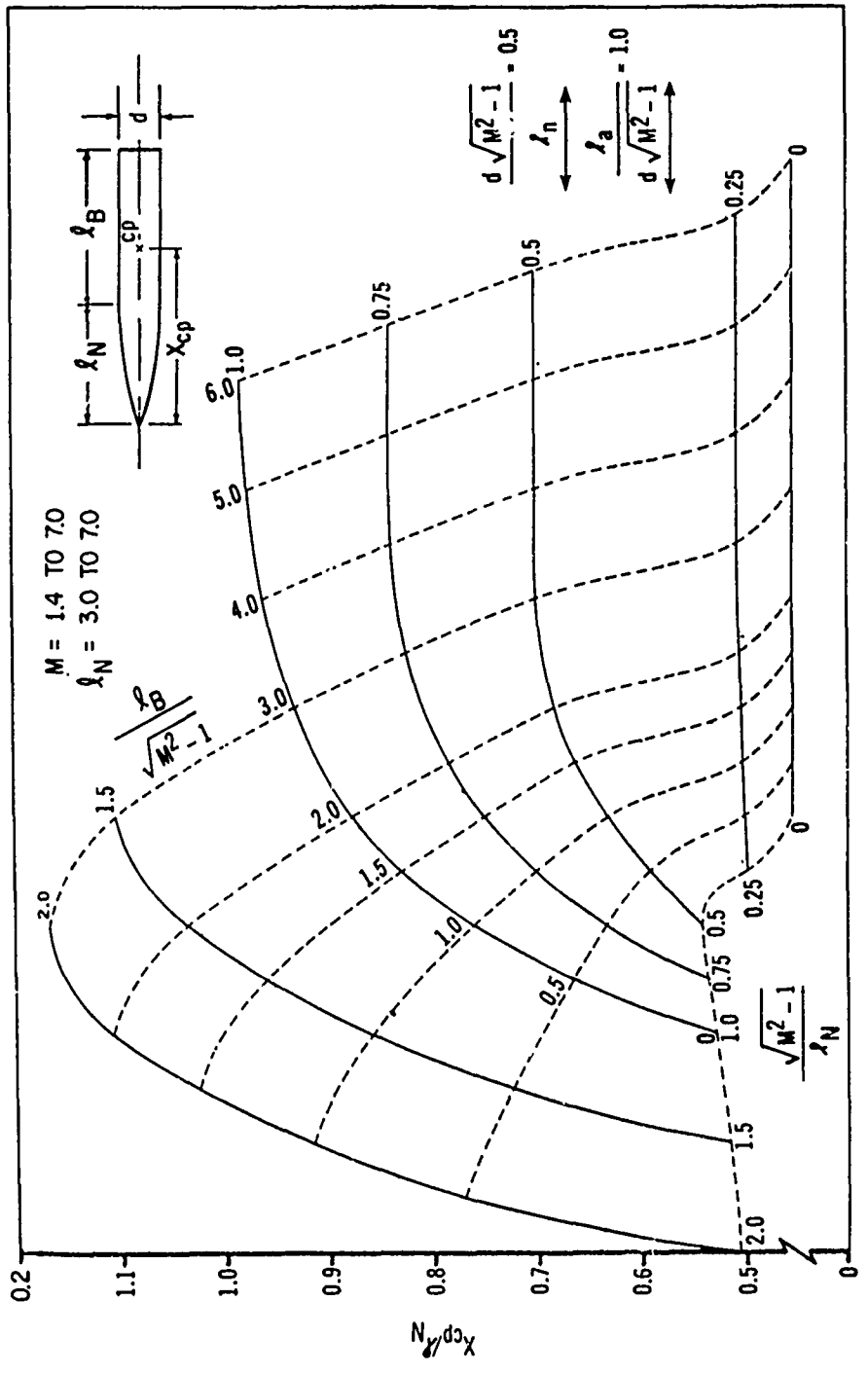

FIG. 20 CENTER OF PRESSURE FOR TANGENT OGIVE-CYLINDER CONFIGURATIONS (REF 2)

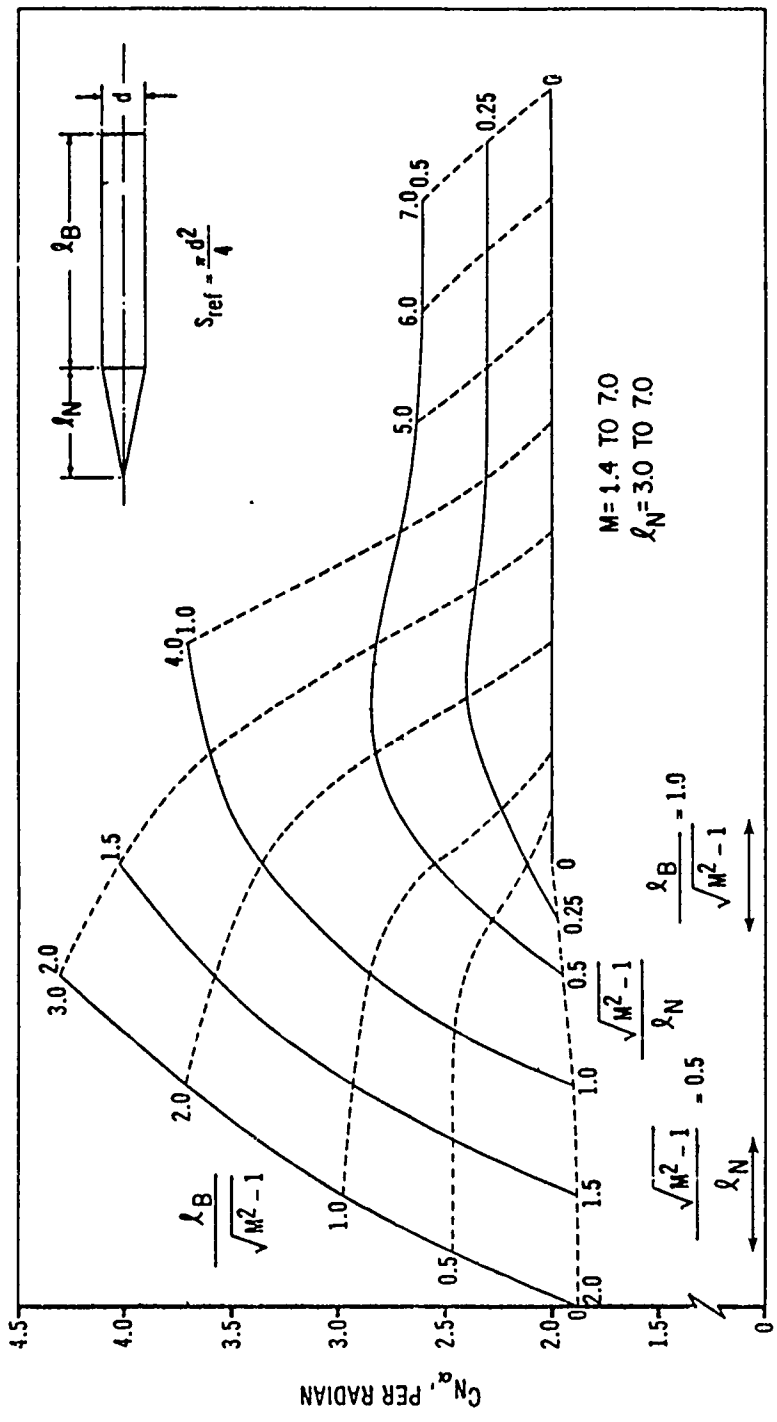

FIG. 21 NORMAL FORCE COEFFICIENT GRADIENT FOR CONE-CYLINDER CONFIGURATIONS (REF 2)

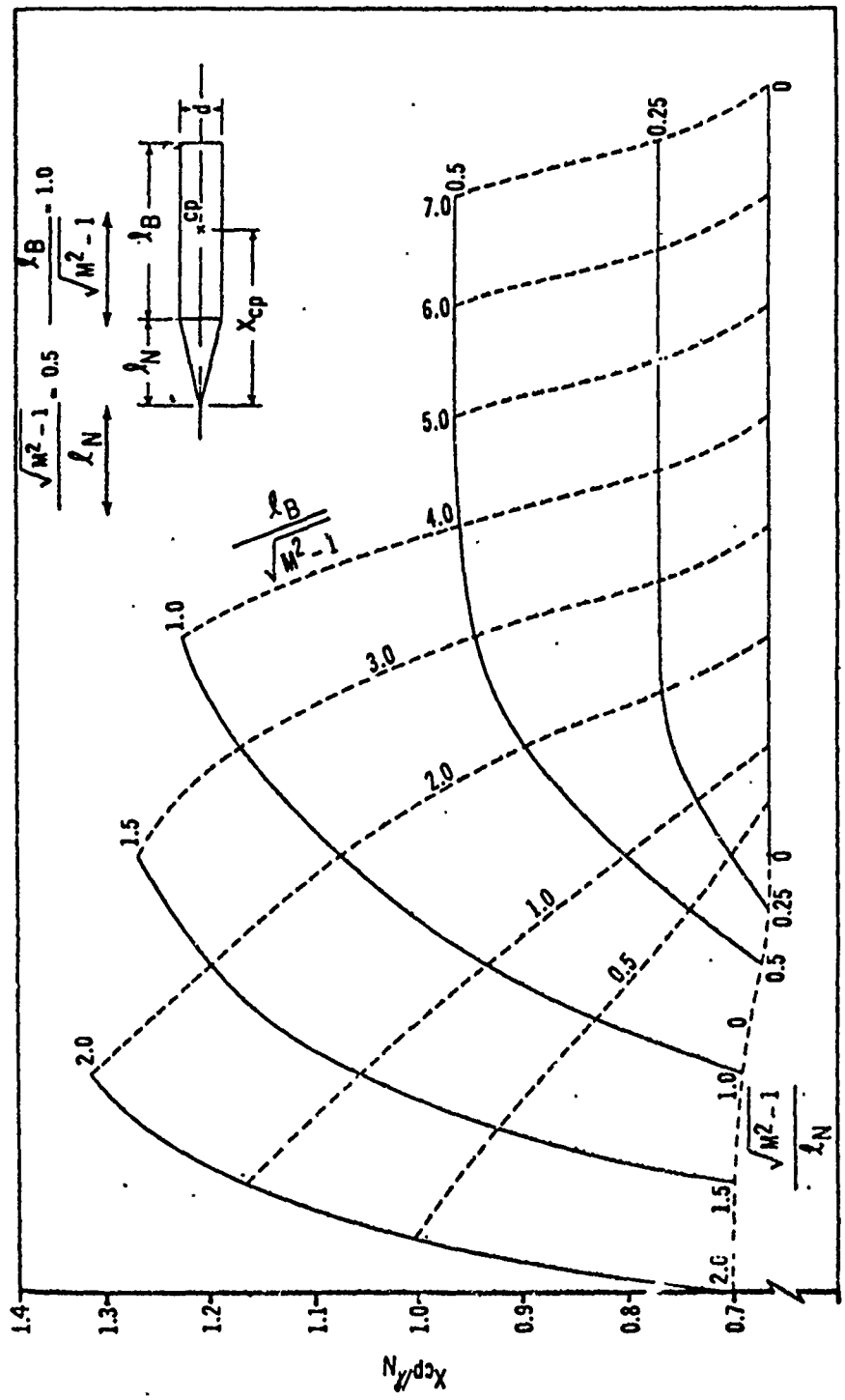

FIG. 22 CENTER OF PRESSURE FOR CONE-CYLINDER CONFIGURATIONS (REF 2)

NORMAL FORCE AND PITCHING MOMENT FOR CONE CYLINDERS WHERE α = 0 TO 90 DEGREES FOR SUBSONIC AND SUPERSONIC SPEEDS

K. D. Thomson formulated a rapid method for calculating C_N and C_m for cone cylinders for the angle-of-attack range of 0 to 60 degrees. The method is good for bodies $\ell/d > 3$ where cone half angle does not exceed 75° and the crossflow Mach number (M_c) does not exceed 0.8 (Ref. (10)). By Thomson's method:

$$C_N = \Delta C_{N_1} + \Delta C_{N_v} \tag{8}$$

where: $\Delta C_{N_1} = \frac{1}{2} C_{N_\alpha} \sin 2\alpha$ (inviscid contribution)

C_{N_α} is found on the appropriate figure

in this report and ΔC_{N_v} = is the viscous flow contribution.

$$\frac{\Delta C_{N_v} S}{KF \sin \alpha \cos \alpha} = \frac{J}{S} \cot \alpha \, [B]_0^{X_N} + [A]_{X_N}^{X_L-E} + H[A]_{X_L-E}^{X_L} \tag{9}$$

For the pitching moment referred to the nose tip:

$$C_m = \Delta C_{m_1} + \Delta C_{m_v} \tag{10}$$

where: $\Delta C_{m_1} = \frac{1}{2} C_{N_\alpha} x_{cp} \sin 2\alpha$ (the inviscid contribution)

x_{cp} is taken from the appropriate figure

$$\frac{(\Delta C_{m_v}) S^2}{KF \cos^2 \alpha} = \frac{J}{S} \cot \alpha \, [C]_0^{X_N} + [B]_{X_N}^{X_L-E} + H[B]_{X_L-E}^{X_L} \tag{11}$$

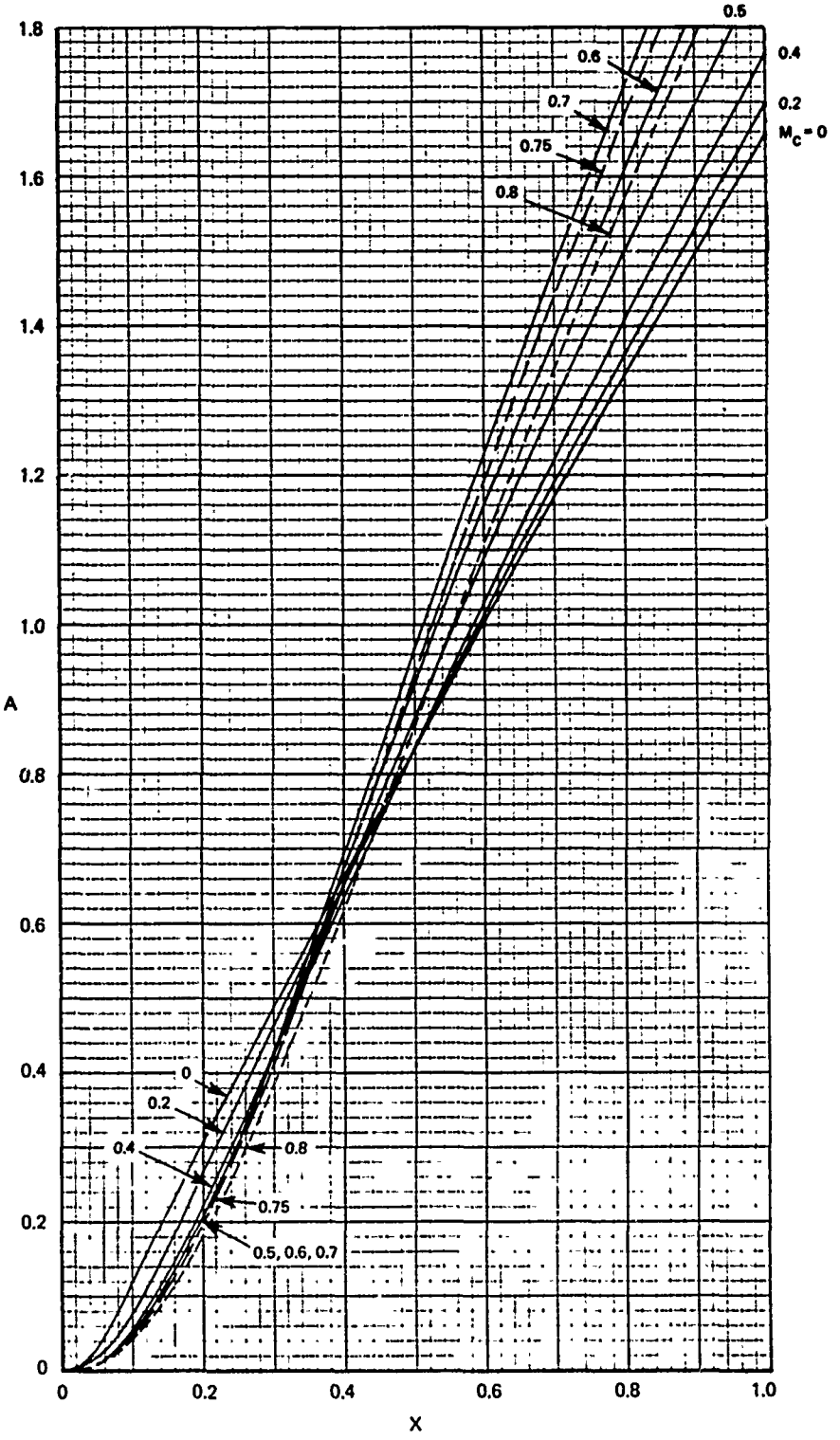

FIG. 23a VARIATION OF THE FUNCTION A WITH X AND M_c
$0 \leq X \leq 1$ (REF 10)

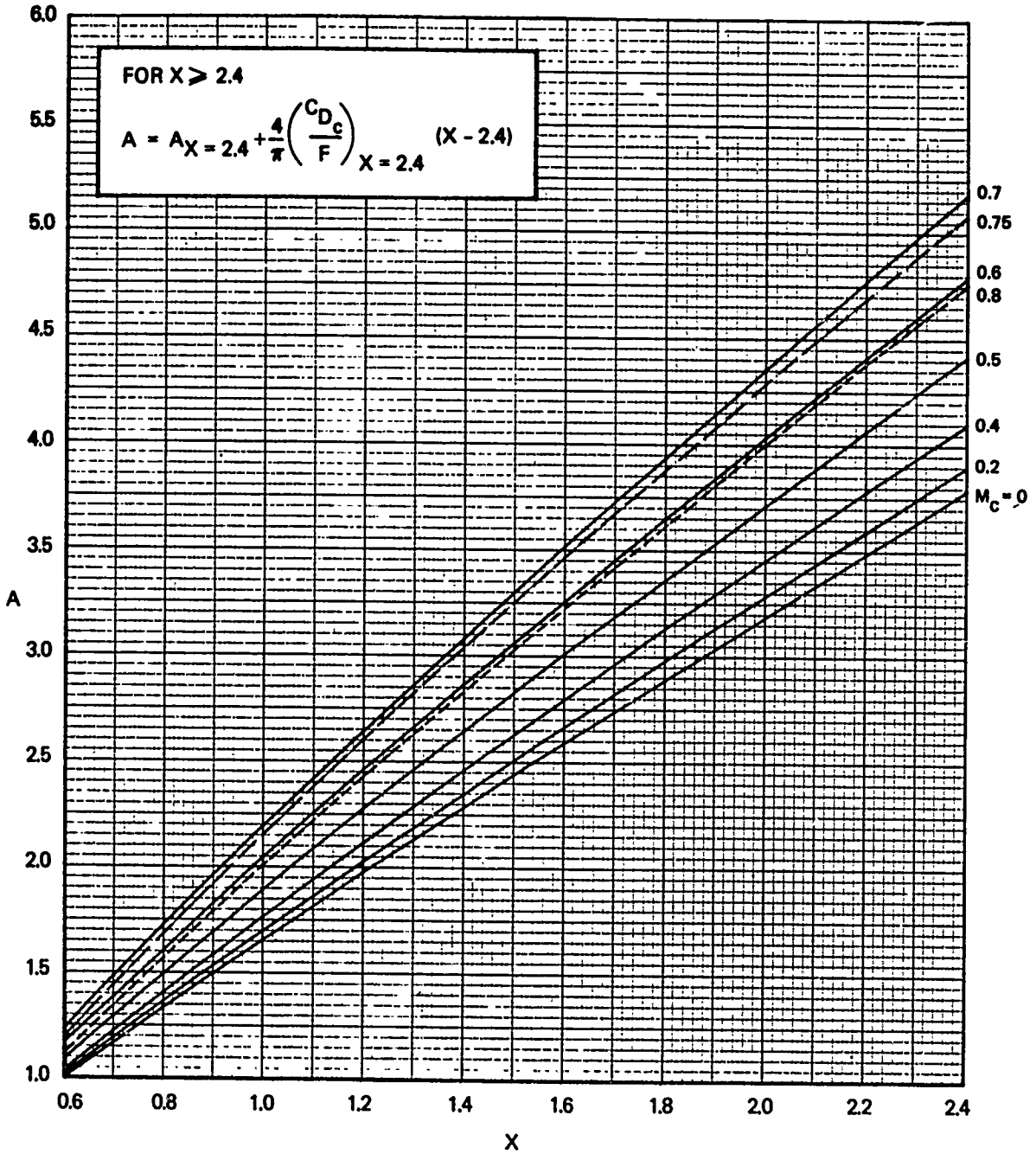

FIG. 23b VARIATION OF THE FUNCTION A WITH X AND M_c
$0.6 \leq X \leq 2.4$ (REF 10)

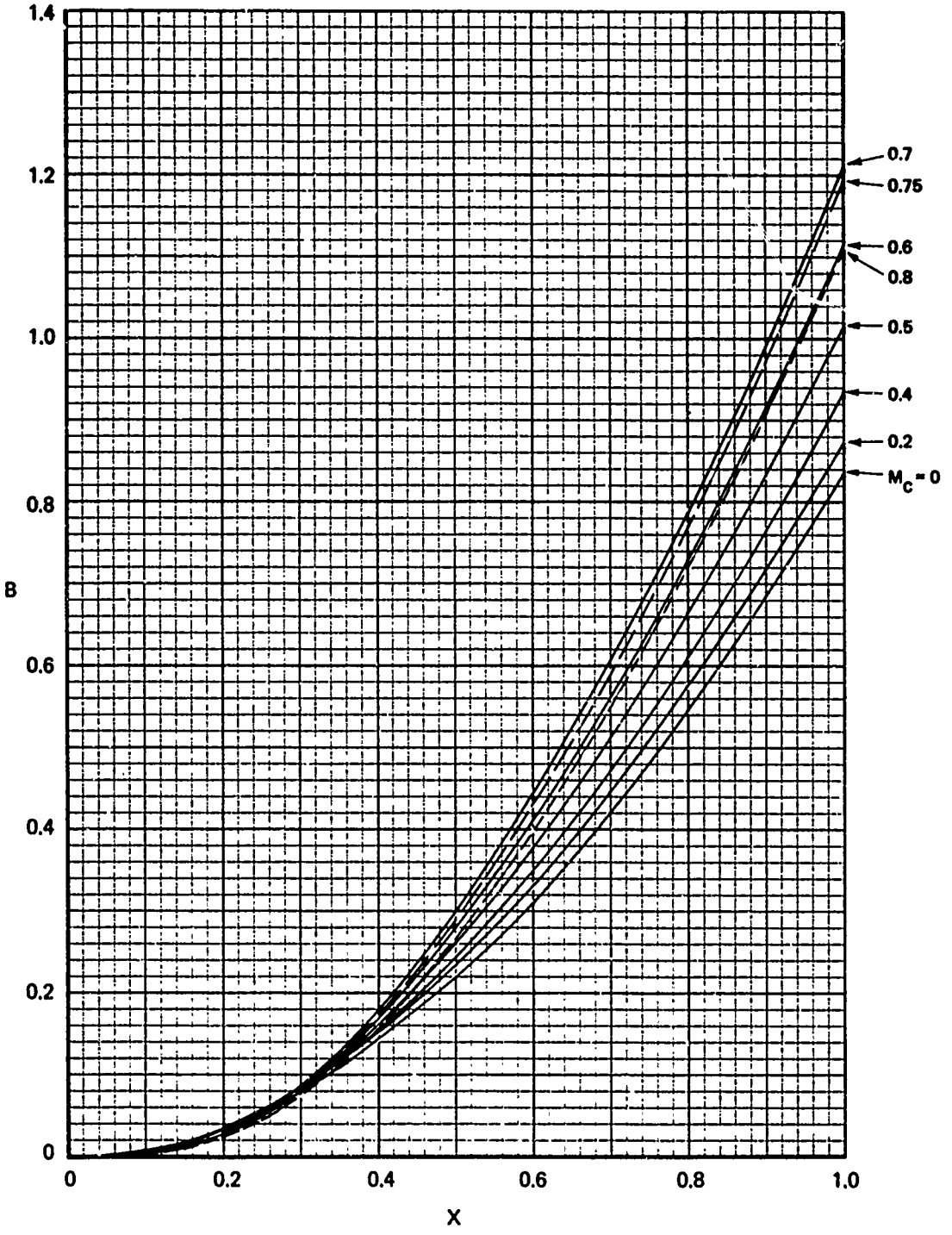

FIG. 24a VARIATION OF THE FUNCTION B WITH X AND M_c
$0 \leq X \leq 1.0$ (REF 10)

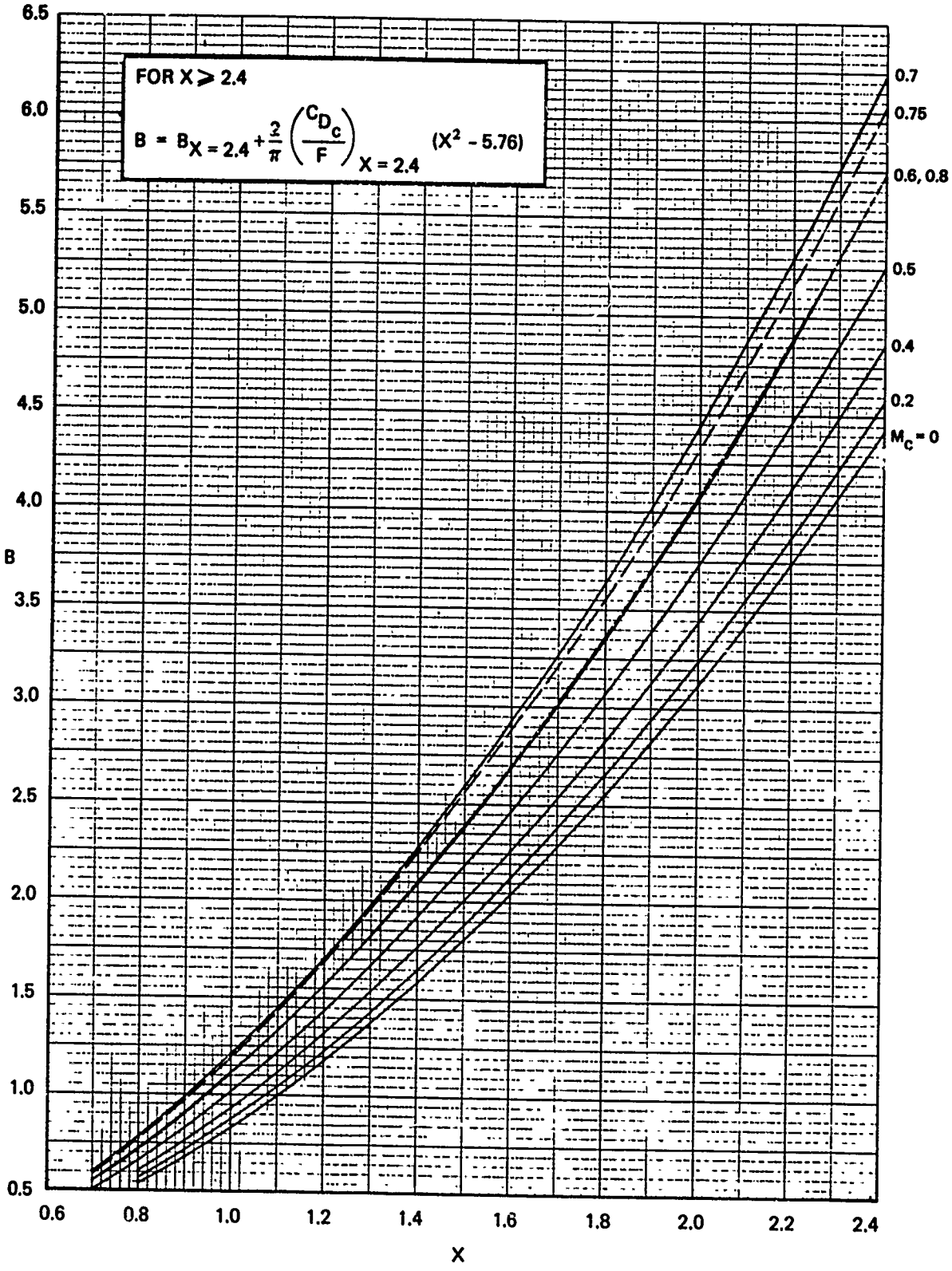

FIG. 24b VARIATION OF THE FUNCTION B WITH X AND M_c
$0.6 \leq X \leq 2.4$ (REF 10)

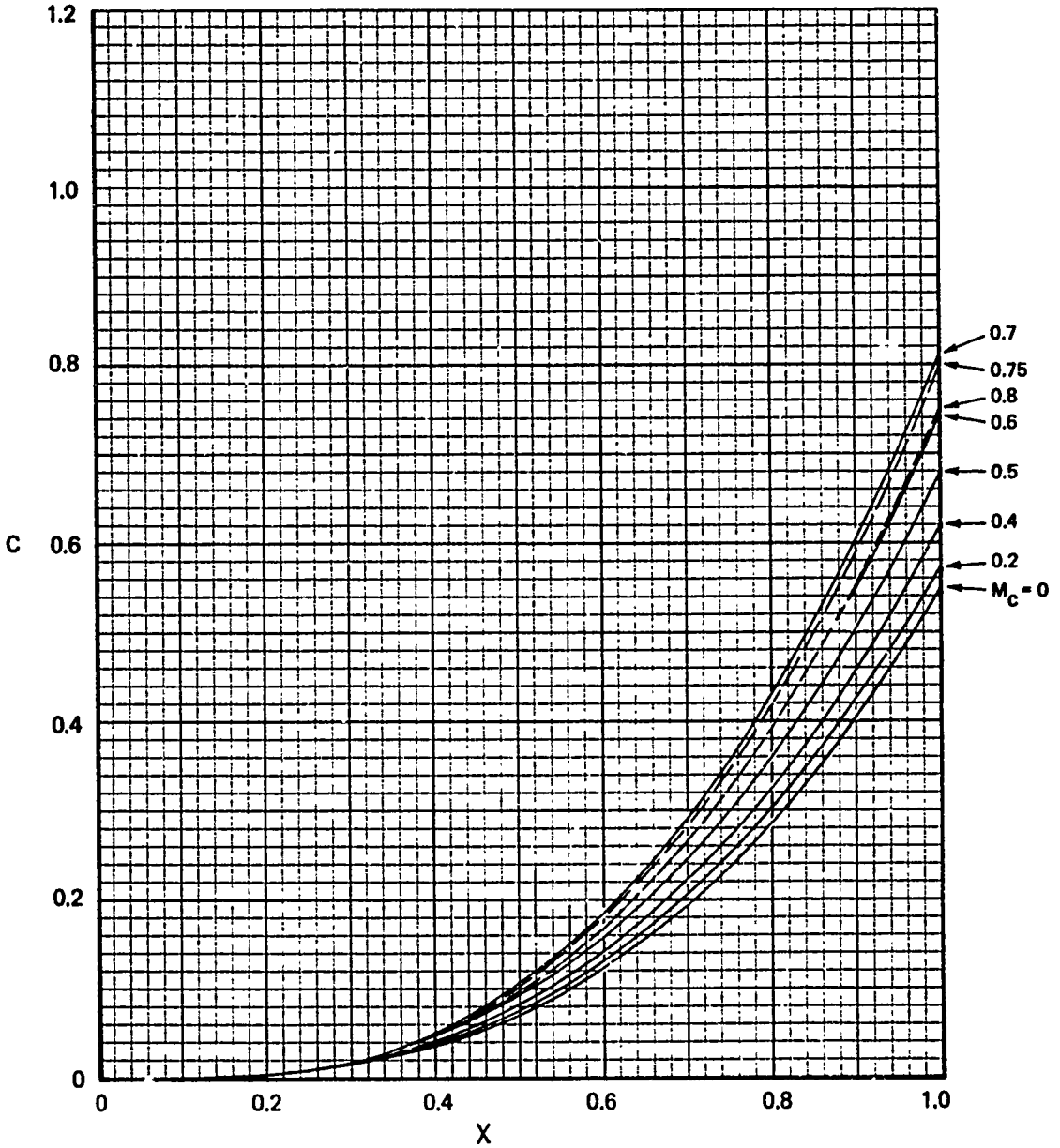

FIG. 25a VARIATION OF THE FUNCTION C WITH X AND M_c
$0 \leq X \leq 1.0$ (REF 10)

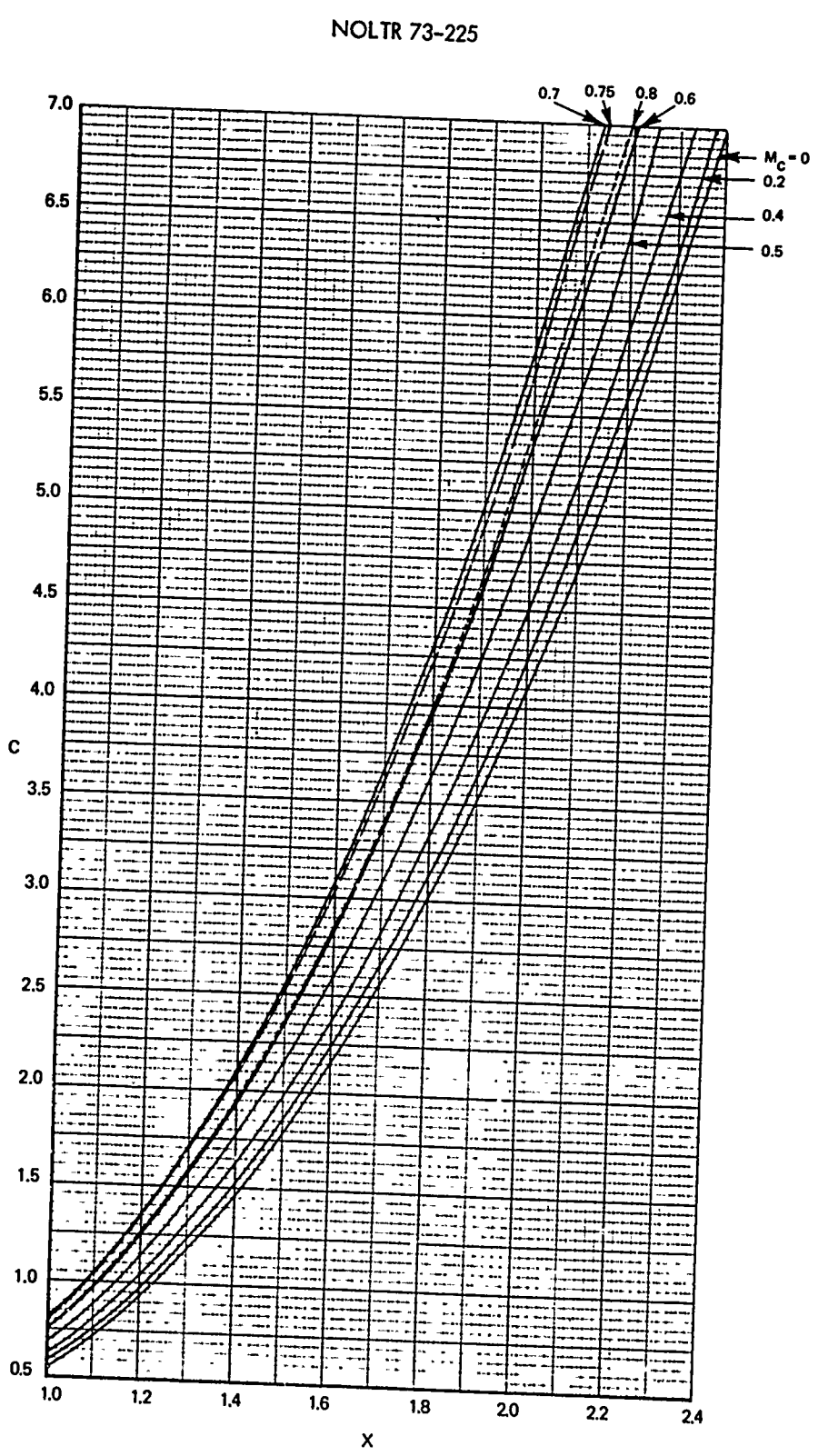

FIG. 25b VARIATION OF THE FUNCTION C WITH X AND M_c
$1.0 \leq X \leq 2.4$ (REF 10)

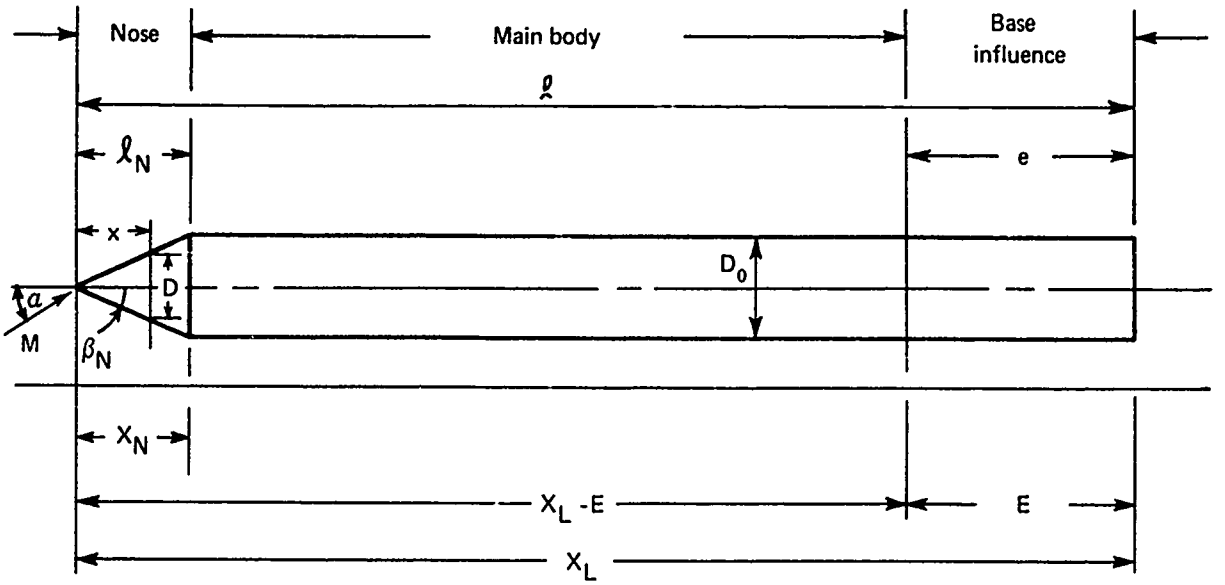

$X_N = \ell_N$ S tan α; $X_L = \ell$ S tan α; E = e S tan α

NOTE: ℓ_N, ℓ, and e are in calibers

FIG. 26 GEOMETRY FOR CONE-CYLINDER AT INCIDENCE (REF 10)

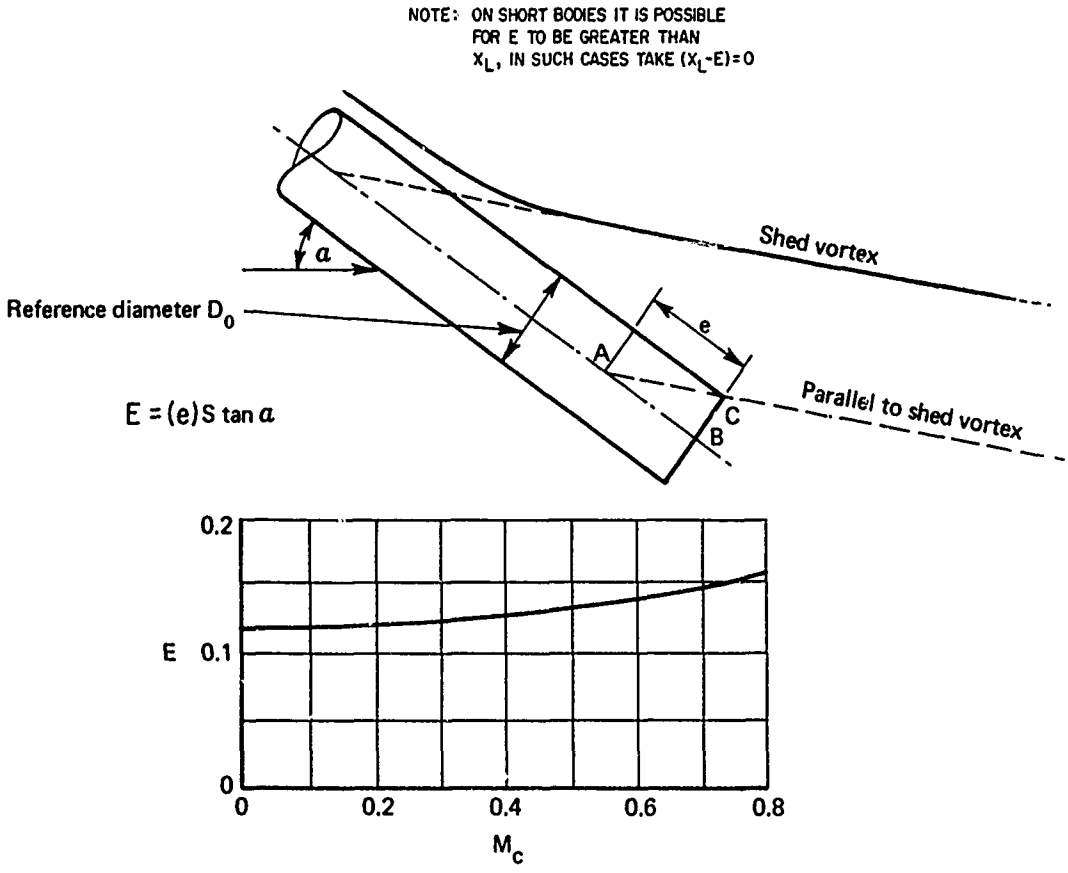

FIG. 27 EXTENT OF UPSTREAM INFLUENCE OF BASE (E) (REF 10)

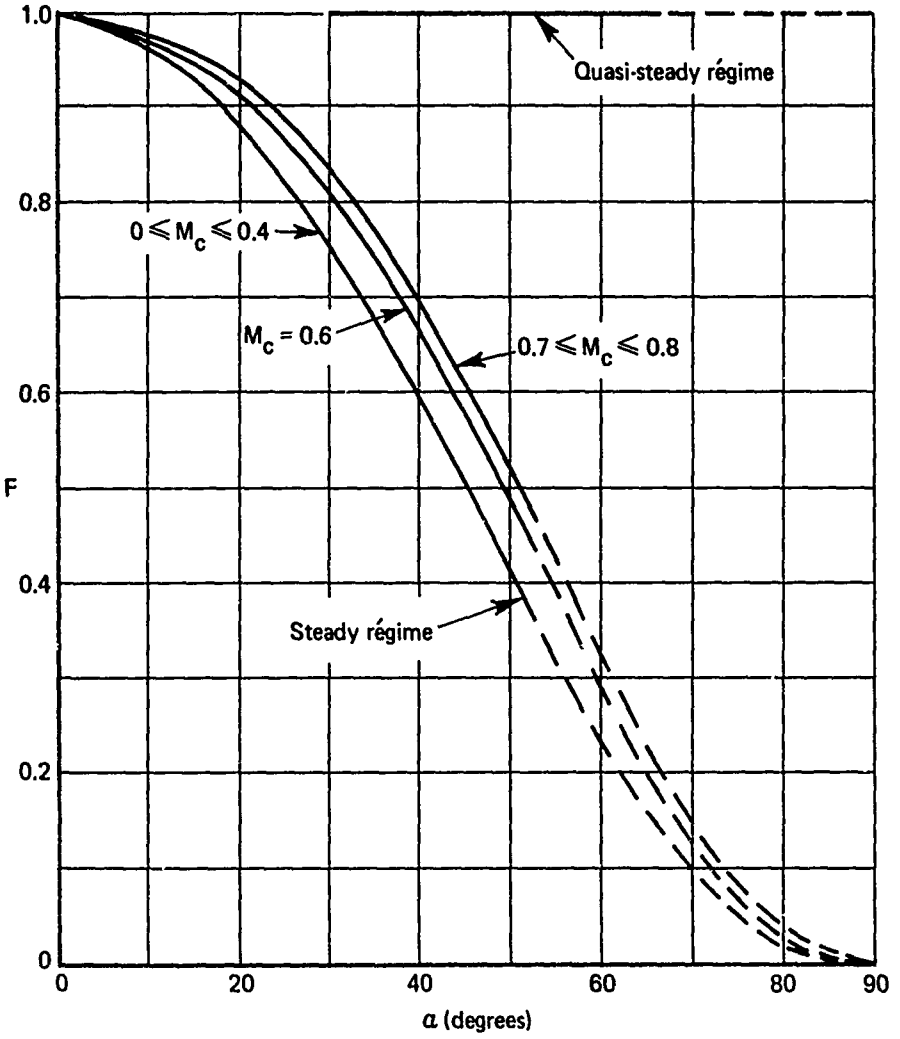

FIG. 28 VARIATION OF VORTEX STRENGTH PARAMETER F WITH CROSS-FLOW MACH NUMBER AND INCIDENCE (REF 10)

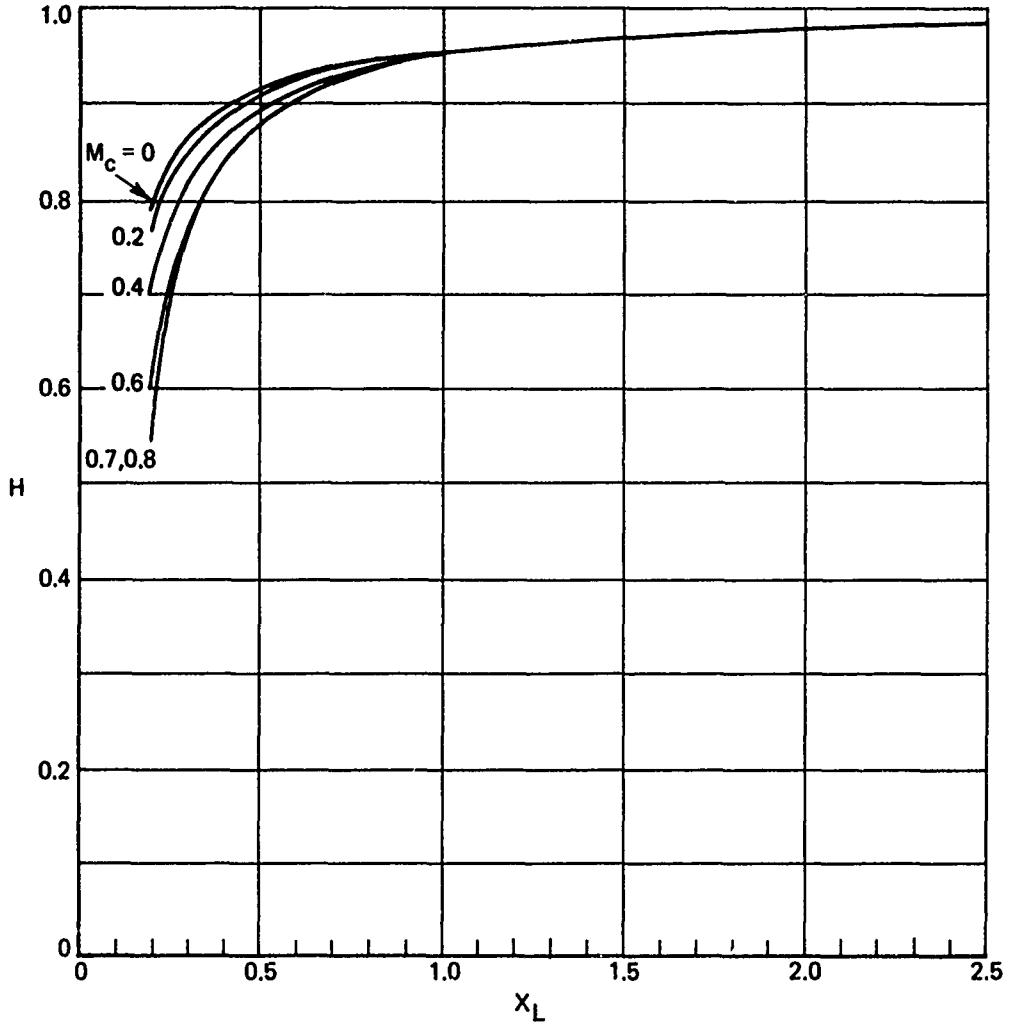

FIG. 29 REDUCTION FACTOR H TO ALLOW FOR EFFECT OF BASE INFLUENCE ON VISCOUS NORMAL FORCE AND PITCHING MOMENT (REF 10)

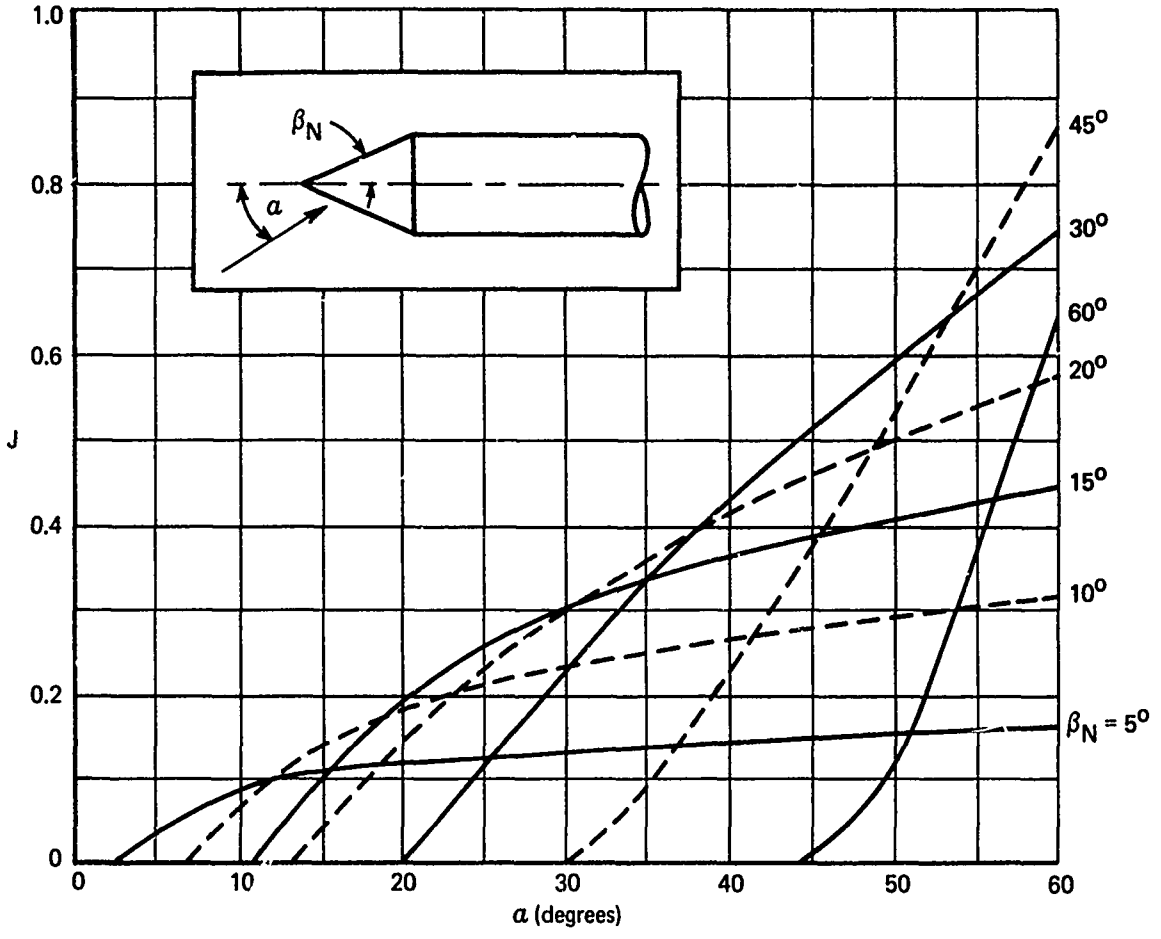

FIG. 30 REDUCTION FACTOR J TO ALLOW FOR EFFECT OF NOSE ON VISCOUS NORMAL FORCE AND PITCHING MOMENT (REF 10)

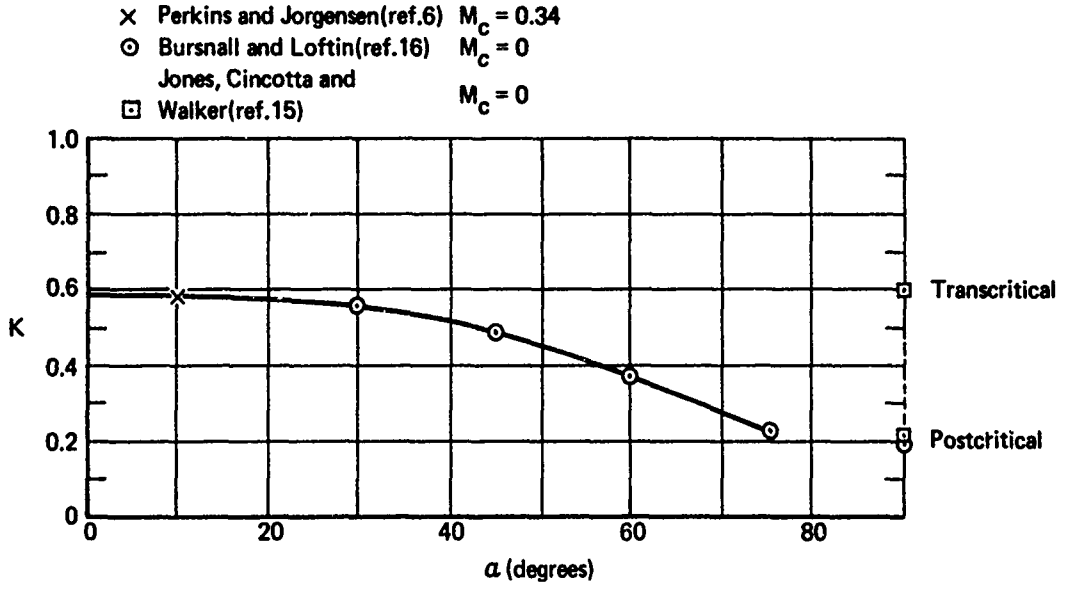

FIG. 31 EFFECT OF INCIDENCE ON $K = \frac{C_{D_c}\ (\text{TURBULENT SEPARATION})}{C_{D_c}\ (\text{LAMINAR SEPARATION})}$ (REF 10)

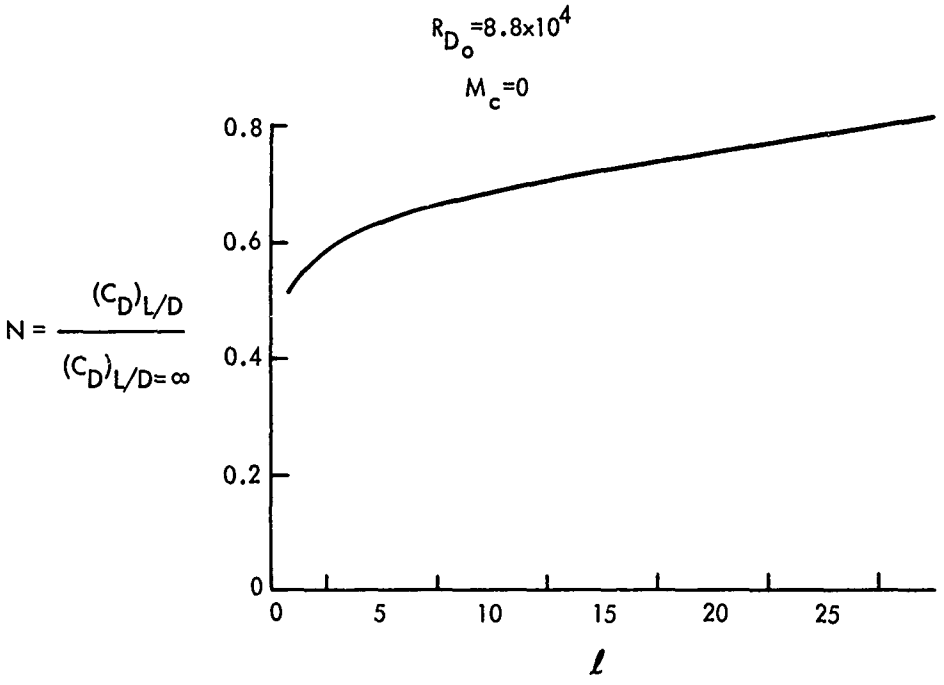

FIG. 32 DRAG OF CIRCULAR CYLINDERS OF FINITE SPAN MOUNTED NORMAL TO FREE STREAM (THE FACTOR N) (REF 10)

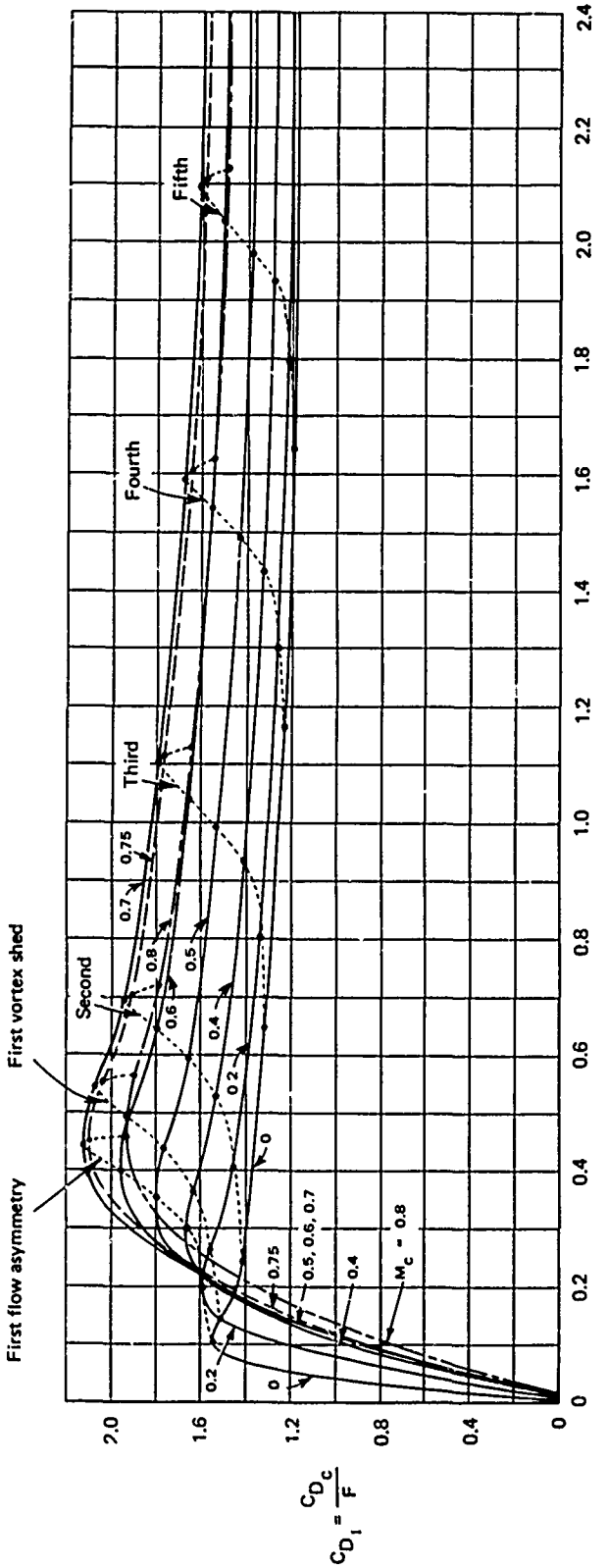

FIG. 33 BASIC CURVES FOR DETERMINING DISTRIBUTION OF CROSS-FLOW DRAG COEFFICIENT (REF 10)

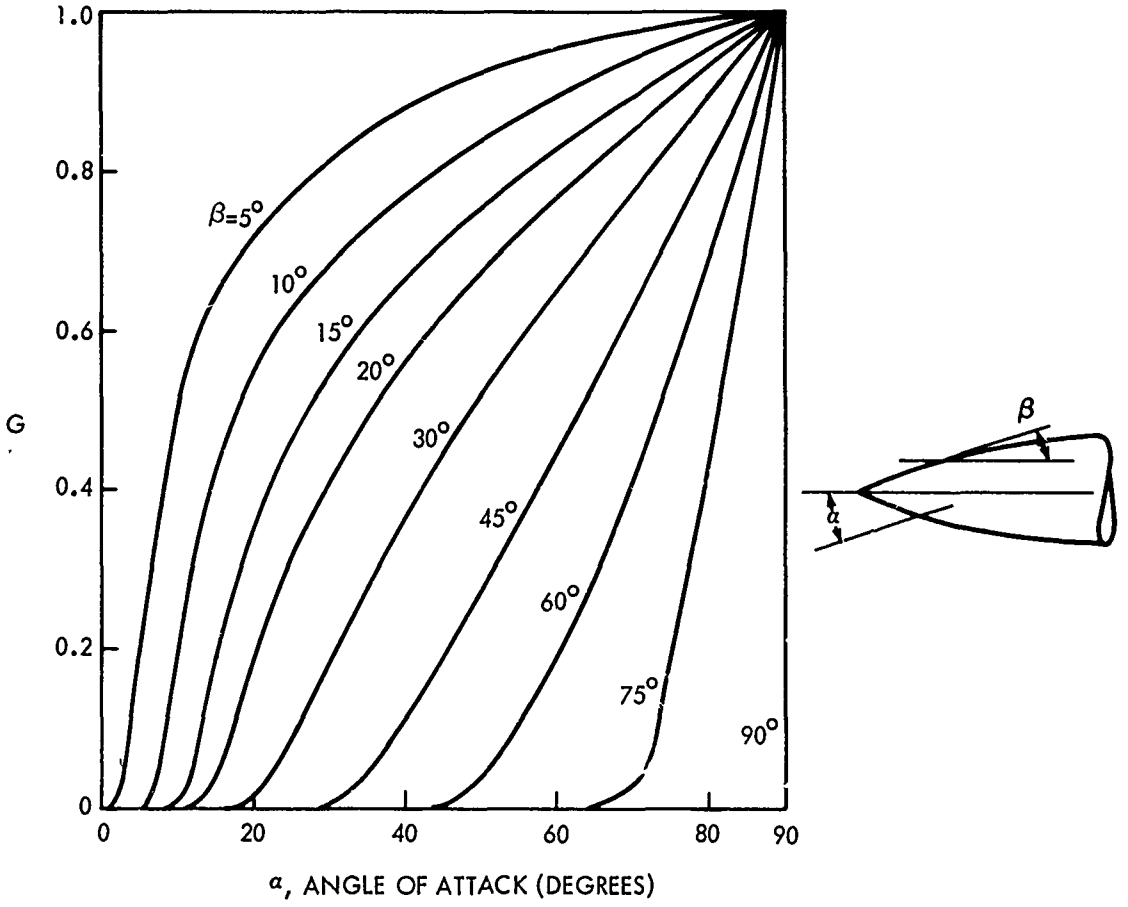

FIG. 34 CROSS-FLOW DRAG CORRECTION FACTOR G DUE TO AXIAL PRESSURE GRADIENT (REF 10)

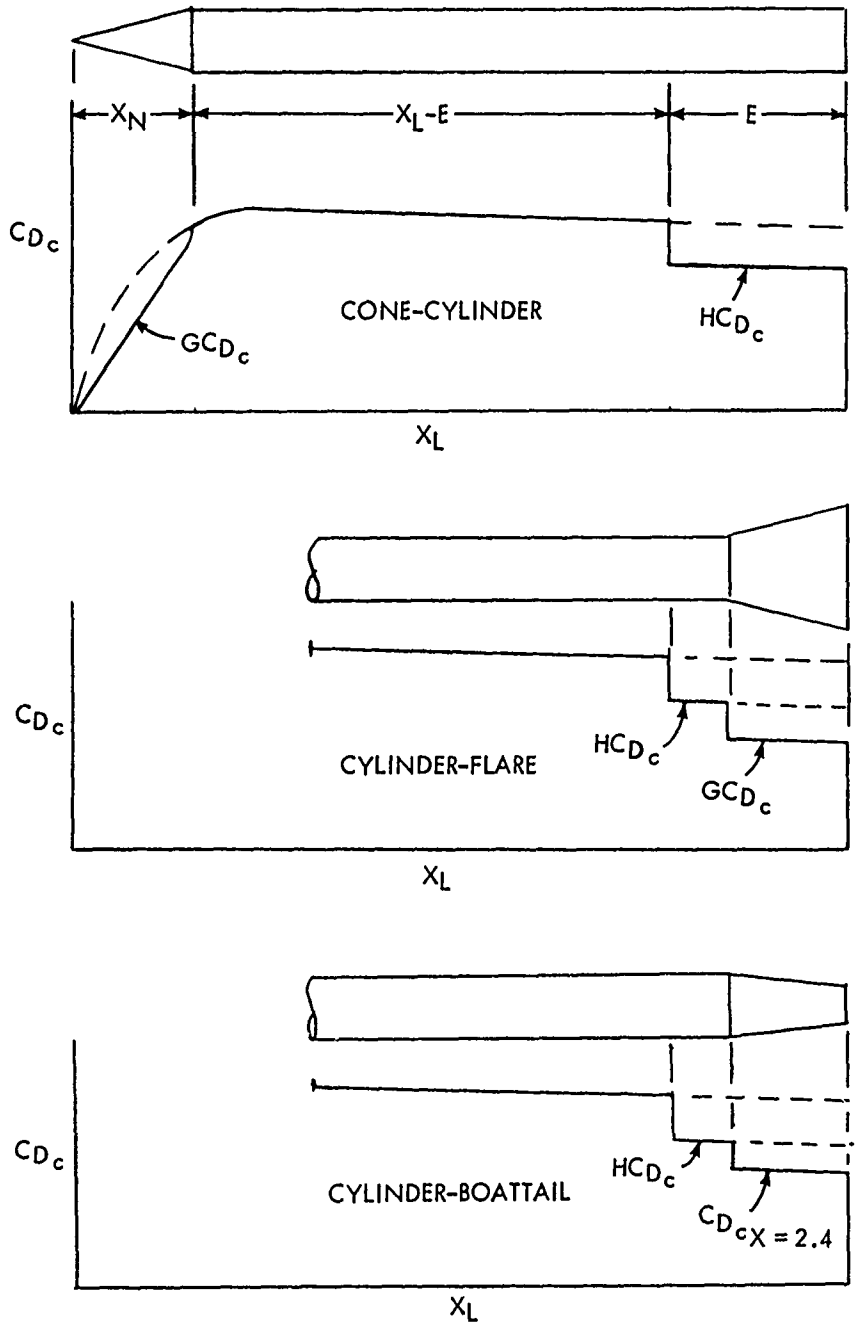

FIG. 35 ILLUSTRATION SHOWING COMPOSITION OF CROSS-FLOW DRAG COEFFICIENT FOR THREE TYPES OF BODIES (REF 10)

In these equations, to find the value of terms such as $[A]_{X_N}^{X_L-E}$, find the value of A at X_L-E and at X_N and take the difference. Figures 23 to 31 give A, B, C, E, F, H, J, and K. In both Equations (9) and (11), S = 0.2 and is the Strouhal number. On Figures 23, 24, and 25 for finding A, B, and C as a function of X_N X_L and X_L-E as defined on Figure 26 where:

$$X_N = \ell_N \, S \tan \alpha$$

$$X_L = \ell \, S \tan \alpha$$

E = e S tan α (found directly on Figure 27).

The following table gives the limits of Equations (9) and (11) and shows how to determine the values of K and F.

α RANGE	CHARACTER OF WAKE	K	F
0° to 40°	Steady, Laminar Separation	1	Fig. 28
	Turbulent Separation	Fig. 31	1
30° to 60°	Quasi-Steady Laminar	1	1
	Turbulent	Fig. 31	Fig. 28

For the range of α = 60° to 90° the body is in the unsteady wake regime and:

$$\Delta C_{N_v} = \sin^2\alpha [C_{D_c} \frac{A_P}{S_{ref}}] \qquad (12)$$

where: $C_{D_c} = KNC_{D_{c_{x=24}}}$, find $C_{D_{c_{x=24}}}$ on Figure 33 and N on Figure 32.

For the pitching moment:

$$\Delta C_{m_v} = \sin^2\alpha[C_{D_c} \frac{A_P}{S_{ref}}] x_{cp} \quad (x_{cp} \text{ at high angles of attack is the centroid of the body}) \tag{13}$$

EFFECTS OF FLARES AND BOATTAILS AT HIGH ANGLES OF ATTACK

Thomson also describes how to calculate the normal force and pitching moment of bodies having flares and boattails. The method is not rapid as the one for cone cylinders described in the previous section but requires integrating the viscous crossflow drag over the body so that:

$$\Delta C_v = \frac{2}{\pi} \frac{\sin 2\alpha}{S} \int_0^{X_L} C_{D_c} \left(\frac{d}{d_{ref}}\right) dx \tag{14}$$

$$\Delta C_m = \frac{-4}{\pi} \frac{\cos 2\alpha}{S^2} \int_0^{X_L} C_{D_c} \left(\frac{d}{d_{ref}}\right) X dx \tag{15}$$

where: C_{D_c} is obtained from Figure 33, S = 0.2 and $X_L = \ell$ S tan α, ℓ = total length of body.

The body is treated as four sections:

(a) nose, where C_{D_c} for X_N is multiplied by G from Figure 34 to account for the effect of pressure gradient on the nose.

(b) body, where C_{D_c} is taken directly from Figure 33.

(e) upstream influence of base, determine E from Figure 27 and H from Figure 29. Find C_{D_c} for E from Figure 33 and multiply by H.

(f) flare or boattail. For a flare multiply C_{D_c} by G using the flair angle as β on Figure 34.

For the boattail, take C_{D_c} at x = 2.4 from Figure 32 as the crossflow drag coefficient for the boattail. Figure 35 shows what the developed crossflow drag coefficient would look like. Keep in mind that such a curve of C_{D_c} versus L has to be corrected to the local body diameter when integrating for the total crossflow drag. Also when finding the turbulent viscous forces, multiply by K from Figure 31 except for the case of the boattail where only the region ahead of the boattail is multiplied by K.

$(\Delta C_{N_\alpha})_{BT}$ - NORMAL FORCE SLOPE COEFFICIENT CONTRIBUTION OF A BOATTAIL NEAR α = 0 DEGREE FOR SUBSONIC AND SUPERSONIC SPEEDS

A boattail causes a negative normal force which subtracts from the normal force of the cylindrical body nose.

$$(\Delta C_{N_\alpha})_{BT} = -K_{BT} \frac{S_{bt}}{S_B} \left[1 - \left(\frac{d_{BT}}{d_c} \right)^2 \right] \qquad (16)$$

$K = 2$ where $d_{BT}/d_c > 0.8$ (Ref. (2))

where: S_{bt} = cross-sectional area of boattail at its smallest diameter

d_{BT} = diameter of boattail at its smallest diameter

d_c = diameter of boattail where it joins body

S_B = reference area of nose-cylinder C_{N_α}

The center of pressure of the boattail is assumed to be located at 0.6 of the boattail length measured from the body boattail juncture. The above expression was derived for boattail angles of 10° or less and ratios of $d_{BT}/d_c > 0.8$.

Where the boattail is replaced by a cylindrical boom of diameter ratio to body of 0.3 or less at attachment point, the C_{N_α} of the boom may be ignored.

For boattails where d_{BT}/d_c is less than 0.8, use Figure 36 to find the factor K_{BT} and the center of pressure of the boattail. At supersonic speeds, Figures 37 and 38 give $C_{N_{\alpha BT}}$ and x_{cp}/ℓ_{BT} for boattails on infinite cylindrical bodies. This means that local flow conditions upstream of the boattail are equal to free-stream conditions. These charts which were taken from the AMC Handbook (Ref. (2)) were derived from linearized theory calculations and slender-body theory predictions.

$(\Delta C_{N_\alpha})_f$ - NORMAL FORCE SLOPE CONTRIBUTION OF A CONICAL-FLARE AFTERBODY α NEAR 0 DEGREE FOR SUBSONIC AND SUPERSONIC SPEEDS

The contribution of a conical-flare afterbody to the normal force based on slender-body prediction is:

$$(\Delta C_{N_\alpha})_f = 2 \frac{S_f}{S_B} \left[1 - \left(\frac{d_c}{d_f} \right)^2 \right] \text{(Ref. (2))} \qquad (17)$$

and the center of pressure is:

$$\left(\frac{x_{cp}}{\ell_f} \right)_f = \frac{\left[\frac{d_c}{d_f} \left(\frac{d_c}{d_f + 1} \right) - 2 \right]}{3 \left[1 - \left(\frac{d_c}{d_f} \right)^2 \right]} , \qquad (18)$$

(an overall value of 60% may be used)

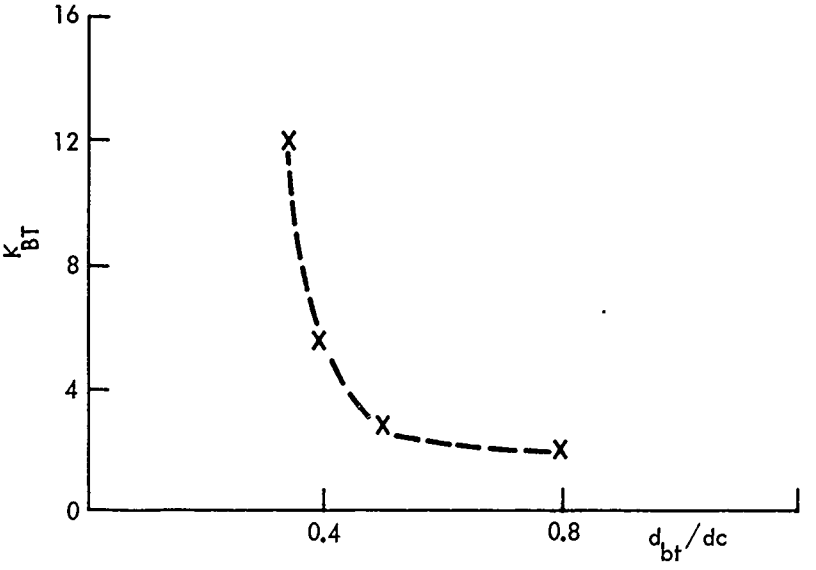

K_{BT} FACTOR USED IN EQUATION (16) FOR C_{N_α} BOATTAIL

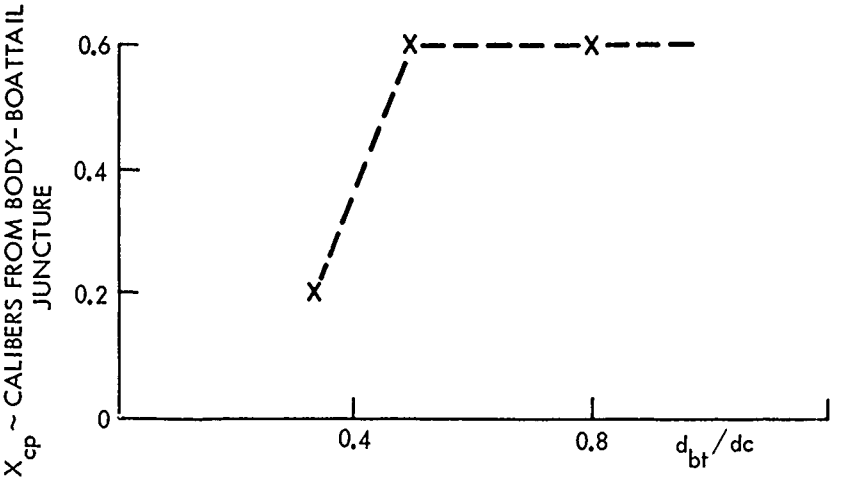

LOCATION OF CENTER OF PRESSURE ON BOATTAIL

FIG. 36 K_{BT} AND CENTER OF PRESSURE FOR BOATTAIL AT SUBSONIC SPEEDS

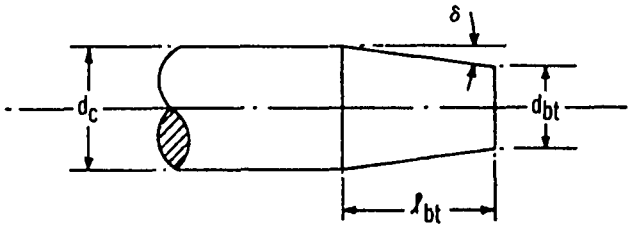

NOTE: M > 1

$$S_{ref} = \frac{\pi d_c^2}{4}$$

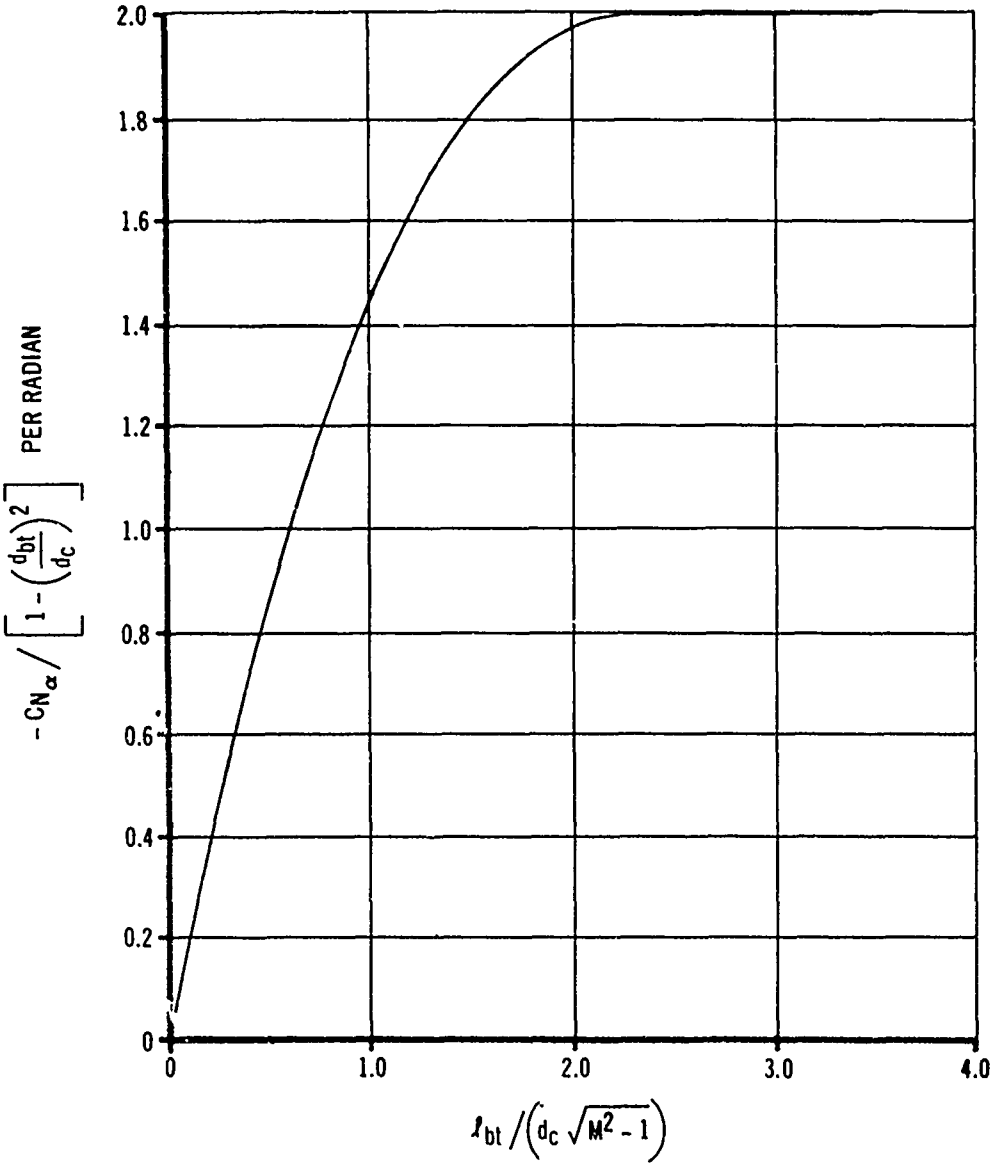

FIG. 37. NORMAL FORCE COEFFICIENT GRADIENT FOR A BOATTAIL (REF. 2)

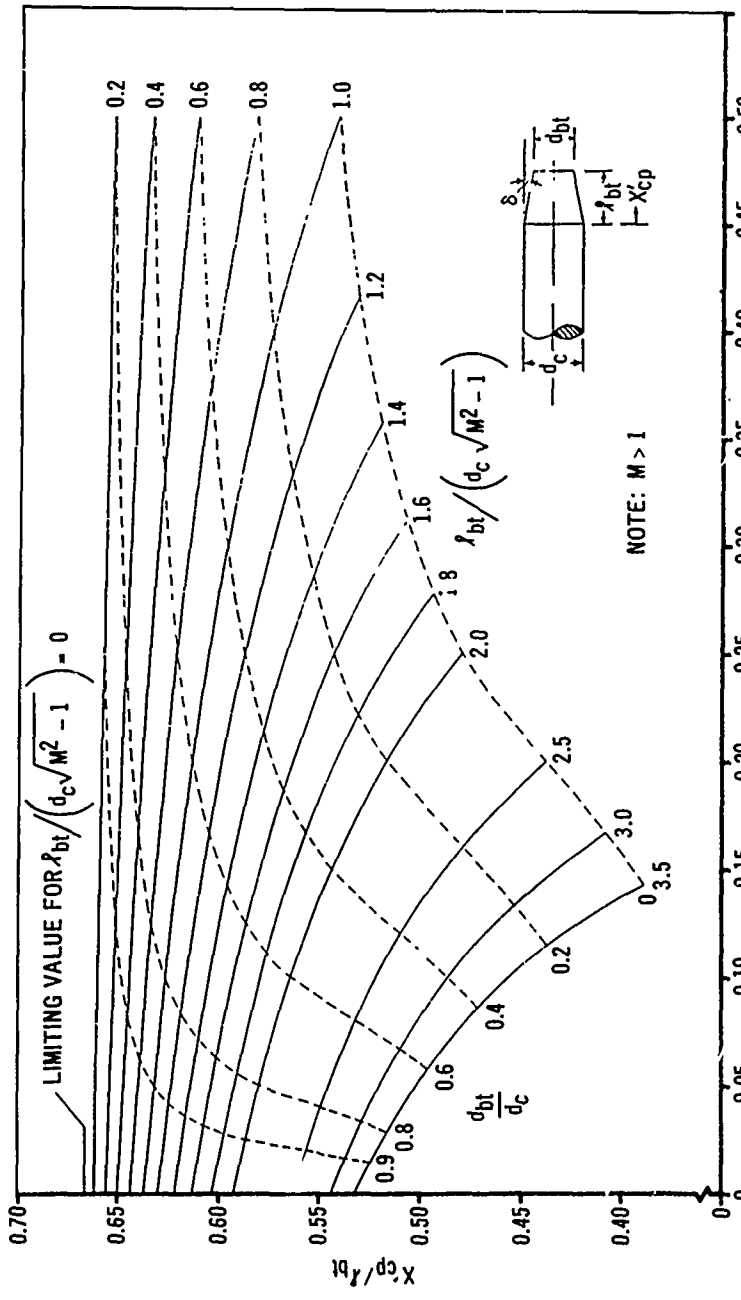

FIG. 38. CENTER OF PRESSURE FOR A BOATTAIL (REF 2)

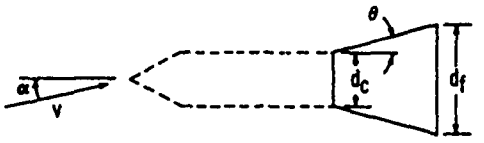

NOTE: $S_{ref} = \frac{\pi d_f^2}{4}$

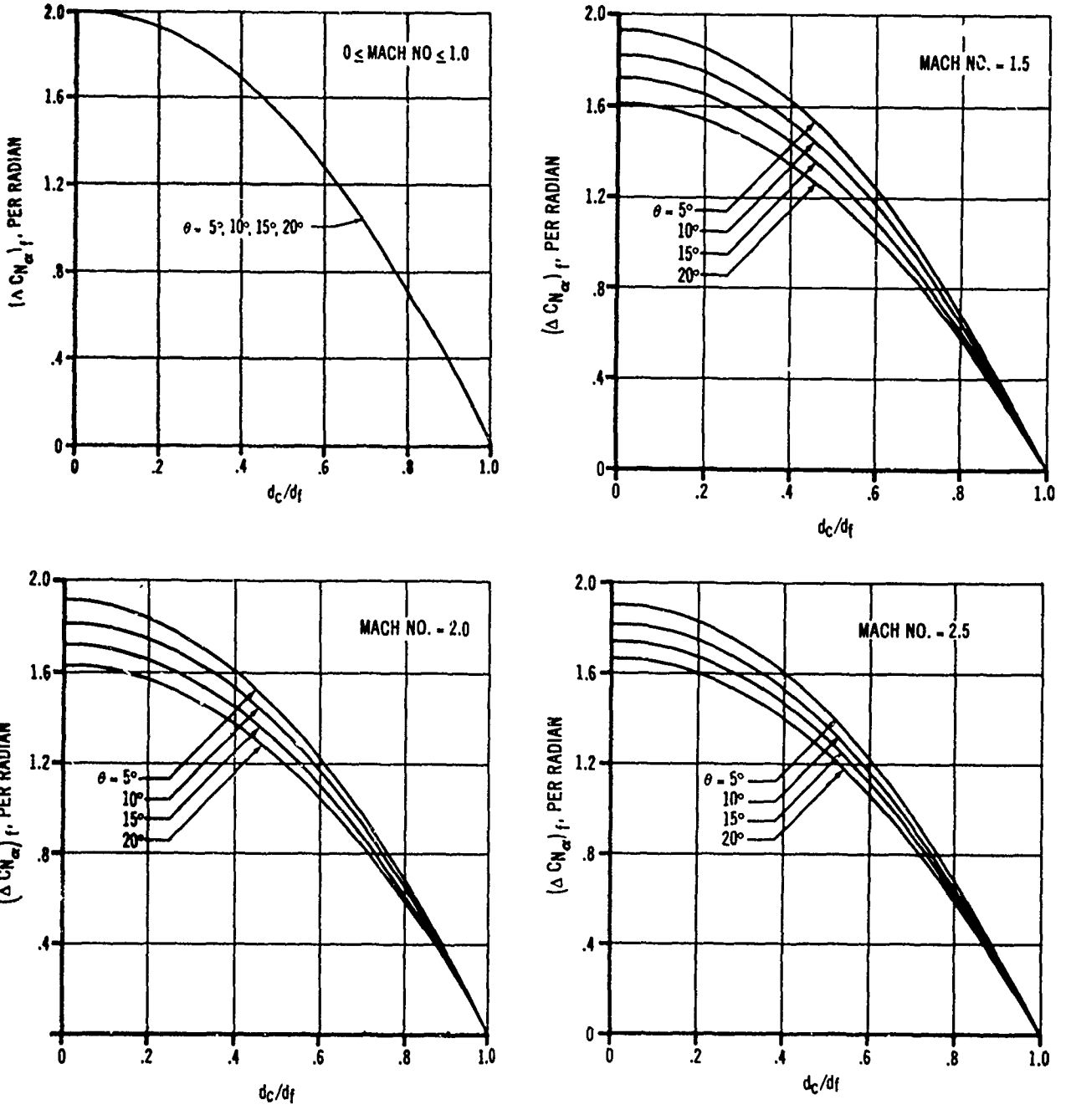

FIG. 39. INCREMENTAL NORMAL-FORCE COEFFICIENT GRADIENT FOR A FLARE. (REF 2)

The important geometric parameter is the ratio of forebody cylinder diameter to base diameter. Flare angle and Mach number do not influence the flare normal force within the limitations of slender-body assumptions. The effect of upstream flow conditions ahead of the flare are not accounted for. Since separation is likely to occur at the body-flare junction, these predictions are not apt to be realistic.

Figure 39 gives $\Delta C_{N_{\alpha f}}$ over a Mach number range of 0 to 2.5 (Ref. AMC Handbook) and should be used in preference to Equation (8).

ESTIMATING NORMAL FORCE AND CENTER OF PRESSURE OF FINS

The basic fin configuration is four fin panels attached to the body in the horizontal and vertical planes. In estimating the normal force contribution of the four panels, only the two panels in the horizontal plane are considered. All of the methods outlined here for estimating $C_{N_{\alpha fe}}$ and x_{cp} are for isolated panels not attached to a body. Body-fin and fin-body influence factors are used to correct the isolated panel normal force to a panel force attached to a body.

SUBSONIC SPEEDS

a. $C_{N_{\alpha fe}}$ AND x_{cp}, α NEAR 0 DEGREE

The normal force of the fins is first calculated as a flat plate detached from the body and positioned in the horizontal plane. The normal force coefficient slope based on lifting line theory is:

$$\frac{C_{N_{\alpha fe}}}{AR} = \frac{2\pi}{2 + \left[(AR)^2\left(\beta^2 + \tan^2\frac{\Lambda c}{2}\right) + 4\right]^{1/2}} \quad \text{(Ref. (2))} \qquad (19)$$

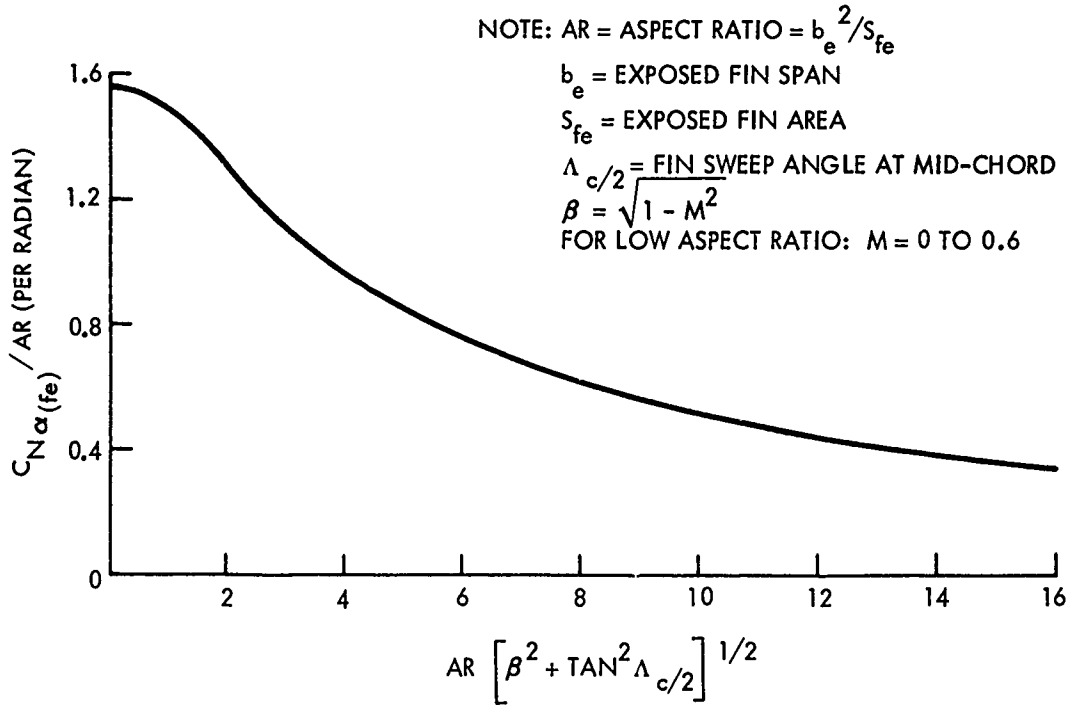

FIG. 40 SUBSONIC FIN NORMAL FORCE COEFFICIENT GRADIENT (REF 2)

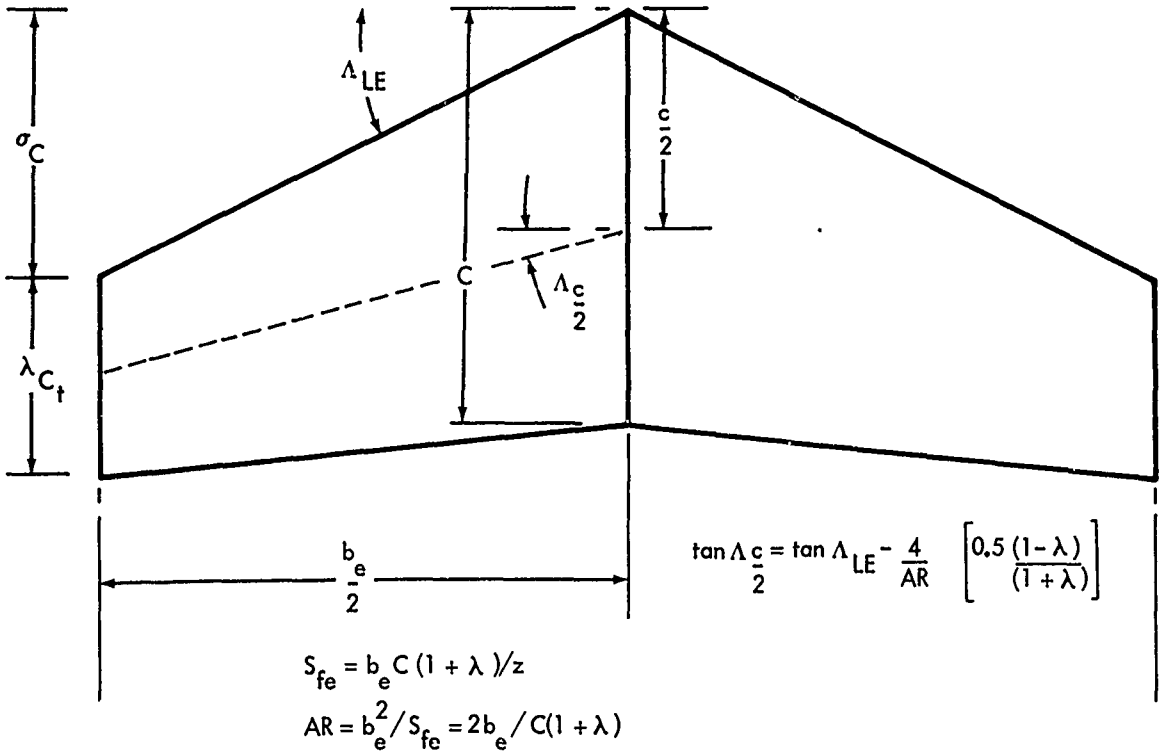

FIG. 41 FIN PANEL GEOMETRY FOR USE WITH FIG. 40 (REF 2)

Figure 40 is a plot of C_{N_α}/AR and is good up to M = 0.6. The center of pressure of the fin is assumed to be 25 percent of the mean aerodynamic chord aft of the leading edge.

Figure 41 illustrates the fin panel and shows how to use Figure 40. It should be noted that there is no significant effect of fin roll orientation on the normal force or x_{cp} of fins as long as there are an even number of fin panels,

b. FIN-BODY INTERFERENCE (SUBSONIC)

When fins are attached to a body of revolution the interference between the fin and body causes an increase in the effectiveness of the fins and brings about a lift over the body portion enclosed between the fins. Figure 42 (Ref. (11)) is a plot of the multiplying factors $K_{f(b)}$, effect of fin on body, and $K_{b(f)}$, effect of body on fin. In the figure the span (b) referred to in the ratio d/b is now the full-fin span as projected through the body. Using $C_{N_{\alpha(we)}}$ from Figure 40 for the fins alone, we have:

$$C_{N_{\alpha fw}} \quad C_{N_{\alpha(fe)}} \quad \frac{S_{fe}}{S_{fw}} \left[K_{f(b)} + K_{b(f)}\right] \quad \text{(Ref. (11))} \qquad (20)$$

where: $S_{fw} = S_{(fe)}$ + (projected fin area passing through body)

S_{fe} = exposed fin area.

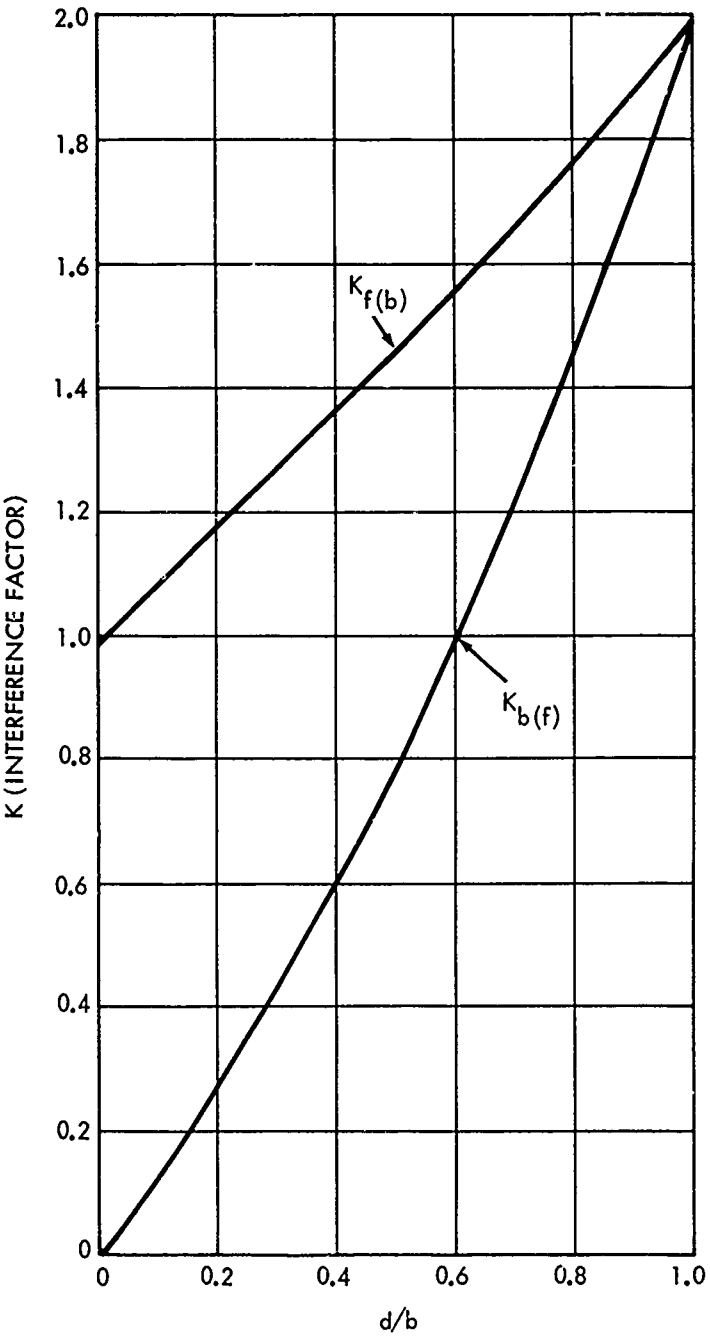

FIG. 42 FIN-BODY INTERFERENCE FACTORS ~ SUBSONIC (REF 2)

To use $C_{N_{\alpha fw}}$ with the body normal force components the coefficient must be referenced to the body area

$$C_{N_{\alpha fB}} = C_{N_{\alpha fw}} \left(\frac{S_{fw}}{S_B}\right) \tag{21}$$

c. FIN-FIN INTERFERENCE

The fin normal force calculations have been for a four-fin configuration where two fins have been assumed to act in the horizontal plane. For six- and eight-fin configurations, multiply the four-fin values by 1.37 and 1.62, respectively (Ref. (2)).

TRANSONIC SPEEDS - $C_{N_{\alpha fe}}$ AND x_{cp} α NEAR 0 DEGREE

For rectangular fins of very low aspect ratio linearized slender-wing theory predicts that $C_{N_\alpha} = (\pi/2)AR$. Utilizing transonic-similarity laws, McDevitt (Ref. AMC Handbook) obtained from experimental data the correlation shown on Figures 43 and 44. Note that here the wing thickness ratio t/c is an important factor.

For M = 0.6 to 1.4 to calculate $C_{N_{\alpha fe}}$ for either rectangular or swept fins, use the method from the U.S. Air Force Stability and Control Handbook (Ref. (1)). This method calls for plotting a curve of $C_{N_{\alpha fe}}$ from M = 0.6 to 1.4. For thin wings or low-aspect ratio wings, the curve shows an increase in slope from M = 0.6 to a high value near the critical Mach number (M_{FB}) and then through M_a and M_b to the value at M = 1.4. The charts of Figures 45a to e are used as follows:

(1) Find $C_{N_{\alpha(fe)}}$ for M = 0.6 from Figure 40

(2) Calculate M_{FB} from Figure 45a for zero wing sweep

(3) For wing with sweep obtain a corrected $M_{(FB)\Lambda}$ from Figure 45b.

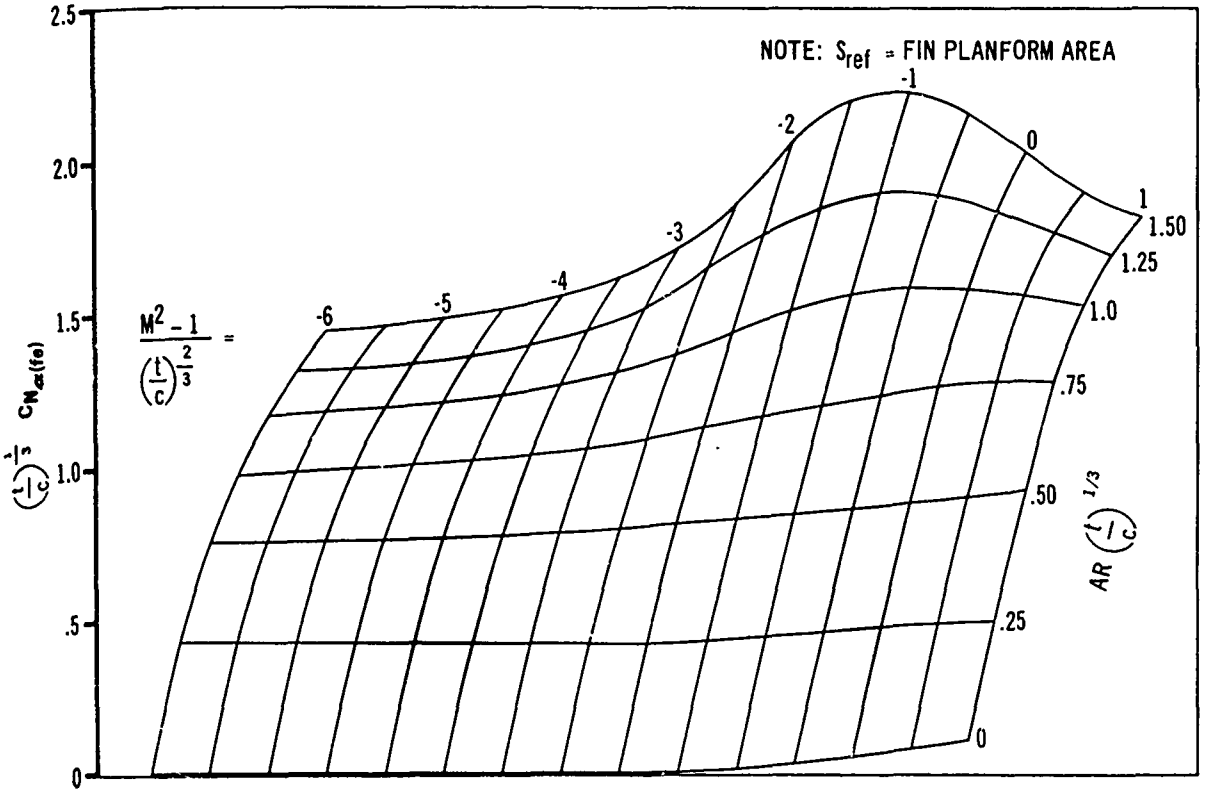

FIG. 43. NORMAL-FORCE COEFFICIENT GRADIENT FOR RECTANGULAR FINS, TRANSONIC SPEEDS (REF 2)

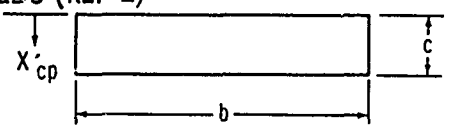

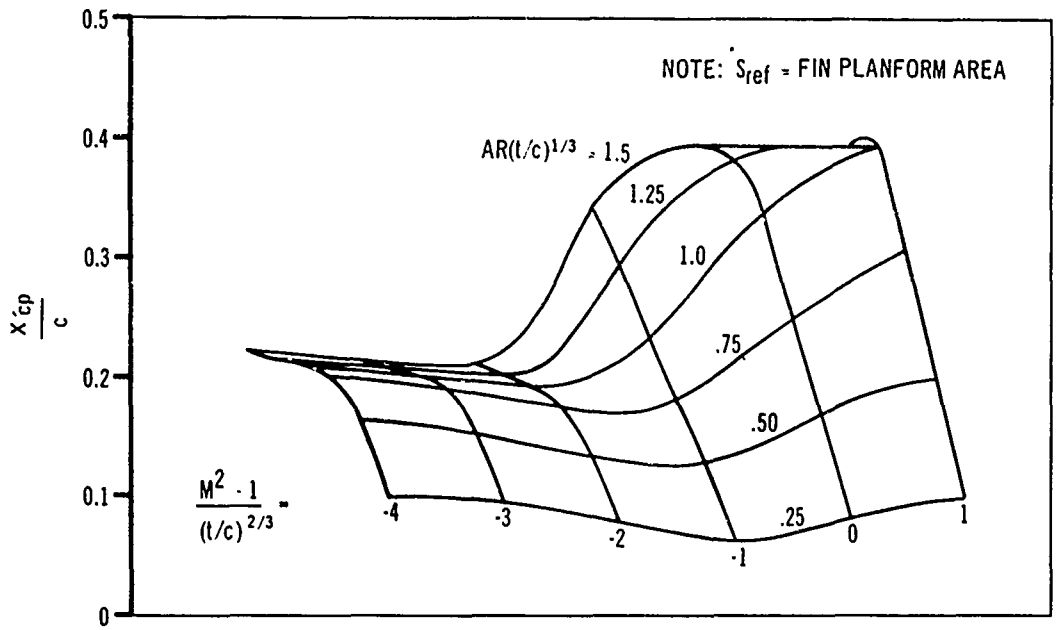

FIG. 44. CENTER OF PRESSURE FOR RECTANGULAR FINS, TRANSONIC SPEEDS (REF 2)

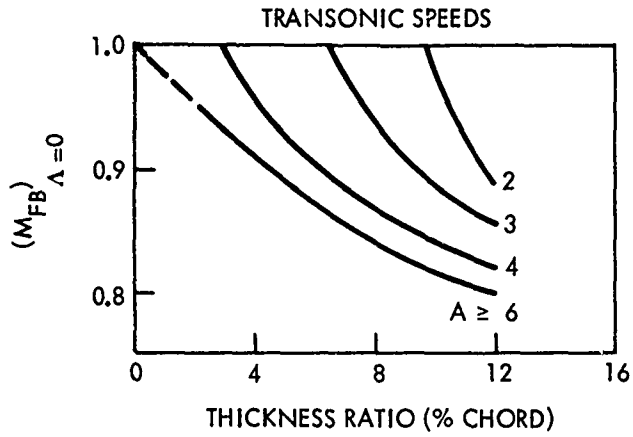

FIG. 45 a TRANSONIC FORCE-BREAK MACH NUMBER FOR ZERO SWEEP (REF 1)

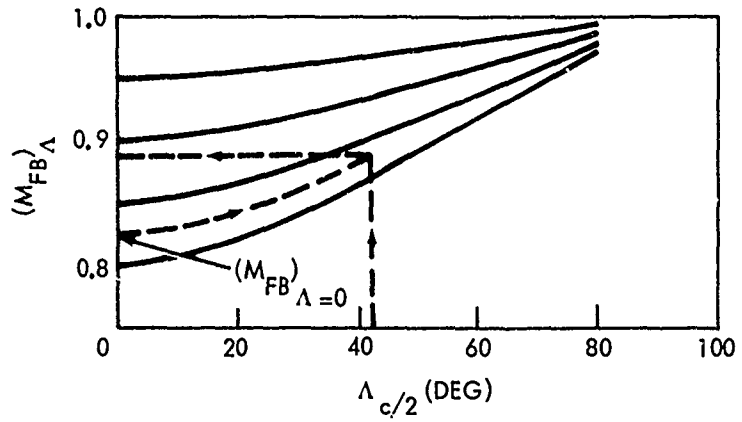

FIG. 45 b TRANSONIC SWEEP CORRECTION FOR FORCE-BREAK MACH NUMBER (REF 1)

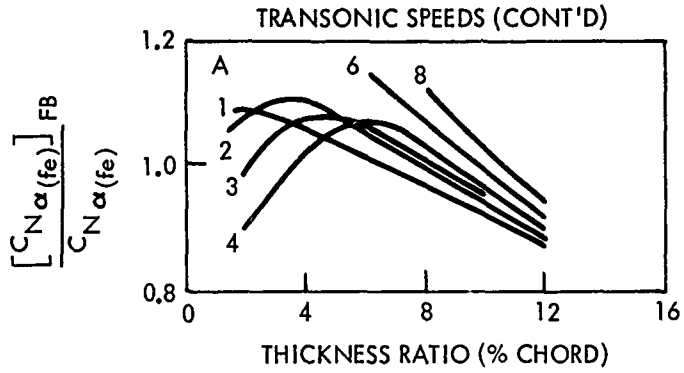

FIG. 45c CORRECTION TO LIFT-CURVE SLOPE AT FORCE-BREAK MACH NUMBER (REF 1)

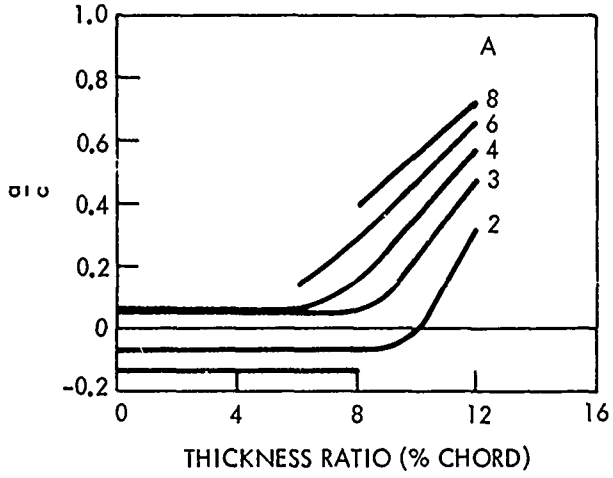

FIG. 45d CHART FOR DETERMINING LIFT-CURVE SLOPE AT M_a (REF 1)

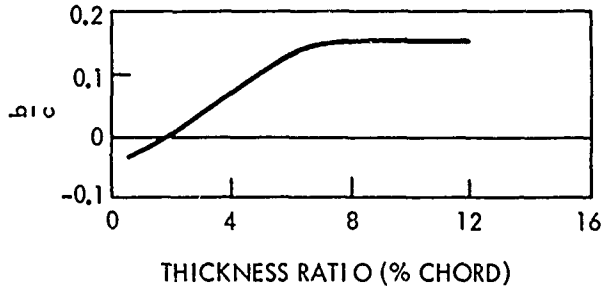

FIG. 45e CHART FOR DETERMINING LIFT-CURVE SLOPE AT M_b (REF 1)

(4) Find $C_{N_{\alpha(fe)}}$ using Figure 40 for M_{FB}

(5) Find actual $[C_{N_{\alpha(fe)}}]_{FB}/C_{N_{\alpha(fe)}}$ from Figure 45c using (t/c) ratio

(6) The value of $M_a = M_{FB} + 0.07$ (22)

(7) $[C_{N_{\alpha(fe)}}]_{\alpha} = (1 - a/c)[C_{N_{\alpha(fe)}}]_{FB}$ where a/c is found on Figure 45d (23)

(8) The value of $M_b = M_{FB} + 0.14$ (24)

(9) $[C_{N_{\alpha(fe)}}]_b (1 - b/c)[C_{N_{\alpha(fe)}}]_{FB}$ where b/c is found on Figure 45e (25)

(10) Find $C_{N_{\alpha(fe)}}$ for M = 1.4 use the methods in the section on $C_{N_{\alpha}}$ of Rectangular Fins at Supersonic Speeds

SUPERSONIC SPEEDS

a. $C_{N_{\alpha fe}}$ AND x_{cp} RECTANGULAR FINS, α NEAR 0 DEGREE

On rectangular fins at supersonic speeds there is a loss of lift on the tips which according to Evvard's theory (Ref. (12)) is half of the two-dimensional value. For a finite fin panel

$$C_{N_{\alpha(fe)}} = \frac{4}{\beta}\left(1 - \frac{1}{2\beta AR}\right) \text{ when } AR > \frac{1}{\beta} \tag{26}$$

When the span is short enough that the Mach cones from the tips intersect, then the expression for normal force slope becomes,

$$C_{N_{\alpha(fe)}} = \frac{2}{\beta}\left[\frac{2A_1 + A_2 + A_3}{A_T}\right] \text{ when } AR < \frac{1}{\beta} \tag{27}$$

(See Fig. 46 note A_4 drops out in the solution)

where: $\beta AR \geq 0.5$ use the chart on Figure 47

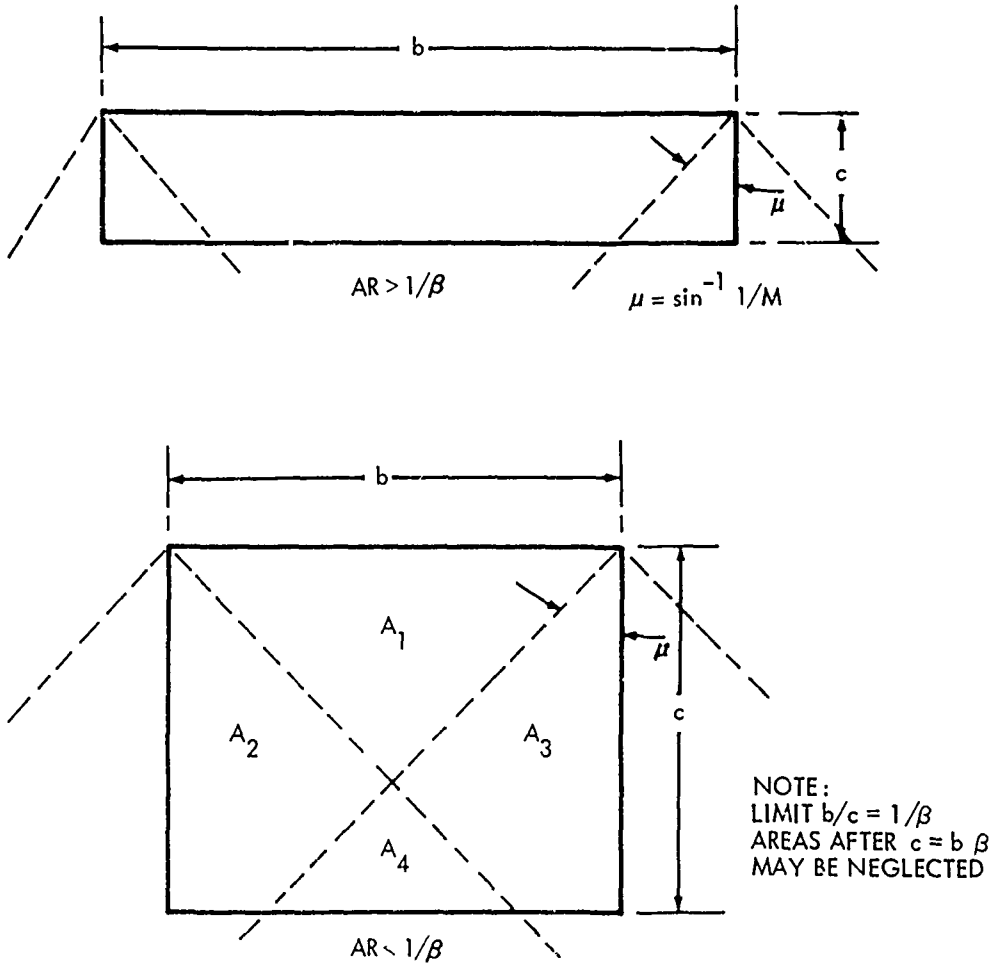

FIG. 46 RECTANGULAR WING PLANFORMS (REF 12)

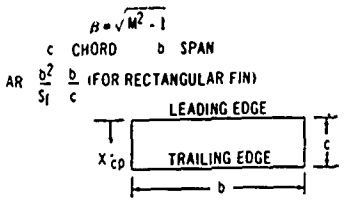

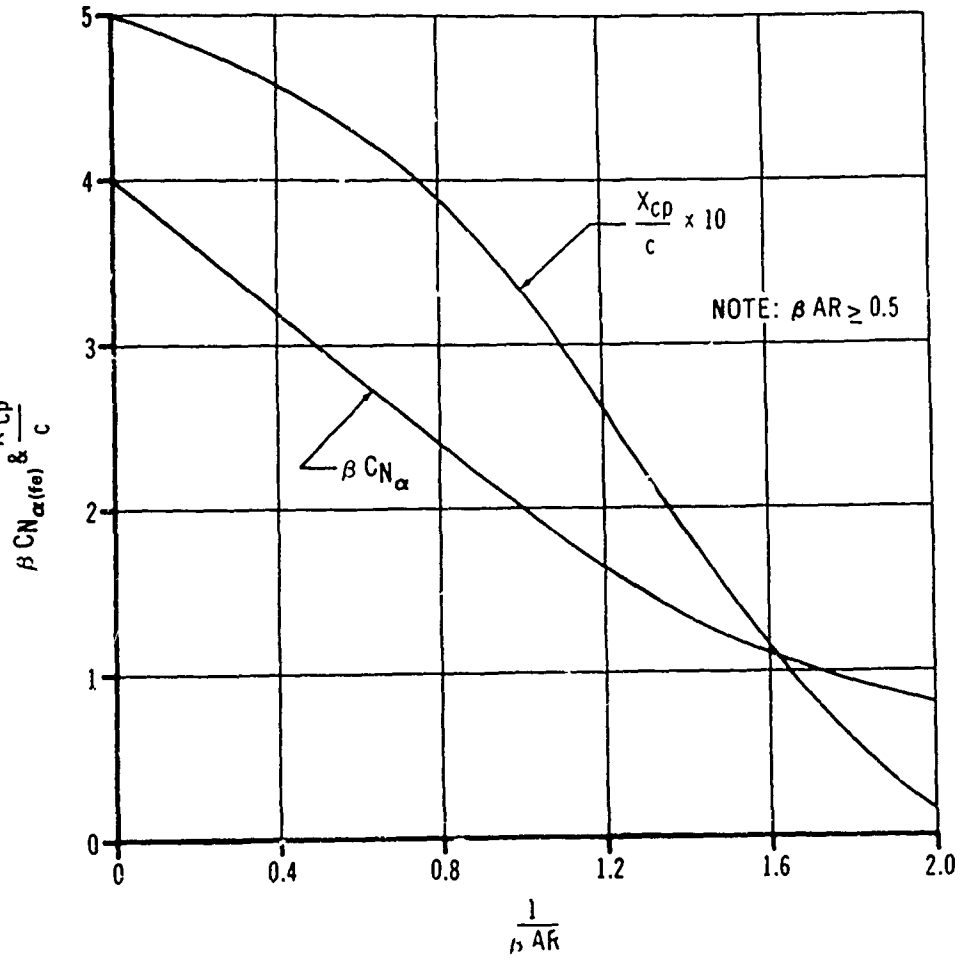

FIG. 47. NORMAL FORCE COEFFICIENT GRADIENT AND CENTER OF PRESSURE FOR RECTANGULAR FINS. (REF 2)

The above expressions are based on linear theory and are good up to $\alpha = +10°$.

b. $C_{N_{\alpha fe}}$ AND x_{cp} SWEPT FINS, α NEAR 0 DEGREE

The charts shown on Figures 48 and 49 (a, b, c) were taken from the AMCP Handbook (Ref. (2)) and are part of a more complete coverage of wing planforms made by E. Lapin. Note that λ is the tip-to-root-chord ratio.

c. FIN-THICKNESS EFFECTS

When Mach lines lie on or near the fin leading edge, there is a loss in normal force from the theoretical value. Figure 50 (Ref. (2)) gives a correction factor for this loss. To use the figure:

(1) find $\Delta y_{\perp}$ equal to the difference between upper surface ordinates at the 6 and 15 percent chord stations (in percent of chord).

(2) $\Delta y_{\perp} = \Delta y / \cos \Lambda_{\ell e}$

(3) for a double-wedge leading edge $\Delta y_{\perp} = 5.85 \tan \delta_{\perp}$ where $\delta_{\perp}$ is the wedge semi-angle

d. FIN-BODY INTERFERENCE

Mach number and the fin plane geometry are important to supersonic fin-body interference when considering the effect of the fin normal force carryover to the body, $K_{b(f)}$. Figure 51 (Ref. (2)) gives $K_{b(f)}$ for the case where the cylindrical body extends past the fin trailing edge and for the case where the body is flush with the fin trailing edge.

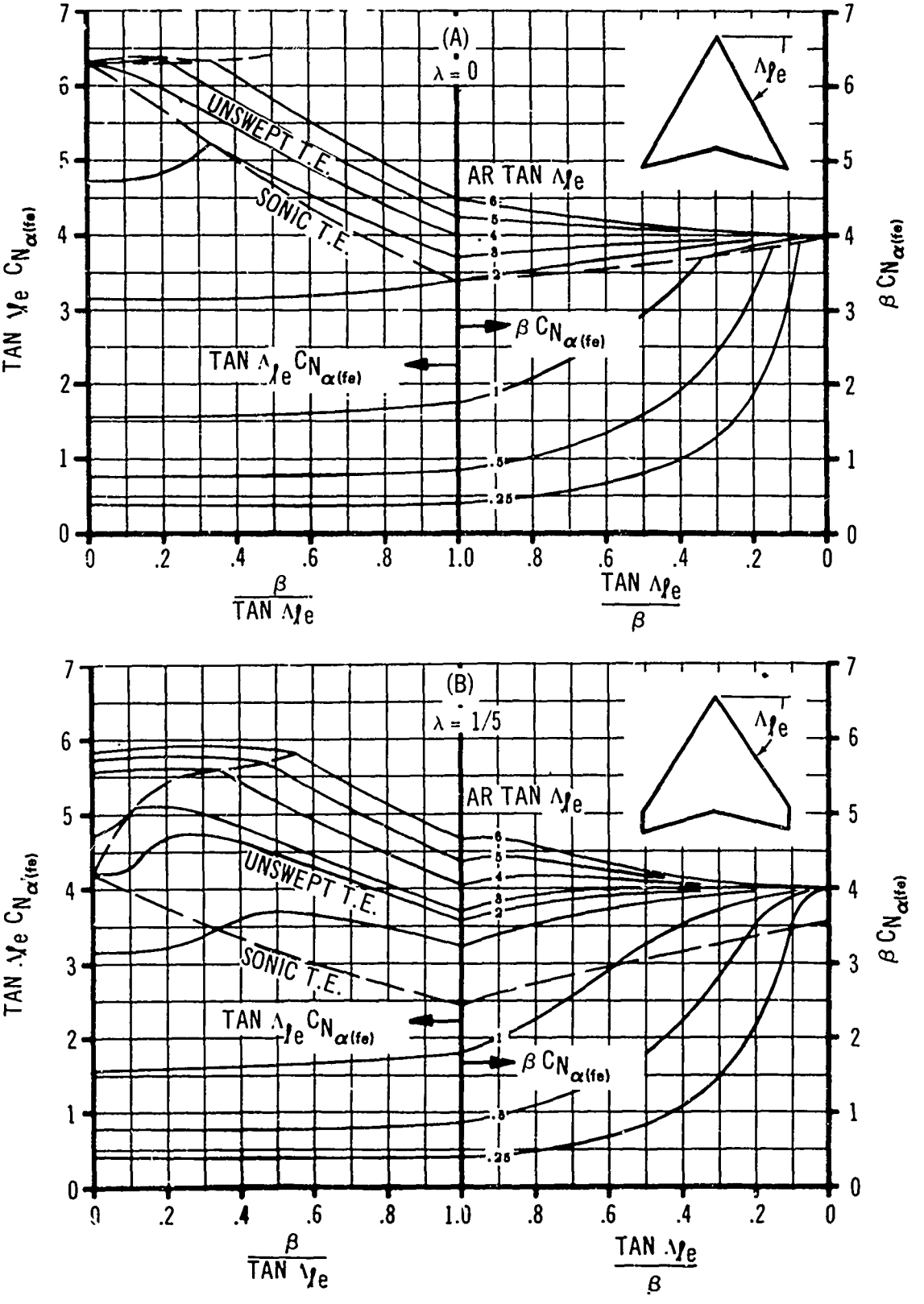

FIG. 48 a FIN NORMAL FORCE COEFFICIENT GRADIENT AT SUPERSONIC MACH NUMBERS (REF 2)

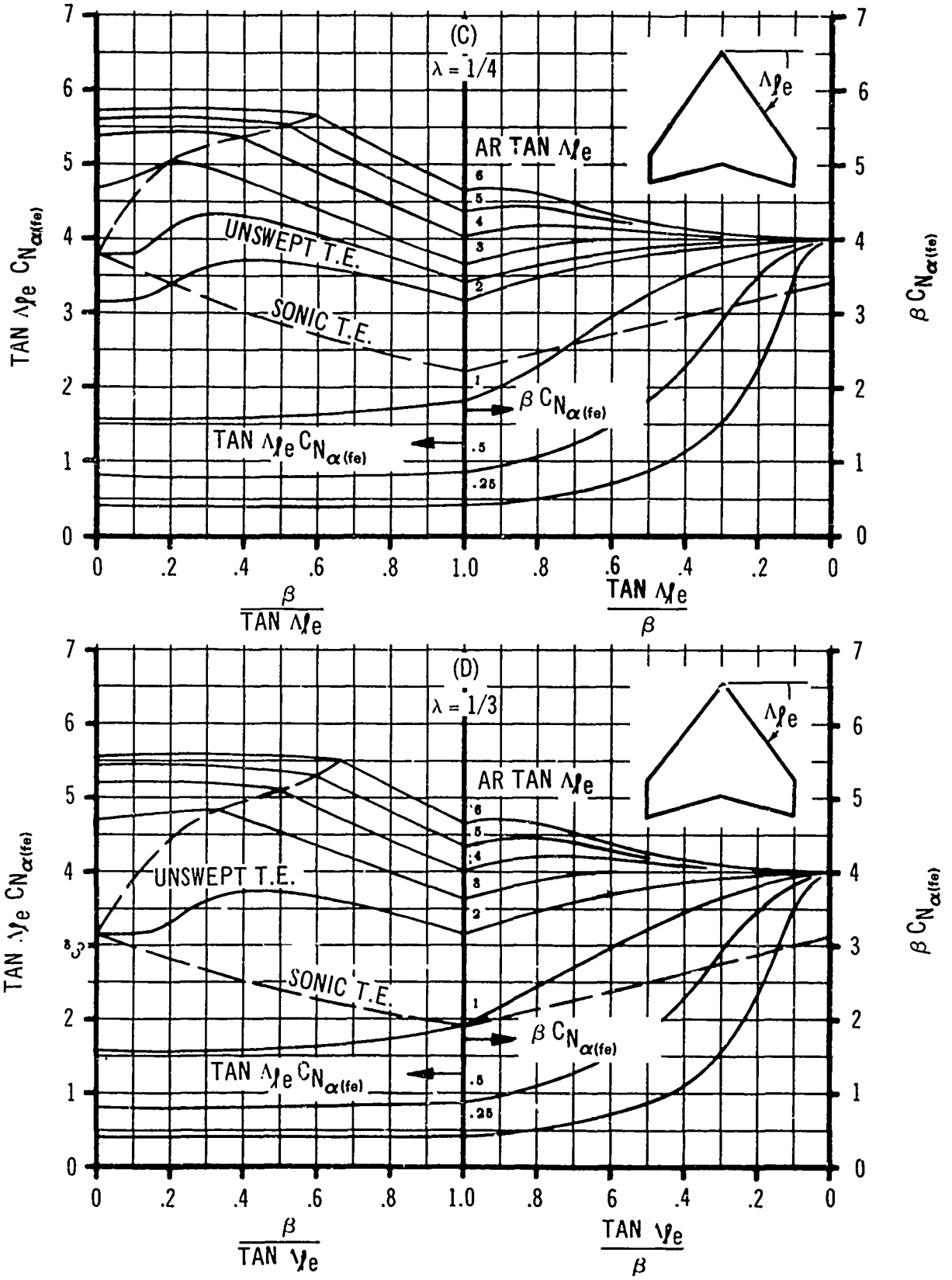

FIG. 48 b. FIN NORMAL FORCE COEFFICIENT GRADIENT AT SUPERSONIC MACH NUMBERS. (REF 2)

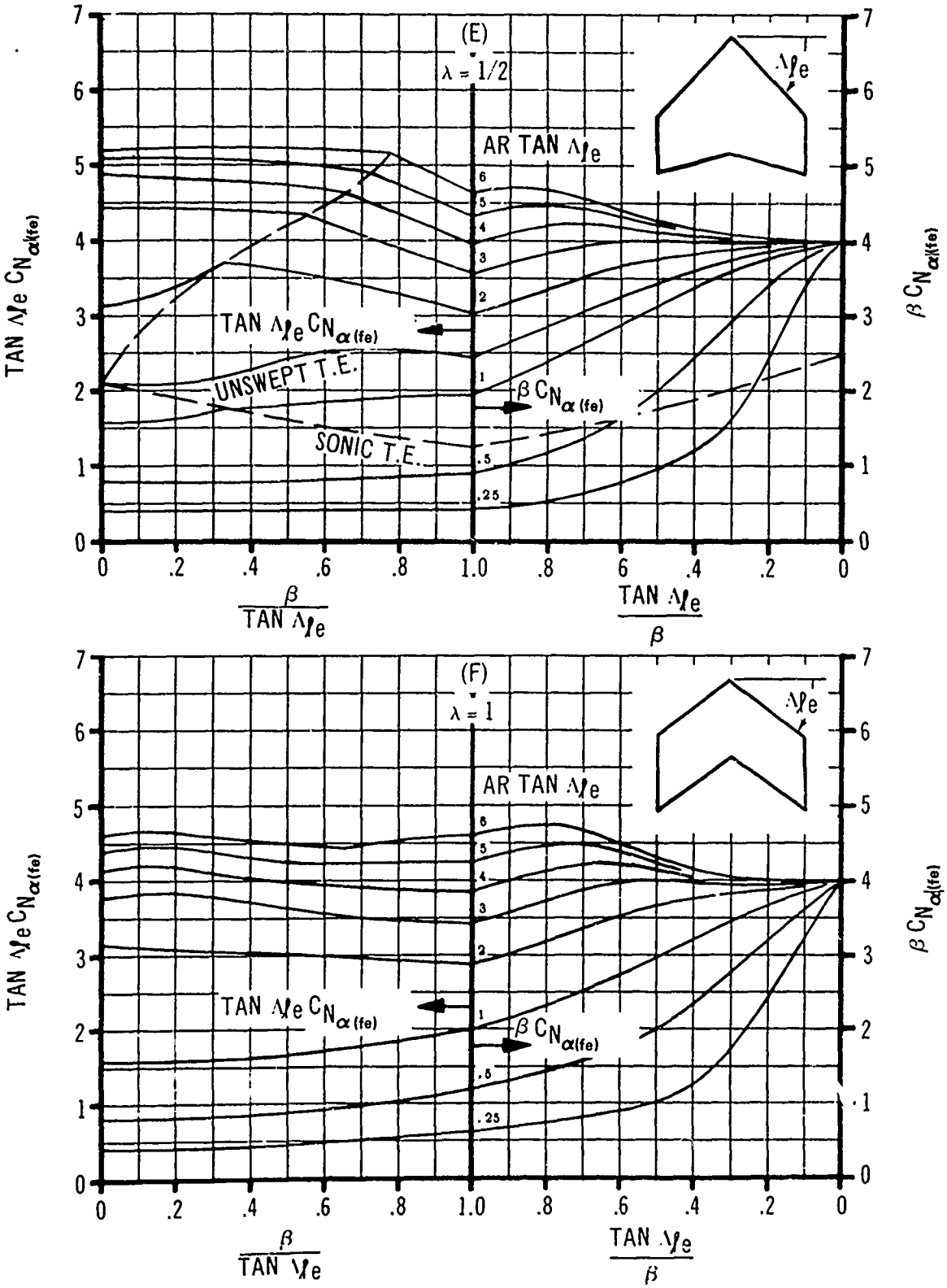

FIG. 48cc . FIN NORMAL FORCE COEFFICIENT GRADIENT AT SUPERSONIC MACH NUMBERS (REF 2)

(A)

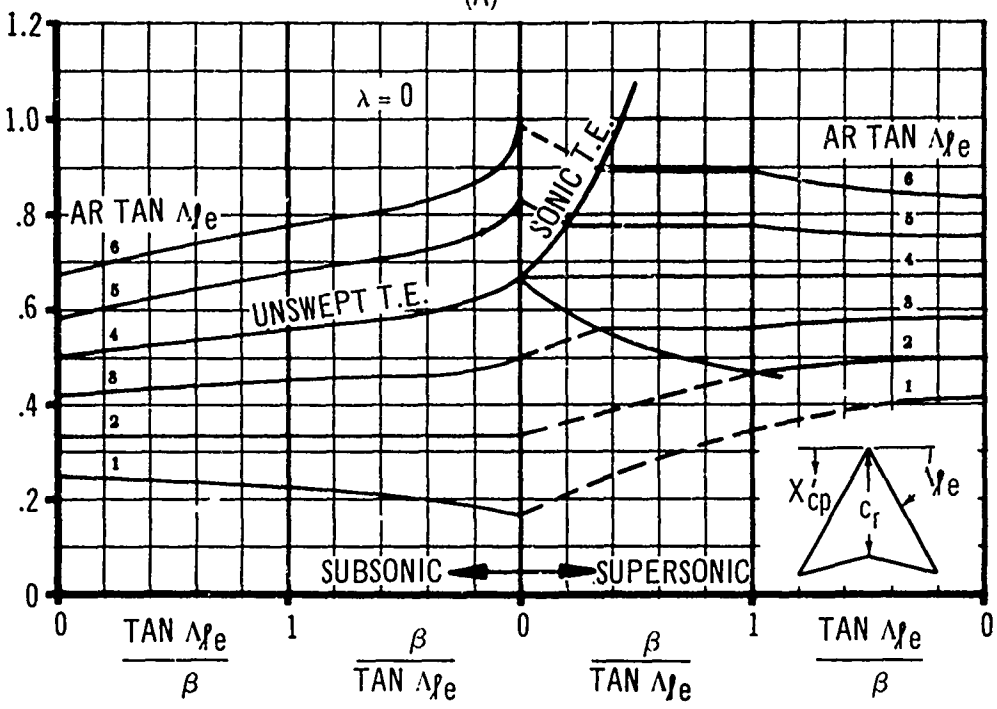

X'_{cp}/c_r

(B)

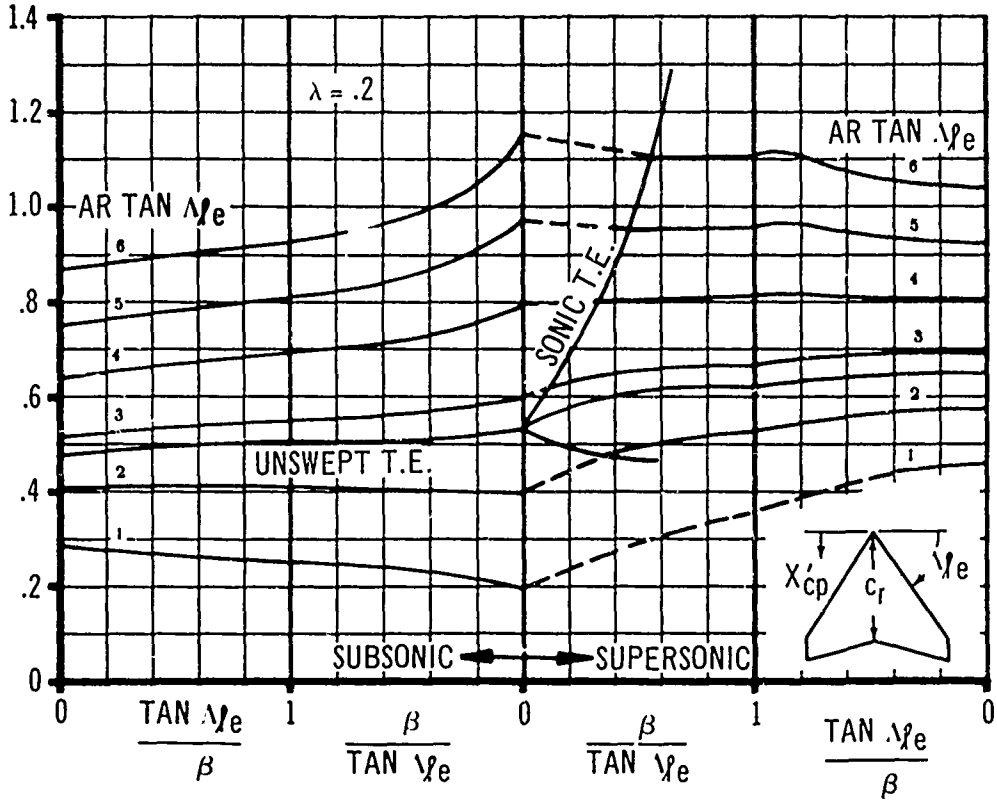

X'_{cp}/c_r

FIG. 49 a FIN CENTER OF PRESSURE (REF 2)

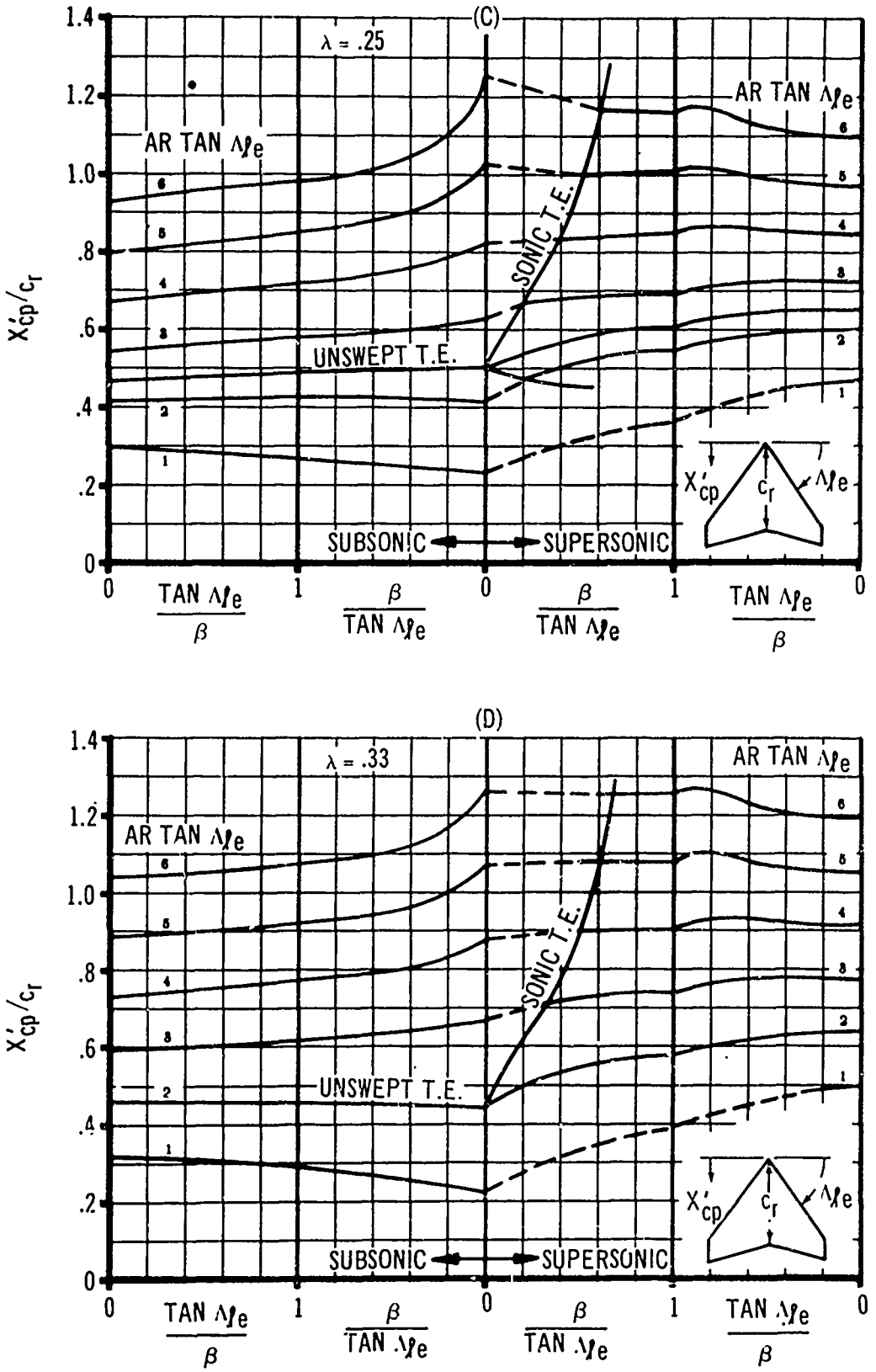

FIG. 49 b. FIN CENTER OF PRESSURE (REF 2)

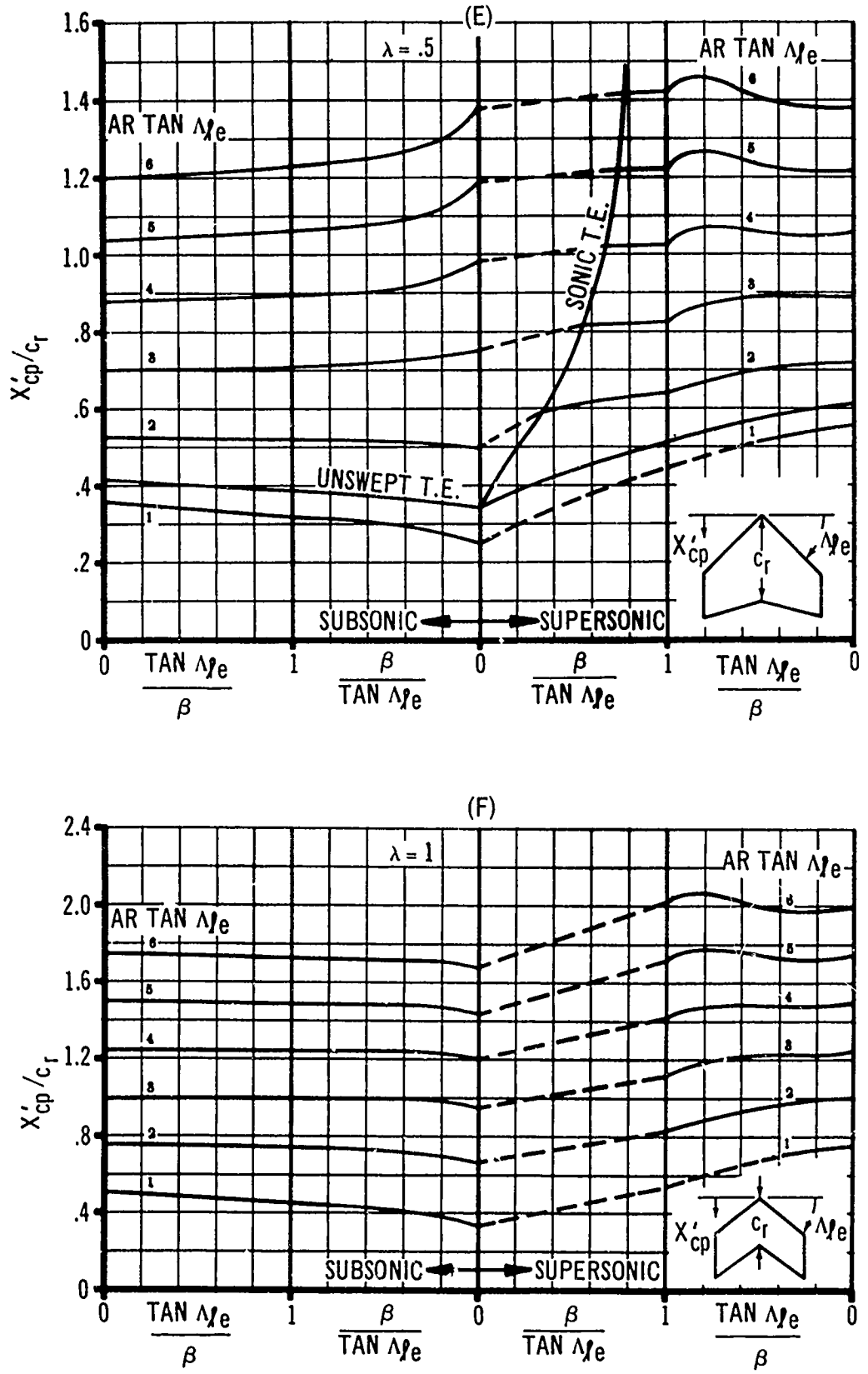

FIG. 49 c FIN CENTER OF PRESSURE (REF 2)

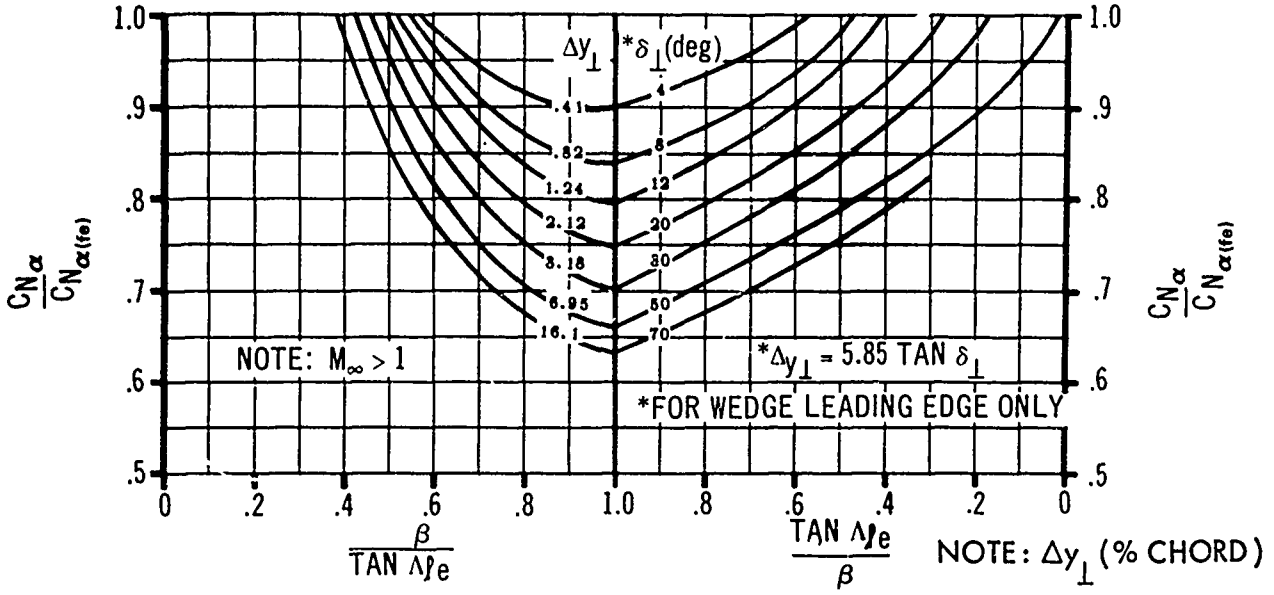

FIG. 50. FIN NORMAL FORCE COEFFICIENT GRADIENT CORRECTION FACTOR FOR SONIC LEADING EDGE REGION. (REF 2)

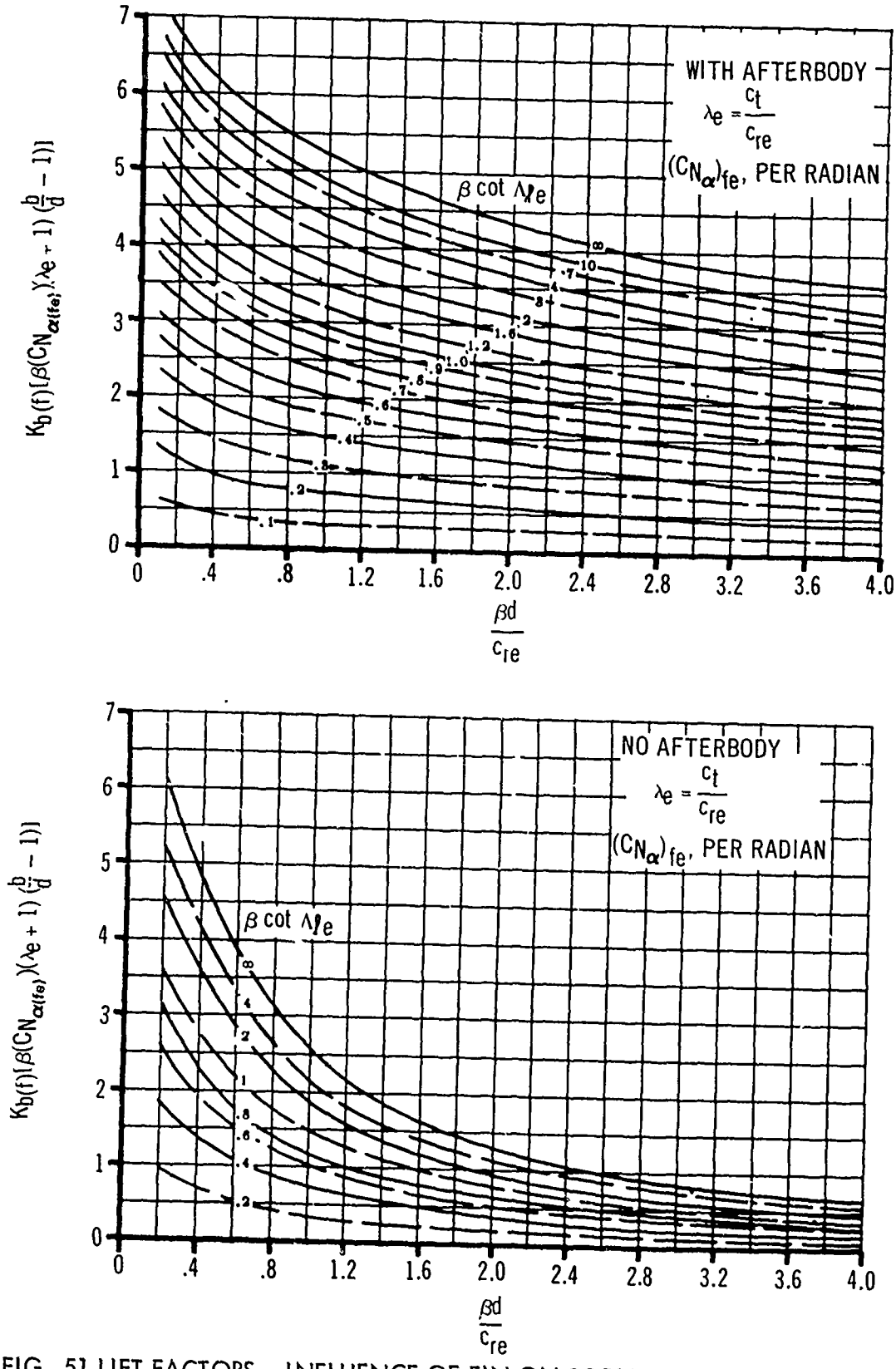

FIG. 51 LIFT FACTORS - INFLUENCE OF FIN ON BODY, SUPERSONIC SPEEDS. (REF.2)

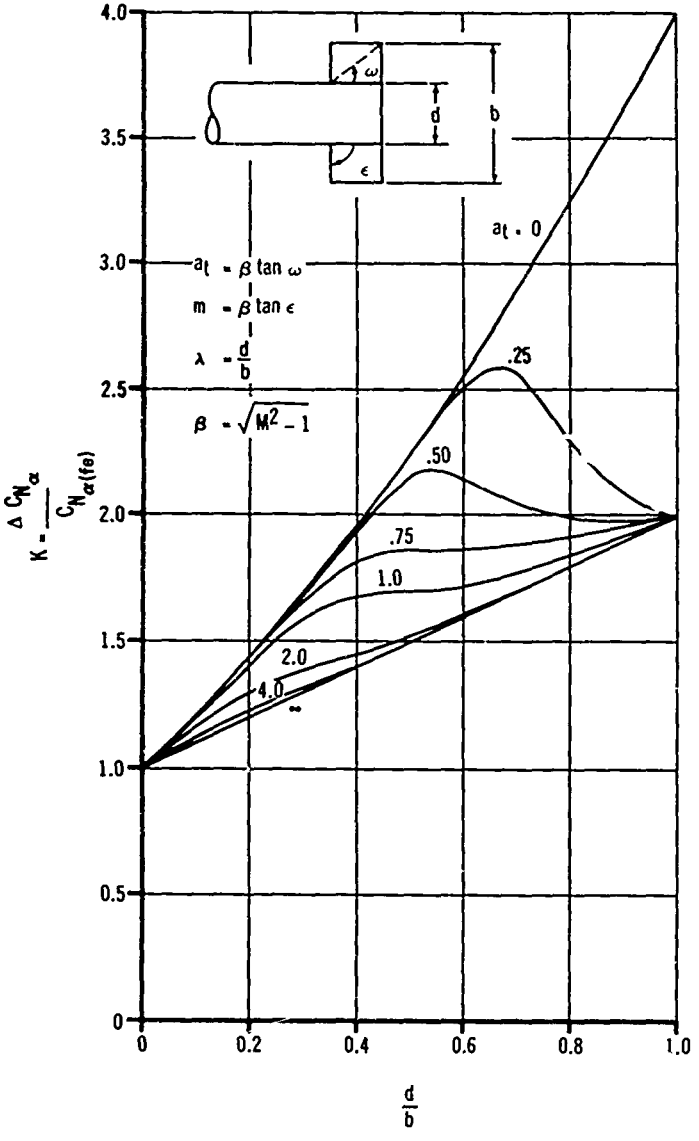

FIG. 52a LIFT OF FIN (BODY) FOR $a_t/m = 0$ (RECTANGULAR FIN) (REF 2)

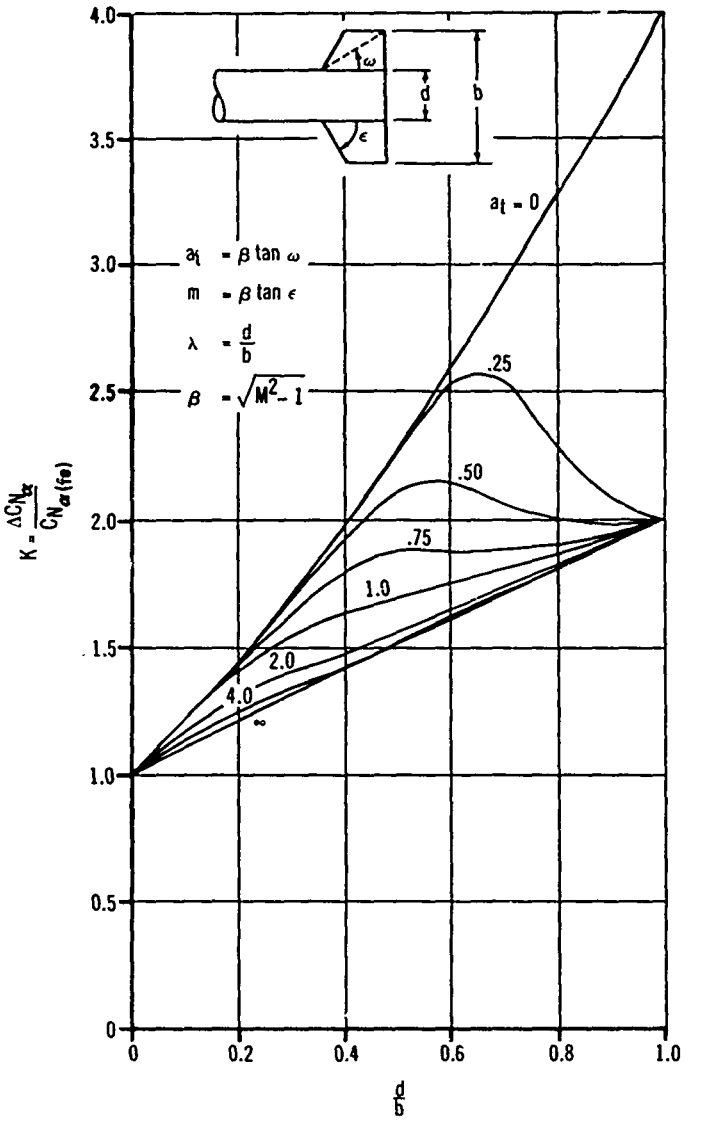

FIG. 52b LIFT OF FIN (BODY) FOR $a_t/m = 0.2$ (CLIPPED DELTA FIN) (REF 2)

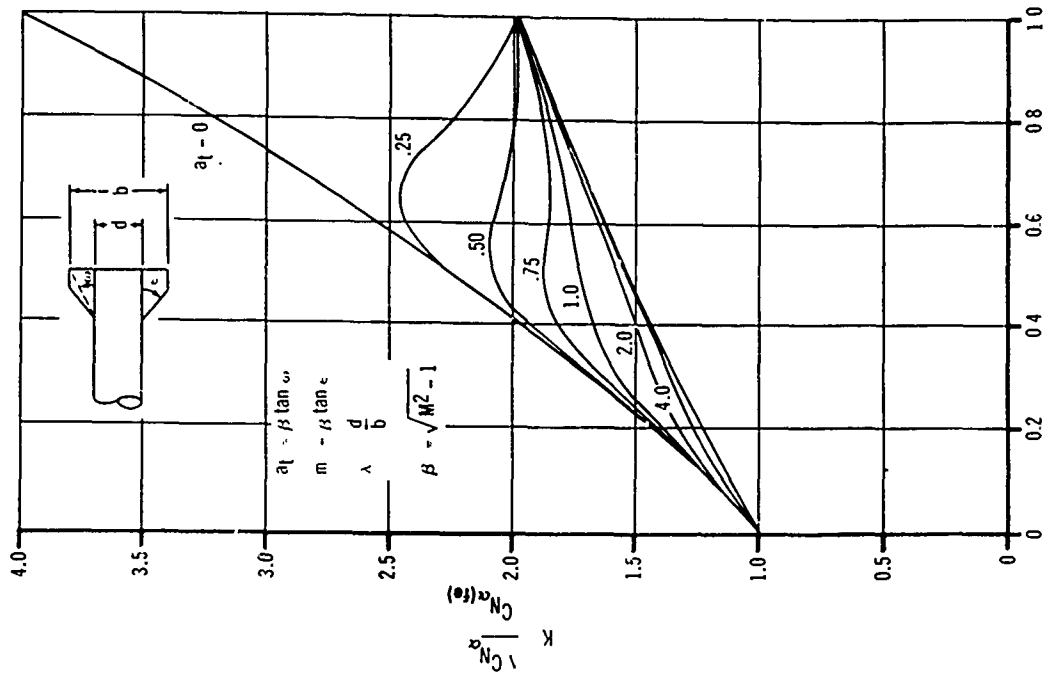

FIG. 52d LIFT OF FIN (BODY) FOR $a_t/m = 0.6$ (CLIPPED DELTA FIN) (REF 2)

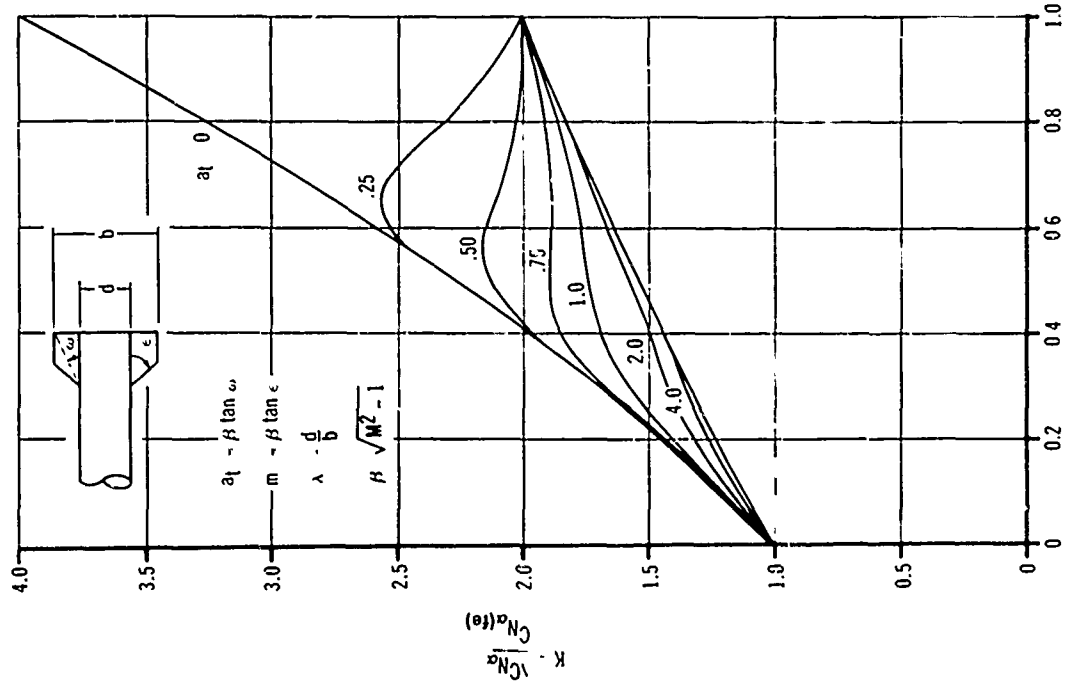

FIG. 52c LIFT OF FIN (BODY) FOR a_t/m 0.4 (CLIPPED DELTA FIN) (REF 2)

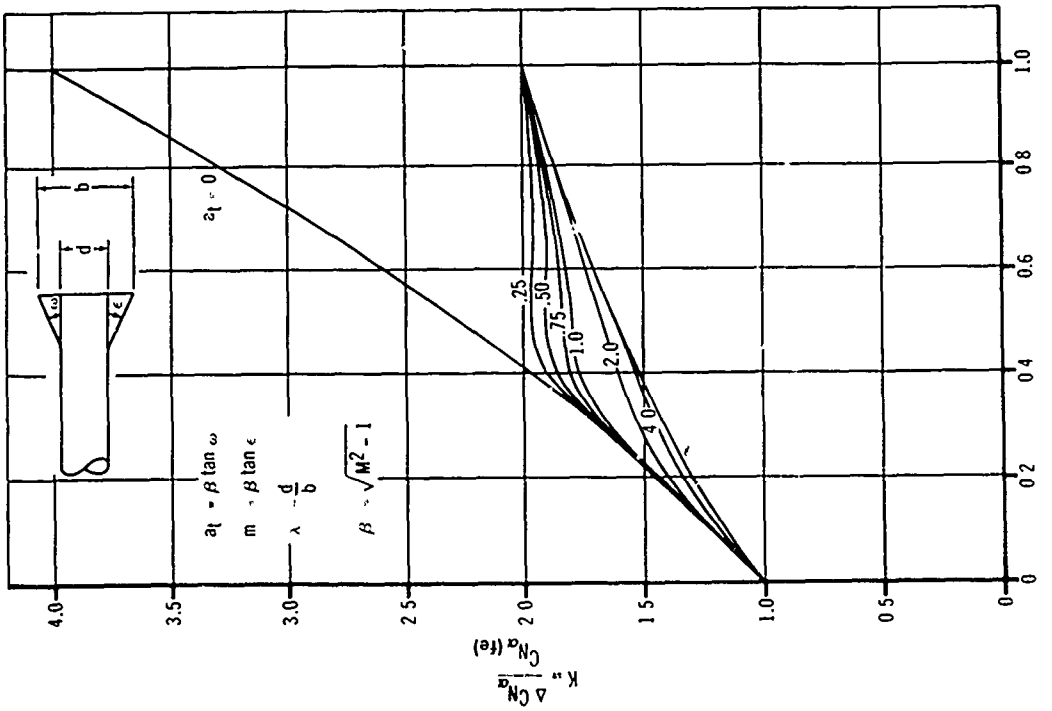

FIG. 52f LIFT OF FIN (BODY) FOR $a_t/m = 1.0$ (DELTA FIN) (REF 2)

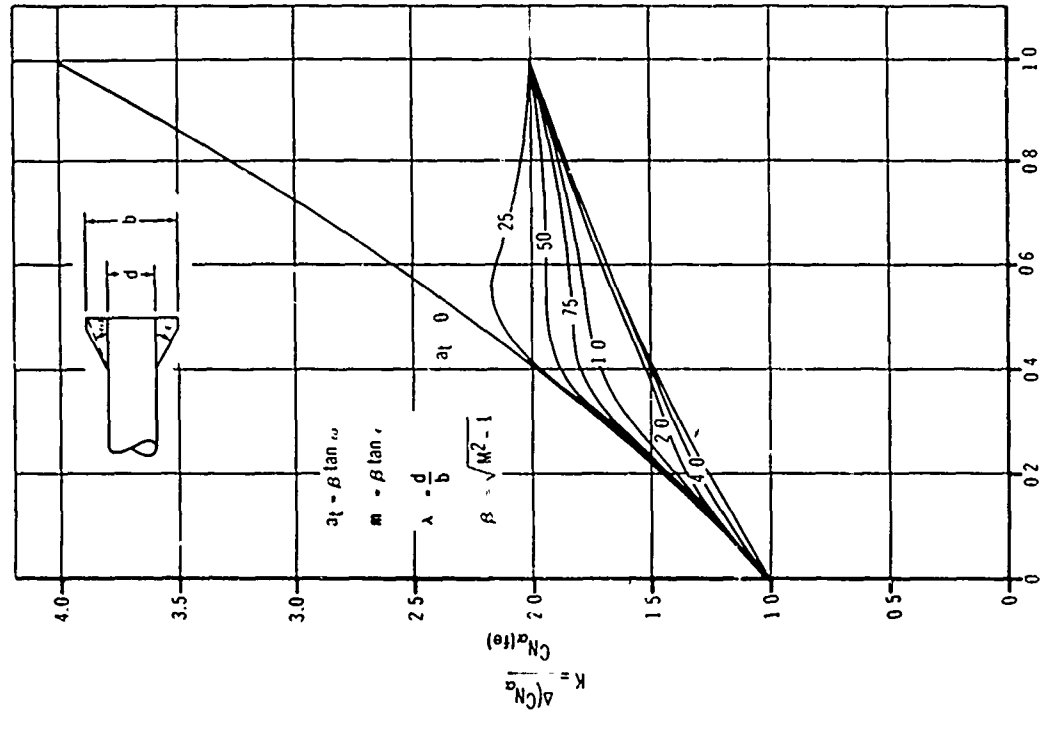

FIG. 52e LIFT OF FIN (BODY) FOR $a_t/m = 0.8$ (CLIPPED DELTA FIN) (REF 2)

The exceptions where Figure 42 is used instead of Figure 51 to find $K_{b(f)}$ are:

(1) If $\beta AR_e \leq 1$ for triangular planforms

(2) If $\beta AR_e(1 + \lambda_e)(\tan \Lambda_{LE}/\beta + 1) \leq 4$ for nontriangular planforms

$K_{f(b)}$ is found using Figure 42 as in the subsonic case.

Another method developed by Morikawa (Ref. (2)) gives a total fin-body interference factor $K = K_{f(b)} + K_{b(f)}$ for use on cylindrical bodies where the trailing edge of the fin is unswept and flush with the base. Figures 52a to f give $K = \Delta C_{N_\alpha}/C_{N_{\alpha(fe)}}$ where $C_{N_{\alpha(fe)}}$ is for the isolated fin panel and ΔC_{N_α} refers to the $C_{N_{\alpha(fe)}}$ with interference. In other words, the K from Figures 52a through f is used the same way as the quantity $(K_{f(b)} + K_{b(f)})$.

e. FIN-FIN INTERFERENCE

Supersonic fin impingement was studied by Potter, Shapiro and Murphree for clipped delta fin configurations where d/b = 1/2 only. The correlation parameter (Ref. (2)):

$$I = \frac{c_r}{\beta d_c \sin \pi/n} \tag{28}$$

where:

c_r = exposed root chord

$\beta = \sqrt{M^2 - 1}$

d = body diameter

n = number of fins

The parameter I is shown on Figure 53 as a function of $C_{N_{\alpha(fe/2)}}$ which is based on an effective area, S_{eff}, which is a function of the number of fins, n, such that:

No. of fins (n)	$S_{eff}/S_{fe/2}$
4	1.63
6	2.43
8	3.24

$S_{fe/2}$ is the exposed area of a single fin: as one of four fins or one of six fins not as in previous calculations where it was two of four fins.

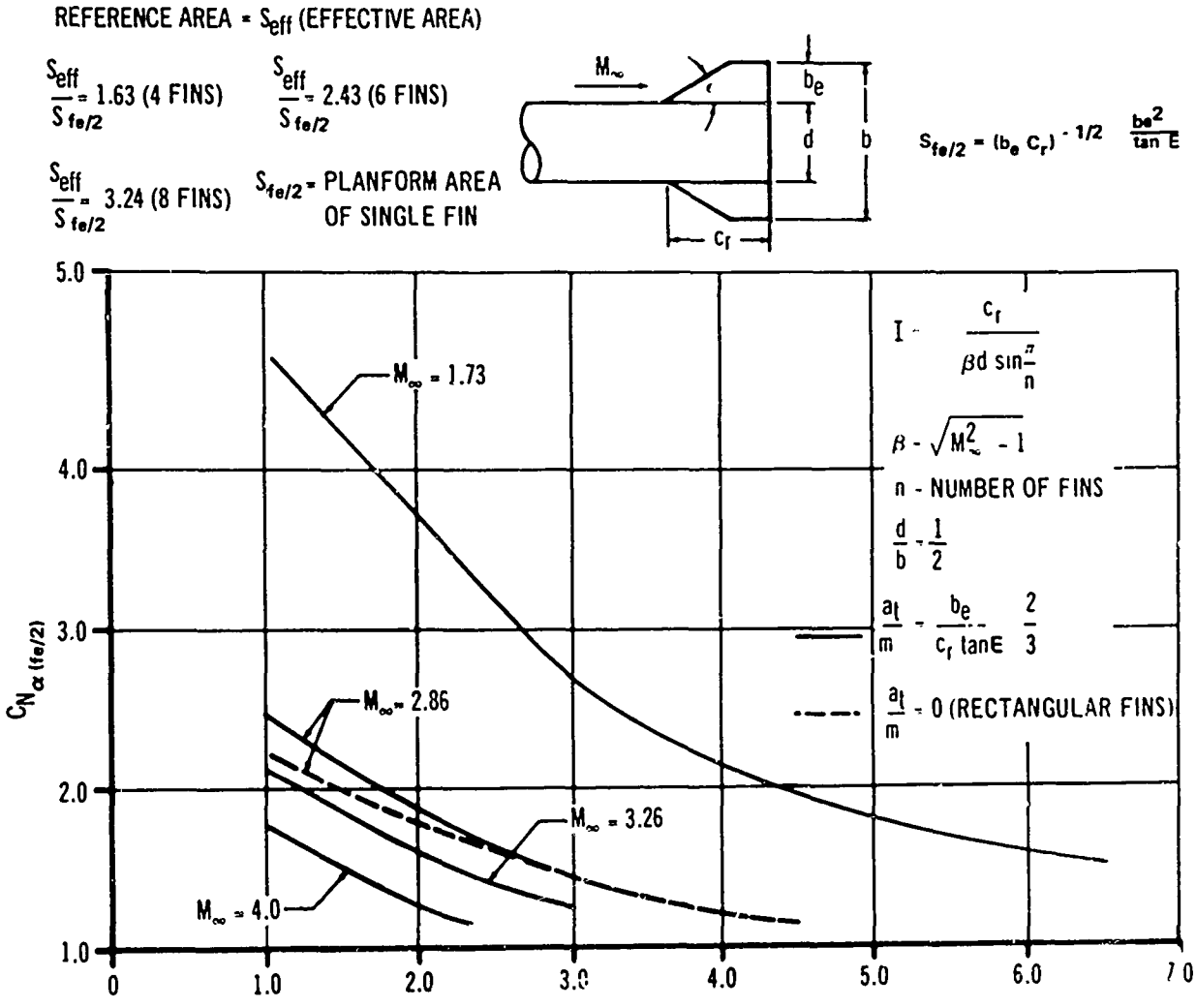

FIG. 53 NORMAL FORCE COEFFICIENT GRADIENT OF MULTIPLE FINS AT SUPERSONIC SPEEDS (REF 2)

To use Figure 53 the steps are:

(1) compute I

(2) find $C_{N_{\alpha fe/2}}$ from Figure 53

(3) multiply $C_{N_{\alpha fin}}$ by appropriate $S_{eff}/S_{fe/2}$

The result gives C_{N_α} for the total number of fins based on the area of one exposed fin panel. Also it is important to note that $C_{N_{\alpha(fe)}}/2$ from Figure 53 does not have to be corrected for fin-body and body-fin interference. To get $C_{N_{\alpha fb}}$, the total fin lift based on body reference area:

$$C_{N_{\alpha(fb)}} = \left(\frac{C_{N_{\alpha(fe)}}}{2}\right)\left(\frac{S_{eff}}{S_{fe/2}}\right)\frac{\left(S_{fe/2}\right)}{S_{ref}} \qquad (29)$$

where: $I < 1$ compute $C_{N_{\alpha(fe)}}$ the regular way for four fins and correct by:

$$\frac{C_{N_{\alpha 6Fins}}}{C_{N_{\alpha 4Fins}}} = 1.50, \quad \frac{C_{N_{\alpha 8Fins}}}{C_{N_{\alpha 4Fins}}} = 2.00 \text{ (Ref. (2))}$$

These fin-fin interference corrections have been derived only for the fins shown on Figure 53 but may be used when making predictions for other fin shapes.

EFFECT OF BOATTAIL ON FINS AT SUBSONIC SPEEDS, α NEAR 0 DEGREE

For subcaliber fins (i.e., where the fin span is less than or equal to the diameter of the boattail body juncture) the fin effectiveness is reduced by a factor which depends on nose bluntness. The fin normal force is calculated as attached to the boattail so

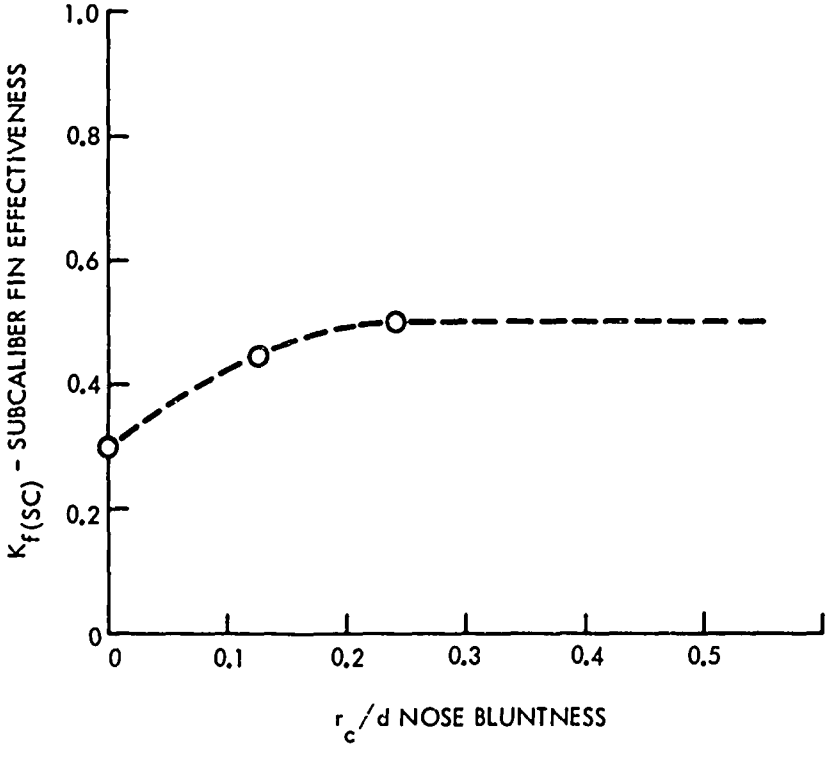

FIG. 54 SUBCALIBER FIN EFFECTIVENESS FACTOR VARIATION WITH NOSE BLUNTNESS

that in finding $K_{f(b)}$ and $K_{b(f)}$ the ratio d/b uses the boattail diameter (d_{BT}). Then $(C_{N_{\alpha f}})_{BT} = C_{N_{\alpha(fe)}} \frac{S_{fe}}{S_w} \left[K_{f(b)} + K_{b(f)}\right]$.

Finally the effect of the boattail is $C_{N_{\alpha f_{ref}}} = K_{f(sc)}(C_{N_{\alpha f}})_{BT} \frac{S_w}{S_{ref}}$ (30)

where $K_{f(sc)}$ is shown on Figure 54.

Where the fin is attached to a boattail and the span is not subcaliber, the percent of the fin area which is not subcaliber is not affected by the boattail. The fin normal force $C_{N_{\alpha fe}}$ is computed as explained above and is separated into the percent affected by the boattail and the percent not affected.

$$C_{N_{\alpha f_{ref}}} = \frac{S_w}{S_{ref}} \left[K_{f(sc)}(x) + 1.0 - x\right]\left(C_{N_{\alpha f\ BT}}\right) \qquad (31)$$

where: x is the percent subcaliber.

For subcaliber ring tails, the boattail reduces the effectiveness of the ring by a factor of 0.8

NONLINEAR NORMAL FORCE ON FINS AT HIGH ANGLES OF ATTACK

Up to 10° angle of attack the previous methods for getting C_N of tail fins holds. J. E. Fidler (Ref. (13)) presents an equation based on empirical methodology where:

$$C_N = C_1\alpha + C_2\alpha^2 \qquad (32)$$

He regards Equation (32) as a truncated power series in α. With the following boundary conditions:

$\alpha = 0$	$\alpha = \pi/2$	$\alpha = \pi$
$C_N = 0$	$C_N = f(\pi/2)$	$C_N = 0$
$C_{N_{\alpha fe}} = f'(0)$	$C_{N_{\alpha fe}} = 0$	$C_{N\alpha fe} = -f'(0)$

The equation becomes:

$$C_{N_{fe}} = f'(0)(\alpha) + \left[\frac{16f\left(\frac{\pi}{2}\right)}{\pi^2} - \frac{5f'(0)}{\pi}\right]\alpha^2 + \left[\frac{8f'(0)}{\pi^2} - \frac{32f\left(\frac{\pi}{2}\right)}{\pi^3}\right]\alpha^3 + \left[\frac{16f\left(\frac{\pi}{2}\right)}{\pi^4} - \frac{4f'(0)}{\pi^3}\right]\alpha^4 \quad (33)$$

$f\left(\frac{\pi}{2}\right)$ may be found on Figure 55. $f'(0)$ or $C_{N_{\alpha fe}}$ may be found from appropriate figures in this report. Equation (33) is good up to a maximum angle of attack α' as determined by Figure 56. With the maximum angle for use of Equation (33) determined, the further determination of $C_{N_{fe}}$ up to $\alpha = 30°$ is as follows.

(1) calculate $C_{N_{fe}}$ up to α' as $(C_{N_{fe}})_{\alpha'}$, with Equation (33)

(2) find $\Delta C_N/\Delta C_{N_m}$ from Figure 57

(3) find ΔC_{N_m} from Figure 58

then: $C_{N_{fe}} = (C_{N_{fe}})_{\alpha'} + (\Delta C_N/\Delta C_{N_m})C_{N_m}$.

From $\alpha = 50°$ to 90° a second equation was developed:

$$C_{N_{fe}} = f(30) + 1.738A - 1.652f'(30) + [4.82f'(30) - 6.6A]\,\alpha + [7.54A - 4.15 + f'(30)]\,\alpha^2 + [1.11f'(30) - 2.31A]\,\alpha^3 \quad (34)$$

where: $A = C_{N_c} - f(30)$ (35)

C_{N_c} from Figure 59

f(30) from Figure 60a, b, c

f'(30) from Figure 61

For a complete curve of $C_{N_{fe}}$ the missing section between $\alpha = 30°$ and $\alpha = 50°$ must be filled in.

a. CENTER OF PRESSURE OF FINS AT HIGH ANGLES OF ATTACK

Fidler in Reference (13) also has a method for calculating the spanwise and chordwise centers of pressure of fins. Only the chordwise calculations are presented here.

Chordwise center of pressure of a fin as measured from the fin root chord body juncture is:

$$\frac{x_{cp}}{c} = \left(\frac{x_{cp}}{c}\right)_{\alpha=90°} - \frac{\Delta x_{cp}}{c}\left[1 + F(M)\right]N \qquad (36)$$

The procedure is as follows:

(a) find $\left(\frac{x_{cp}}{c}\right)_{\alpha=90°}$ as a function of λ from Figure 62

(b) find $\frac{x_{cp}}{c}$ as a function of α for the proper AR and λ for $M = 0.98$ from Figure 63

(c) find the variation of $\frac{\Delta x_{cp}}{c}$ from $M = 0.98$ to M being calculated from Figure 64 as F(M).

(d) find N from Figure 65.

Equation 36 in workable form is:

$$\frac{x_{cp}}{c} = \left(\frac{x_{cp}}{c}\right)_{\alpha=90°} - \left\{\left[\left(\frac{x_{cp}}{c}\right)_{\alpha=90°} - \left(\frac{x_{cp}}{c}\right)_{M=0.98}\right]\left[1 \pm F(M)\right]N\right\} \qquad (37)$$

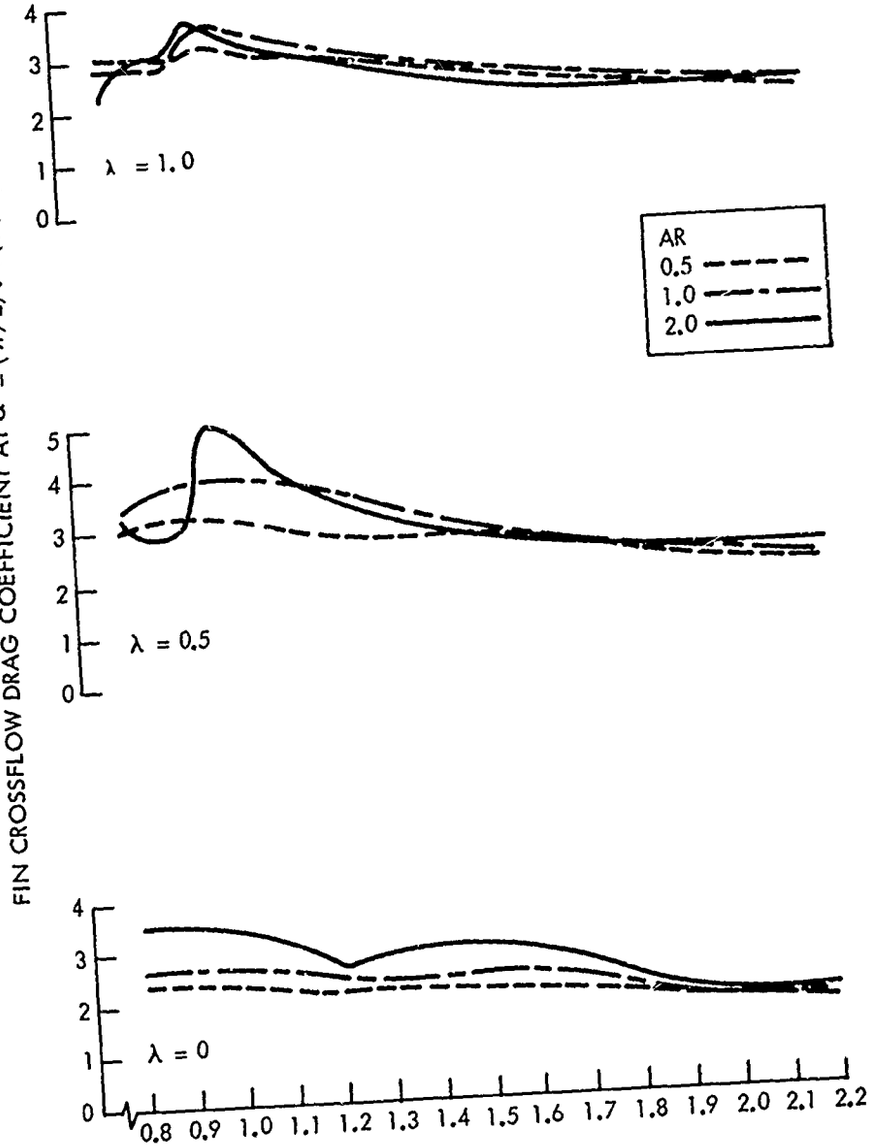

FIG. 55 VARIATION OF f (π/2) WITH MACH NUMBER, $0 \leq \alpha^{\circ} \leq 30$ (REF 13)

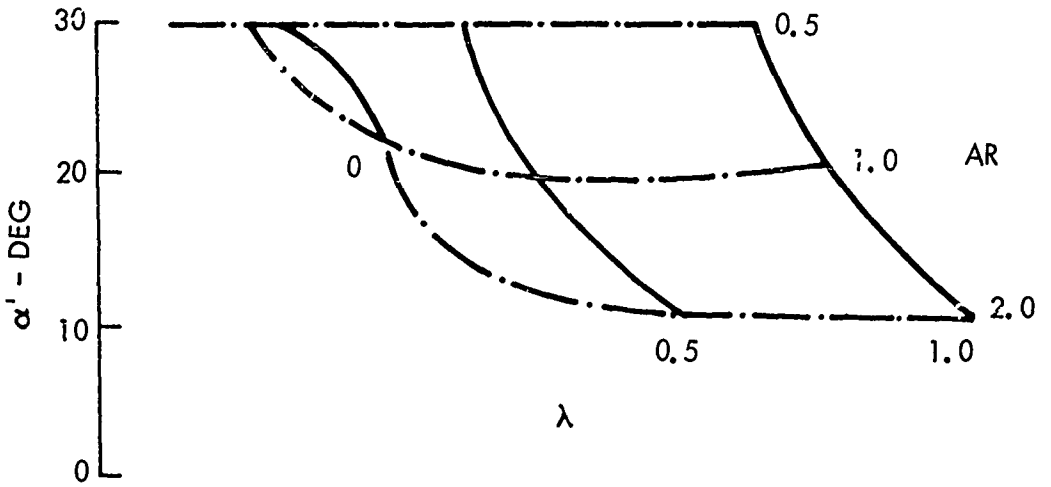

FIG. 56 α' - ANGLE OF ATTACK ABOVE WHICH ΔC_N MUST BE APPLIED (SUBSONIC MACH NUMBER ONLY) (REF 13)

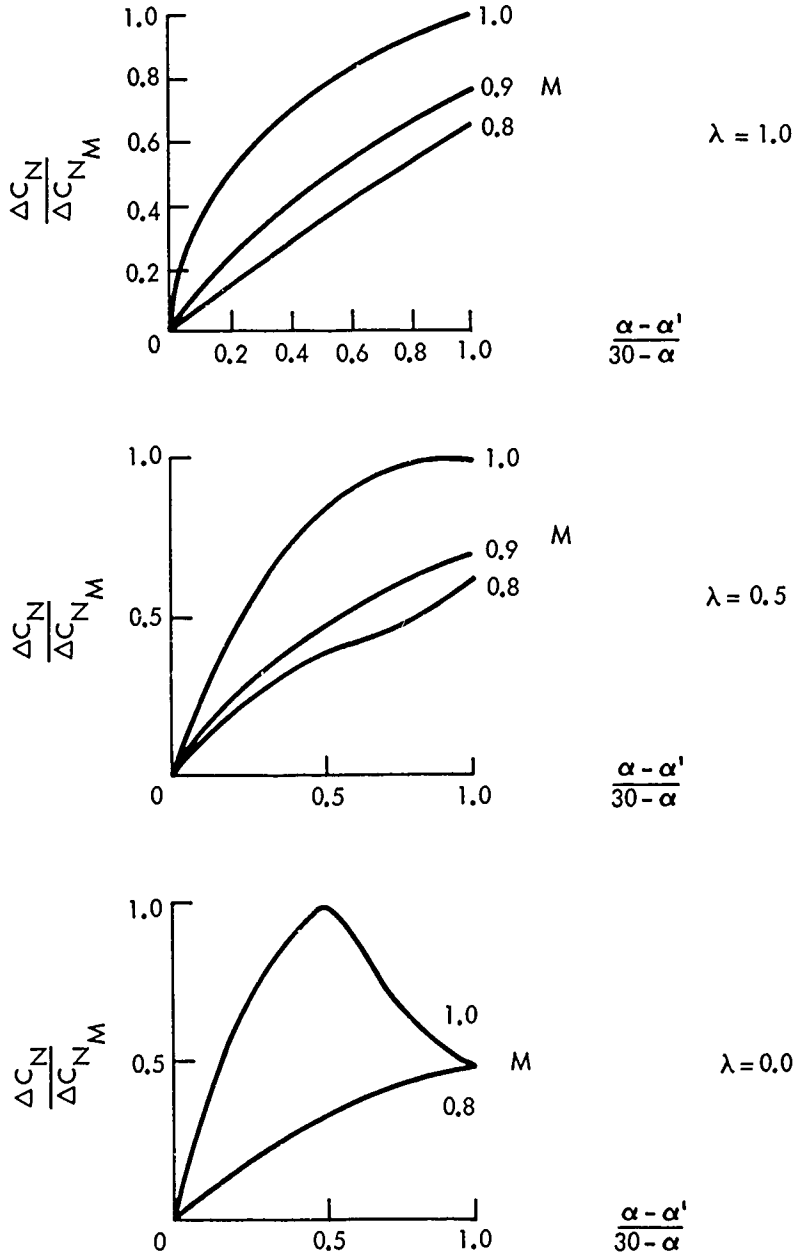

FIG. 57 DIMENSIONLESS C_N INCREMENT ABOVE α' (REF 13)

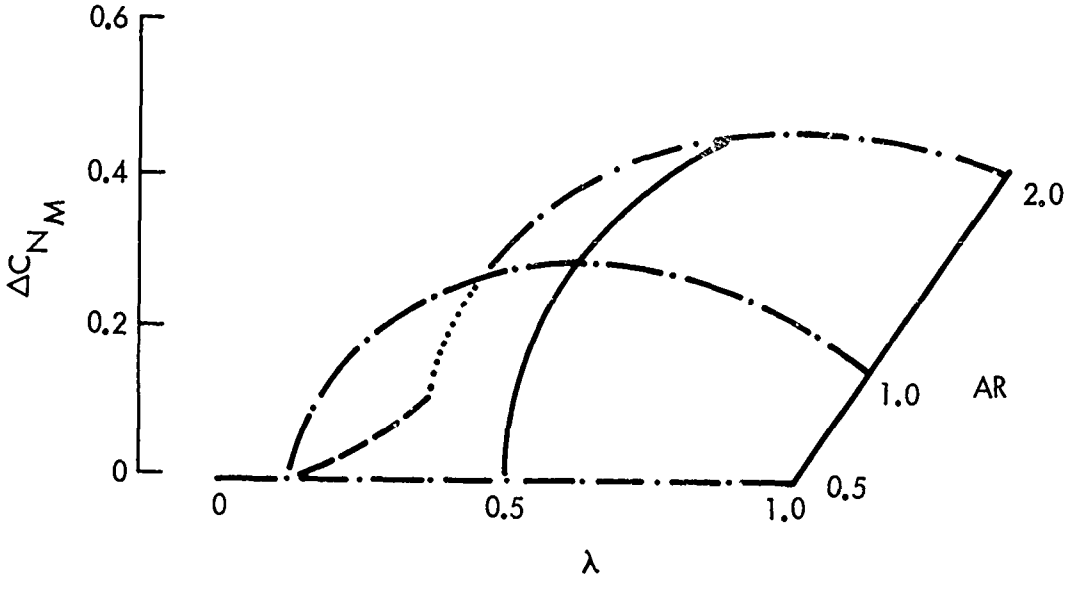

FIG. 58 ΔC_{NM} - MAXIMUM INCREMENT OF NORMAL FORCE ABOVE α' (SUBSONIC MACH NUMBER ONLY) (REF 13)

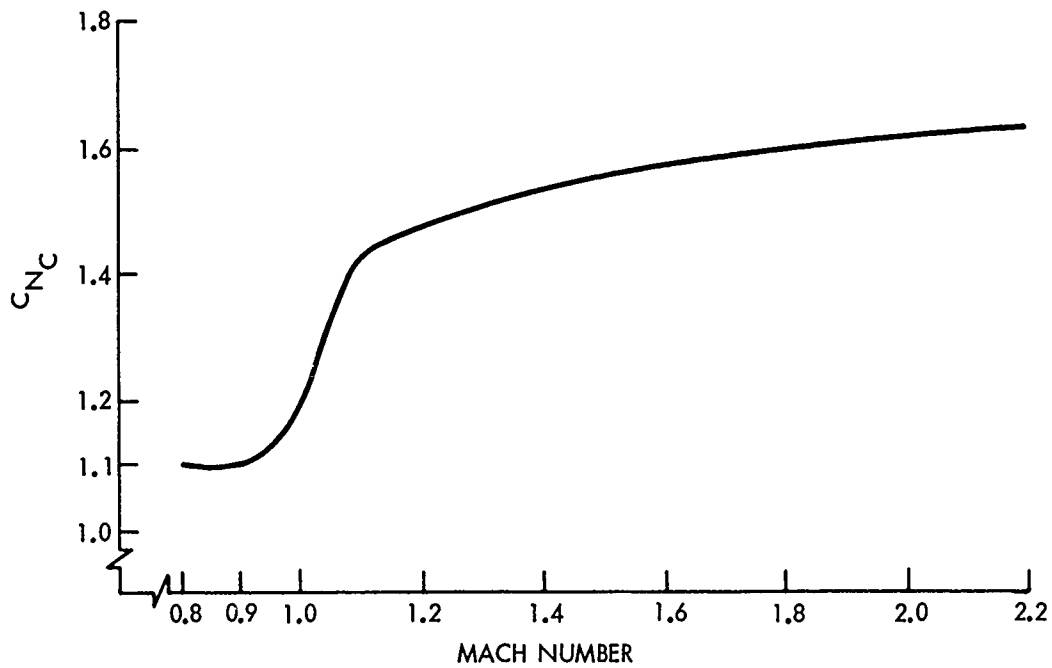

FIG. 59 VARIATION OF FIN NORMAL FORCE WITH MACH NUMBER (α = 90 DEGREES) (REF 13)

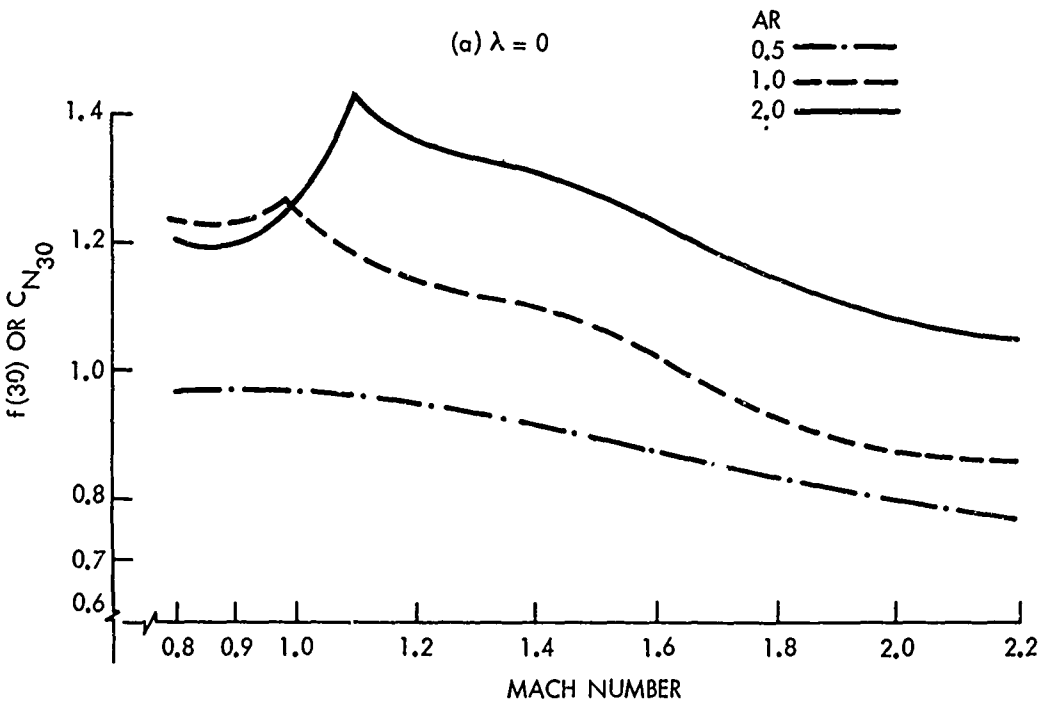

FIG. 60 a VARIATION OF NORMAL FORCE WITH MACH NUMBER (α = 30 DEGREES) (REF 13)

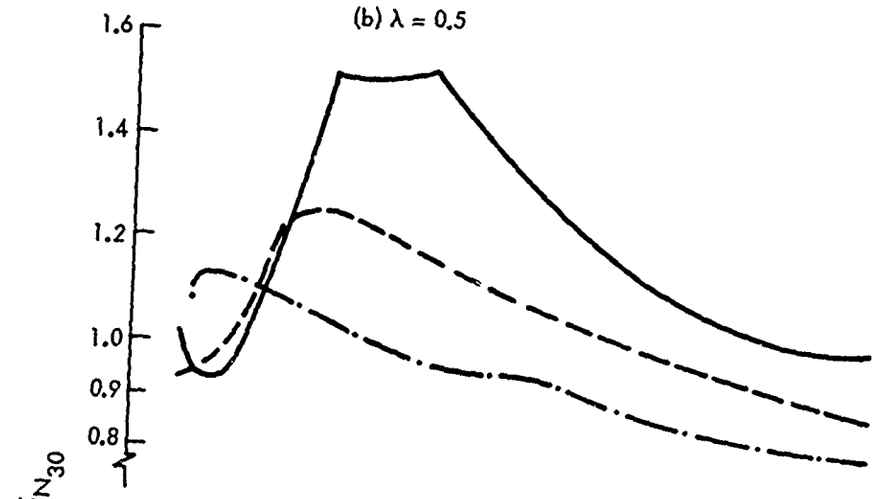

FIG. 60 b VARIATION OF NORMAL FORCE WITH MACH NUMBER (α = 30 DEGREES) (CONT'D) (REF 13)

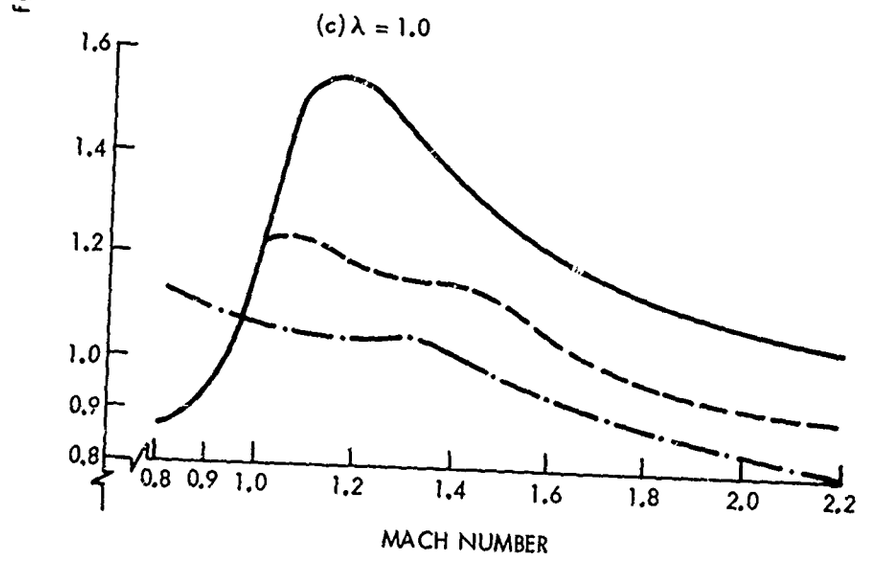

FIG. 60 c VARIATION OF NORMAL FORCE WITH MACH NUMBER (α = 30 DEGREES) (CONT'D) (REF 13)

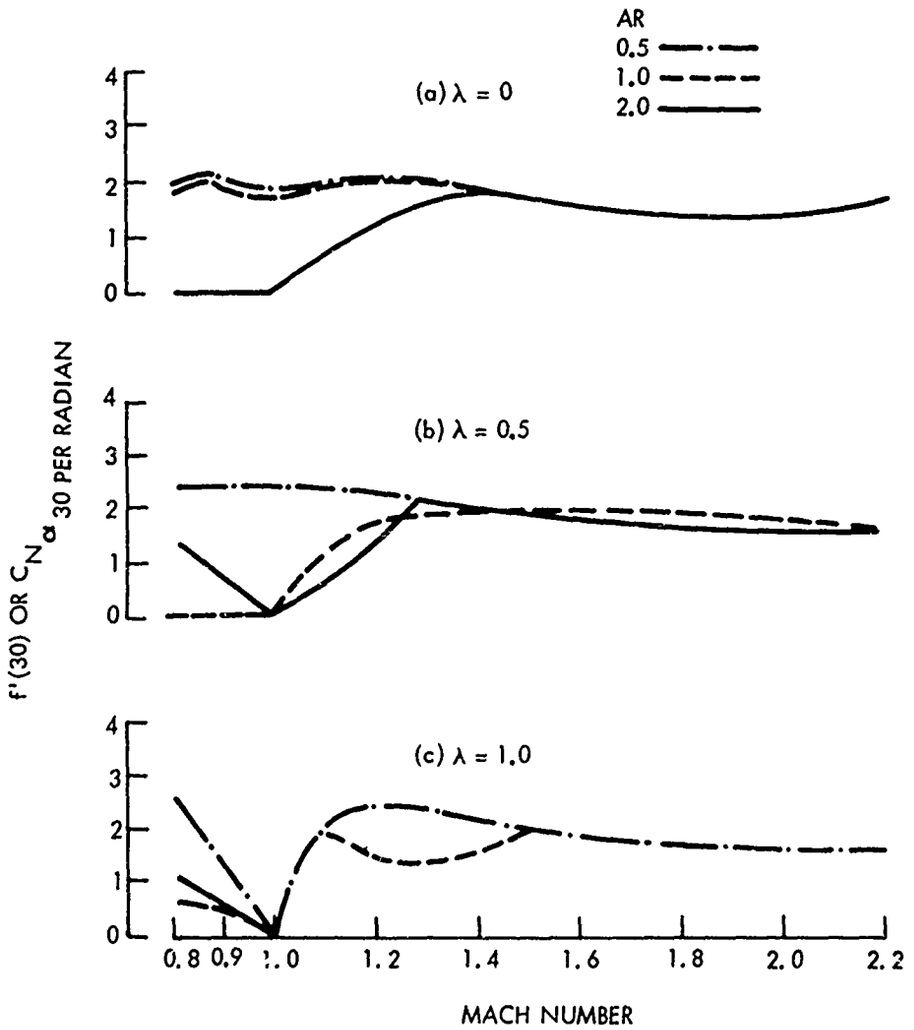

FIG. 61 VARIATION OF NORMAL FORCE CURVE SLOPE WITH MACH NUMBER (α = 30 DEGREES) (REF 13)

CENTER OF PRESSURE COINCIDES WITH FIN CENTROID

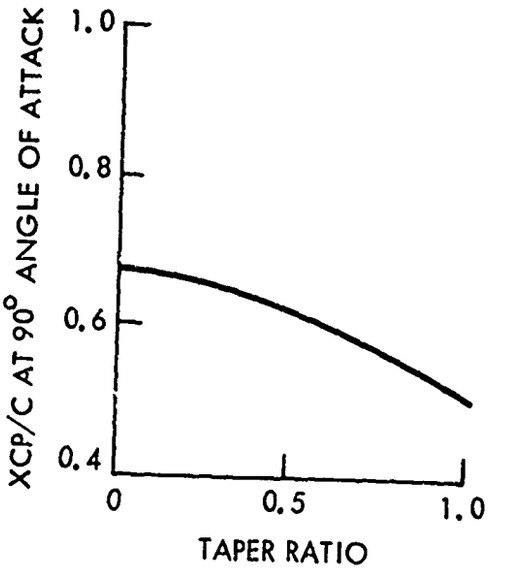

FIG. 62 CHORDWISE CENTER OF PRESSURE AT 90 DEGREES VERSUS TAPER RATIO (REF 13)

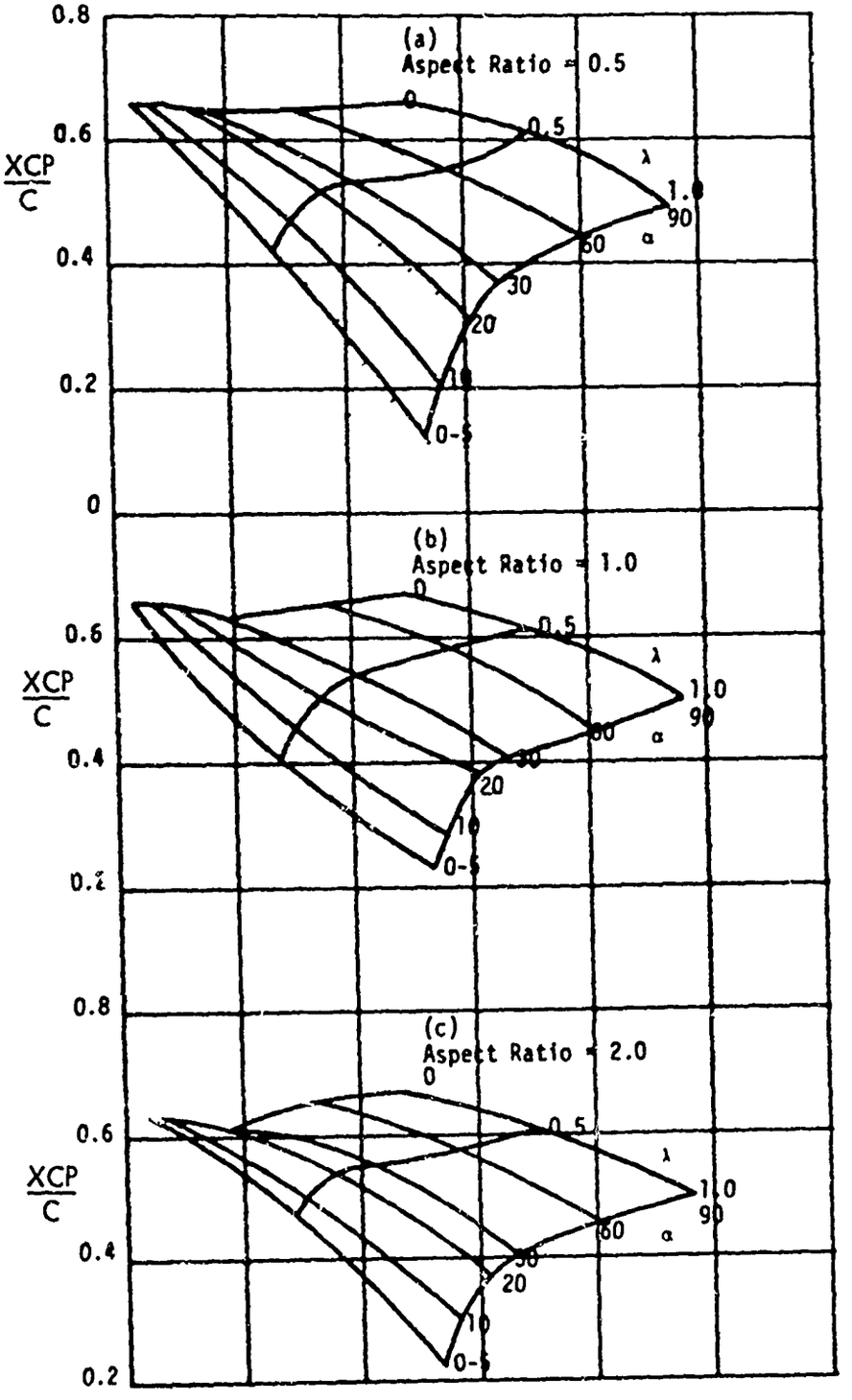

FIG. 63 BASIC CURVES FOR XCP/C AT REFERENCE MACH NUMBER 0.98 (0-90 DEGREES) (REF 13)

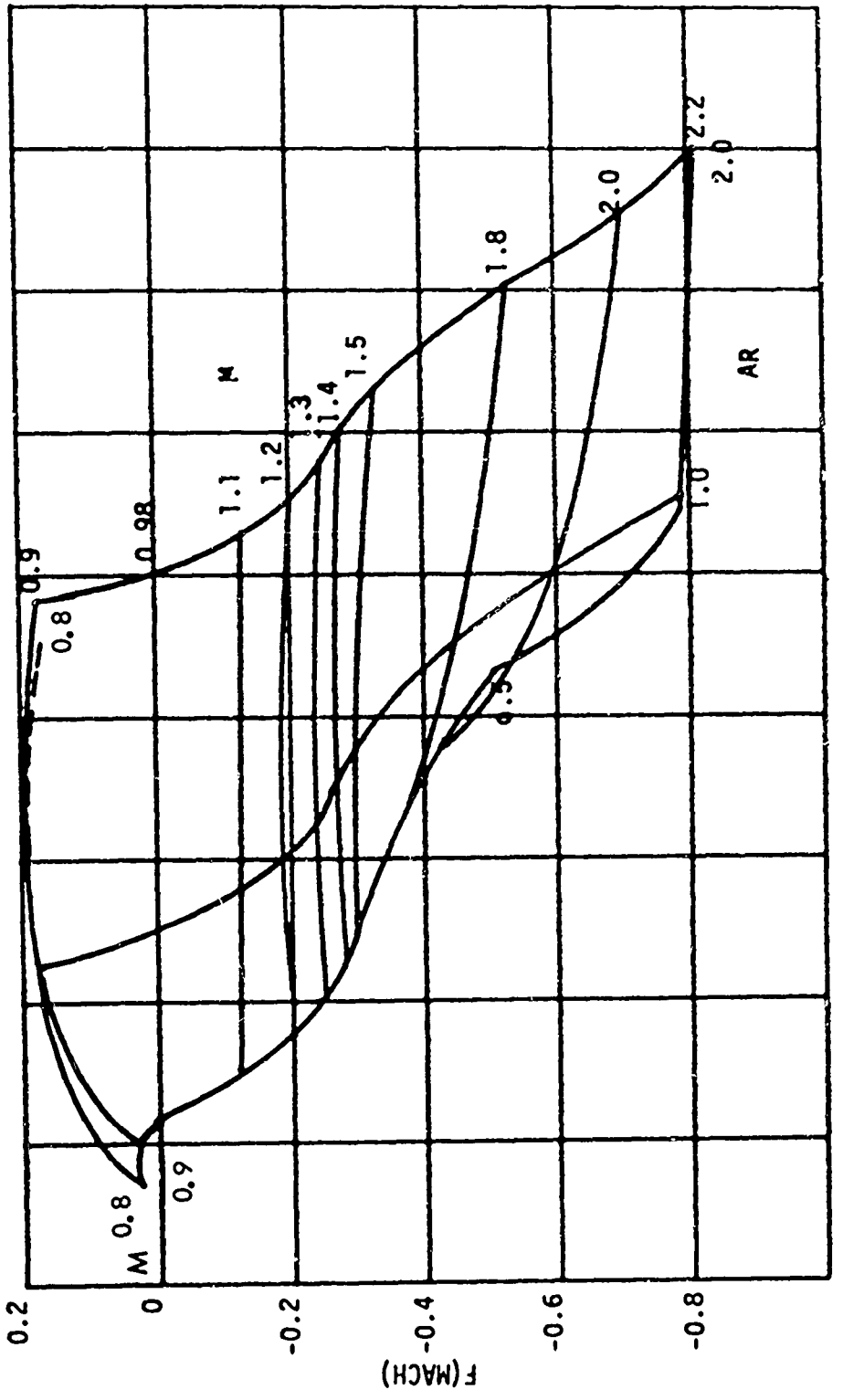

FIG. 64 VARIATION FACTOR OF ΔXCP/C VERSUS MACH NUMBER (REF 13)

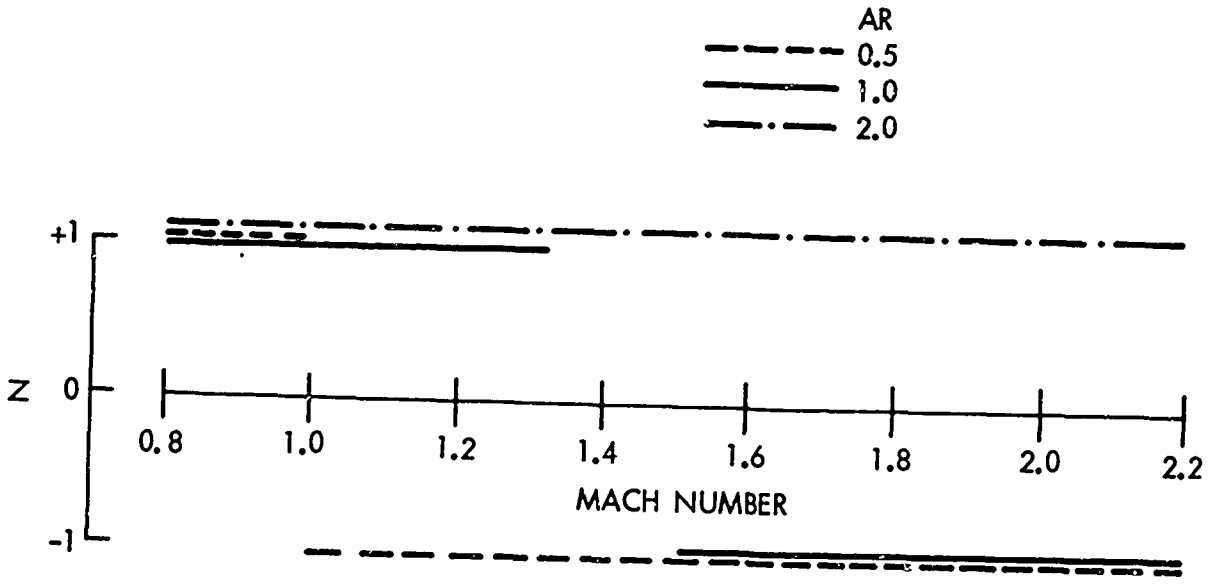

FIG. 65 VARIATION OF SIGN FACTOR N WITH MACH NUMBER (DELTA FINS ONLY) (REF 13)

NORMAL FORCE OF RING TAILS SUBSONIC AND SUPERSONIC

Figures 66a to f give C_{N_α} for ring tails attached to cylindrical afterbodies over a Mach number range of 0.8 to 3.0. The data were obtained experimentally from wind-tunnel tests on a particular 4° double wedge ring set at a 4° angle of attack to the body. The center of pressure of the ring may be assumed to be at mid-chord (Ref. (2)).

EFFECT OF NOSE BLUNTNESS AND BODY LENGTH ON FIN NORMAL FORCE AT α = 0 DEGREE AND 12 TO 15 DEGREES FOR SUBSONIC AND SUPERSONIC SPEEDS

At subsonic speeds, nose bluntness reduces the effectiveness of fins where $r_c/r_d > 0.25$. Figure 67 shows this effect and applies here for AR up to 1.8. Also note that body length has the opposite effect. This curve was developed mainly from the AEDC experimental data from Reference (6). To use the factor $K_{f(N)}$, first find $C_{N_{\alpha fb}}$ by the theoretical method corrected for body interference effects and referenced to the body area.

$$C_{N_{\alpha f(N)b}} = C_{N_{\alpha fb}} K_{f(N)} \tag{38}$$

At supersonic speeds, Figure 68 gives the factor $K_{f(N)}$ also derived from Reference (8). The body length has no effect with the bluntness. Above an aspect ratio of 1.0, and M > 1.2 there is no effect of nose bluntness.

In the range of α = 12° to 15° at subsonic speeds, the nose shape has little effect on fin normal force; however, there is still an effect of body length and fin-aspect ratio. Figure 67b shows $K_{f(N)}$ at α = 12° to 15° for subsonic speeds. At supersonic speeds,

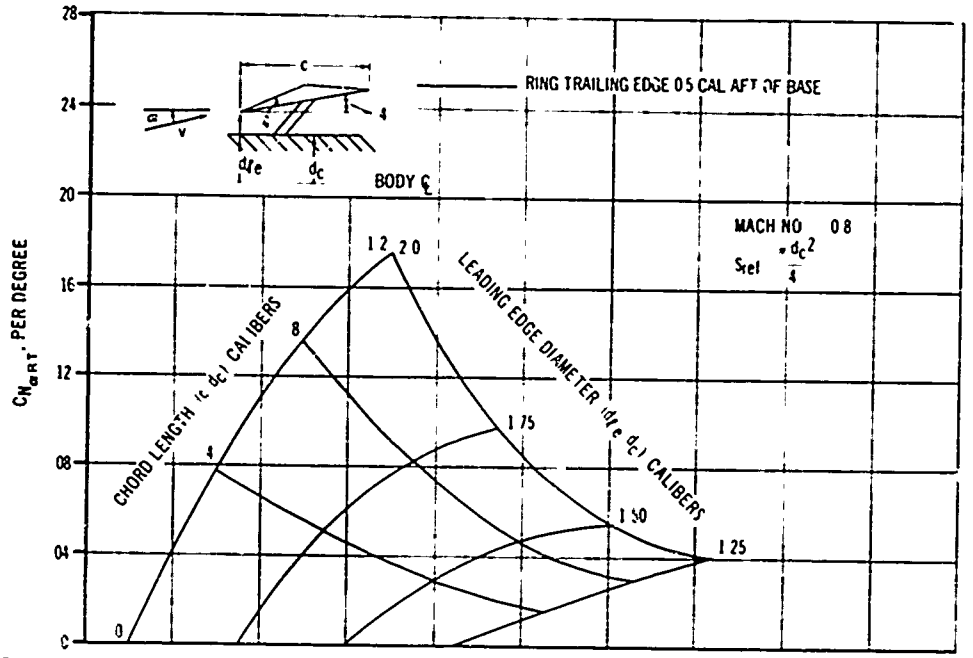

FIG. 66 a . INCREMENTAL NORMAL FORCE COEFFICIENT GRADIENT FOR A RING TAIL MOUNTED ON A CYLINDRICAL AFTERBODY (REF 2)

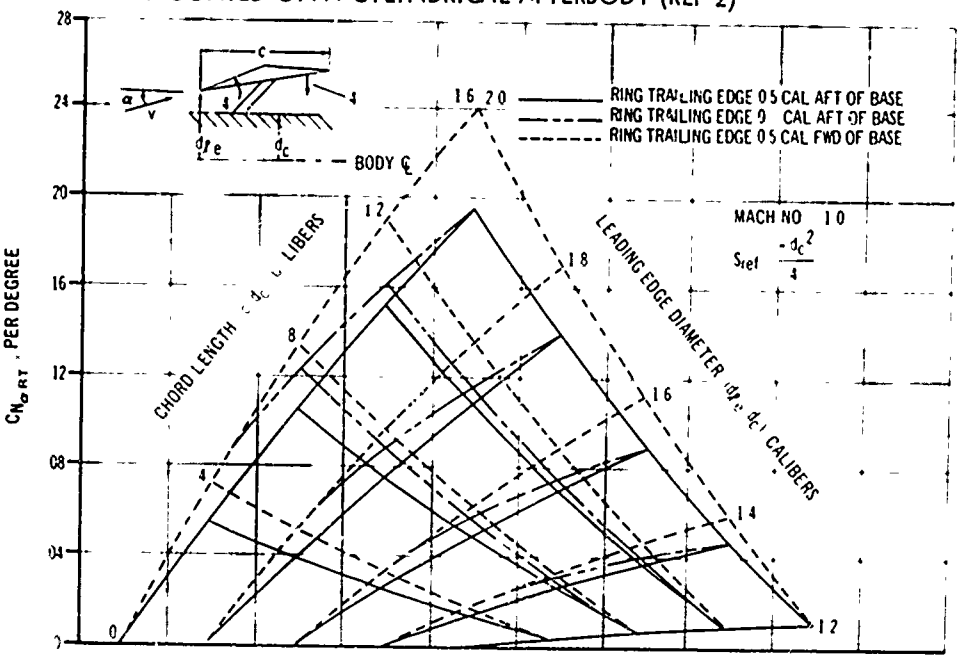

FIG. 66 b . INCREMENTAL NORMAL FORCE COEFFICIENT GRADIENT FOR A RING TAIL MOUNTED ON A CYLINDRICAL AFTERBODY. (REF 2)

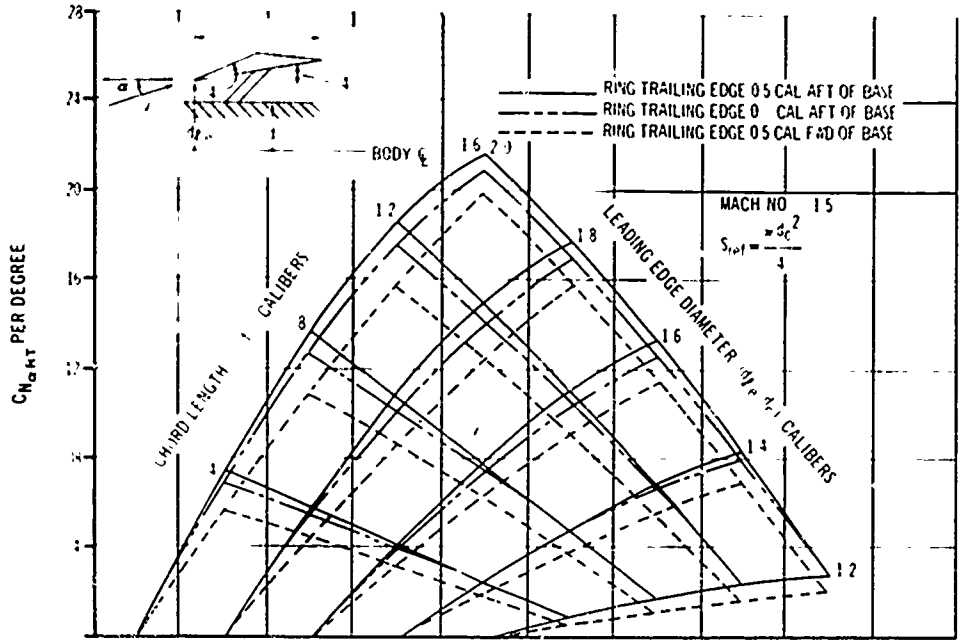

FIG. 66 c . INCREMENTAL NORMAL FORCE COEFFICIENT GRADIENT FOR A RING TAIL MOUNTED ON A CYLINDRICAL AFTERBODY (REF 2)

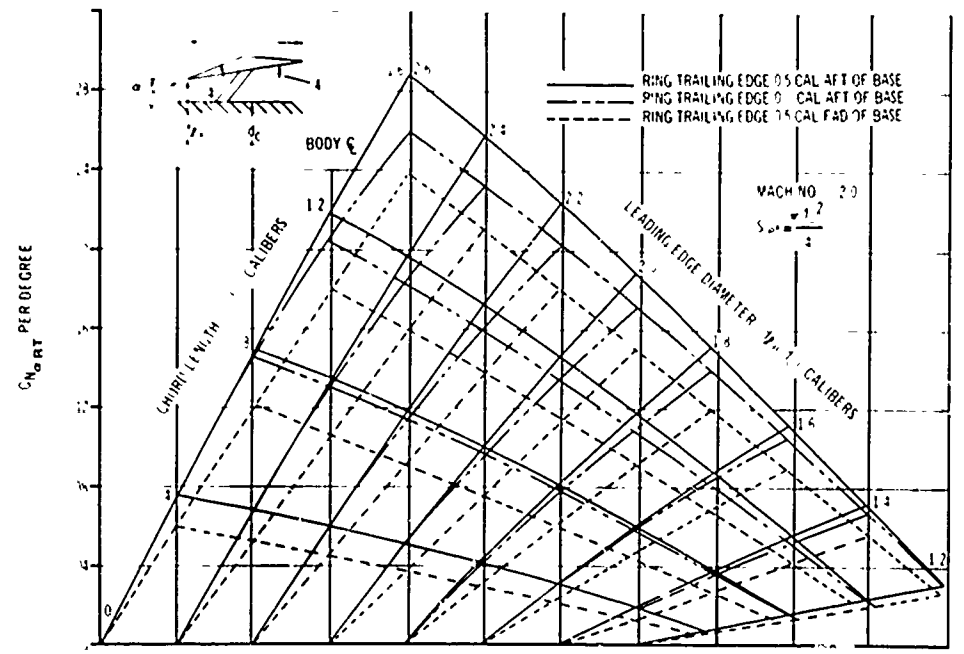

FIG. 66 d . INCREMENTAL NORMAL FORCE COEFFICIENT GRADIENT FOR A RING TAIL MOUNTED ON A CYLINDRICAL AFTERBODY (REF 2)

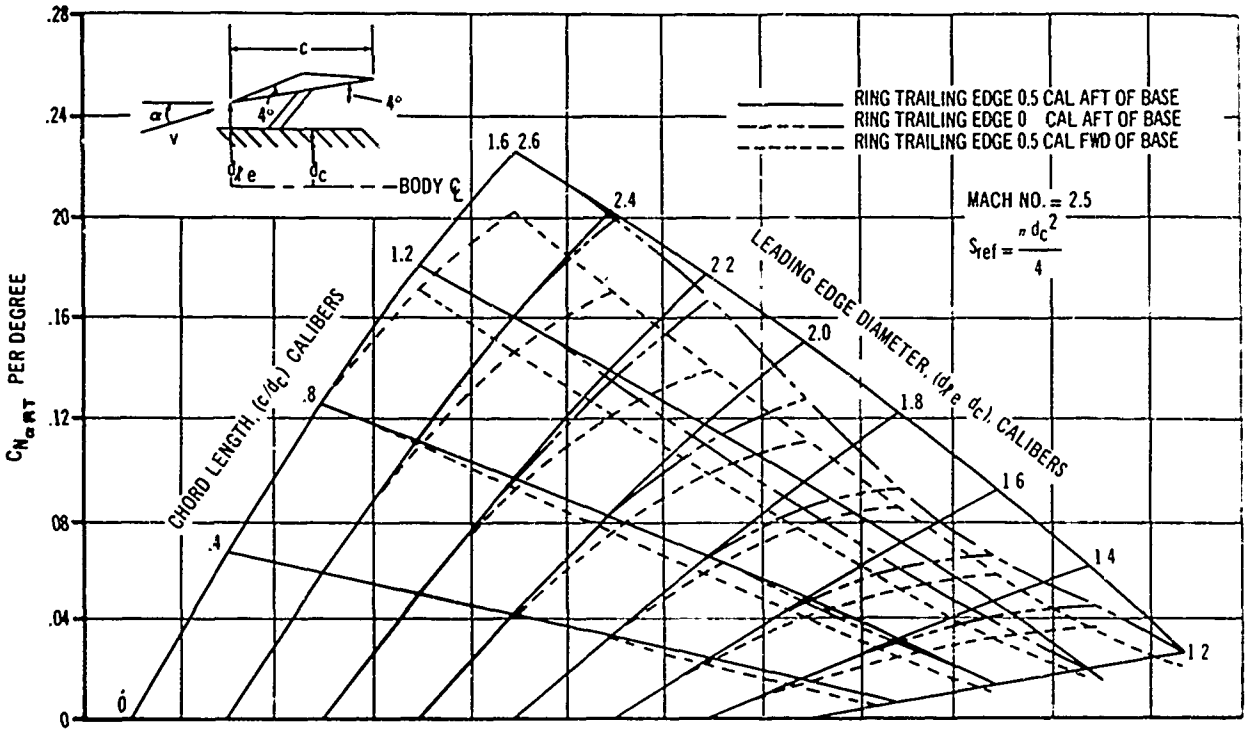

FIG. 66e INCREMENTAL NORMAL FORCE COEFFICIENT GRADIENT FOR A RING TAIL MOUNTED ON A CYLINDRICAL AFTERBODY. (REF 2)

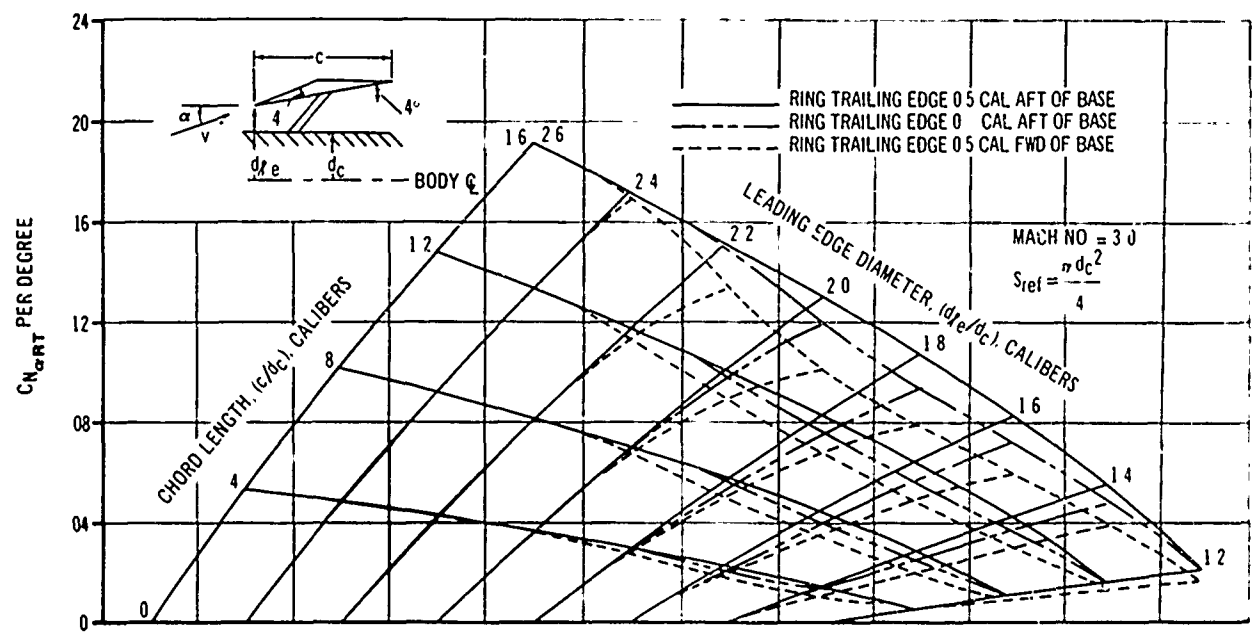

FIG. 66f INCREMENTAL NORMAL FORCE COEFFICIENT GRADIENT FOR A RING TAIL MOUNTED ON A CYLINDRICAL AFTERBODY. (REF 2)

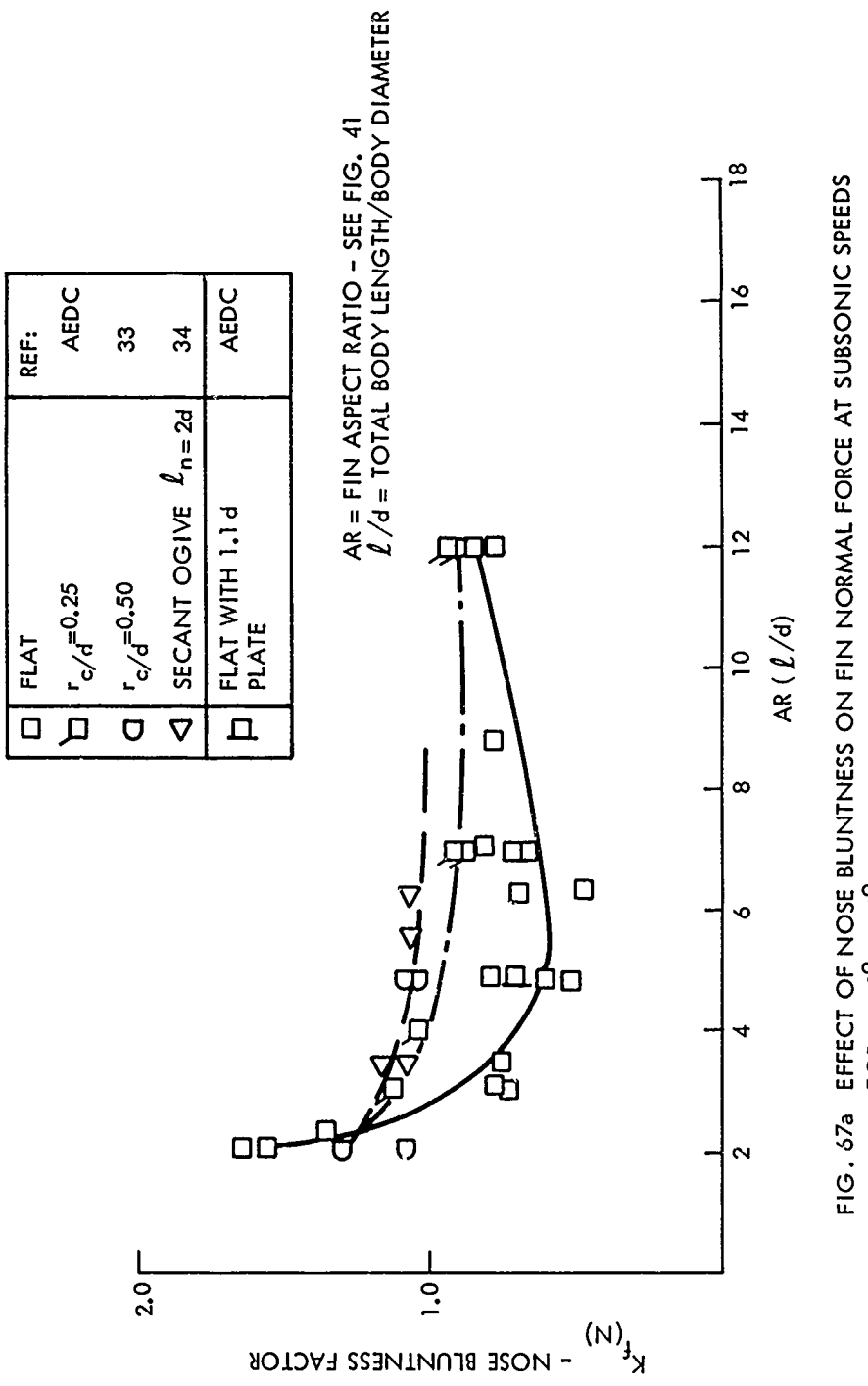

FIG. 67a EFFECT OF NOSE BLUNTNESS ON FIN NORMAL FORCE AT SUBSONIC SPEEDS FOR $\alpha = 0^{\circ}$ TO 6°

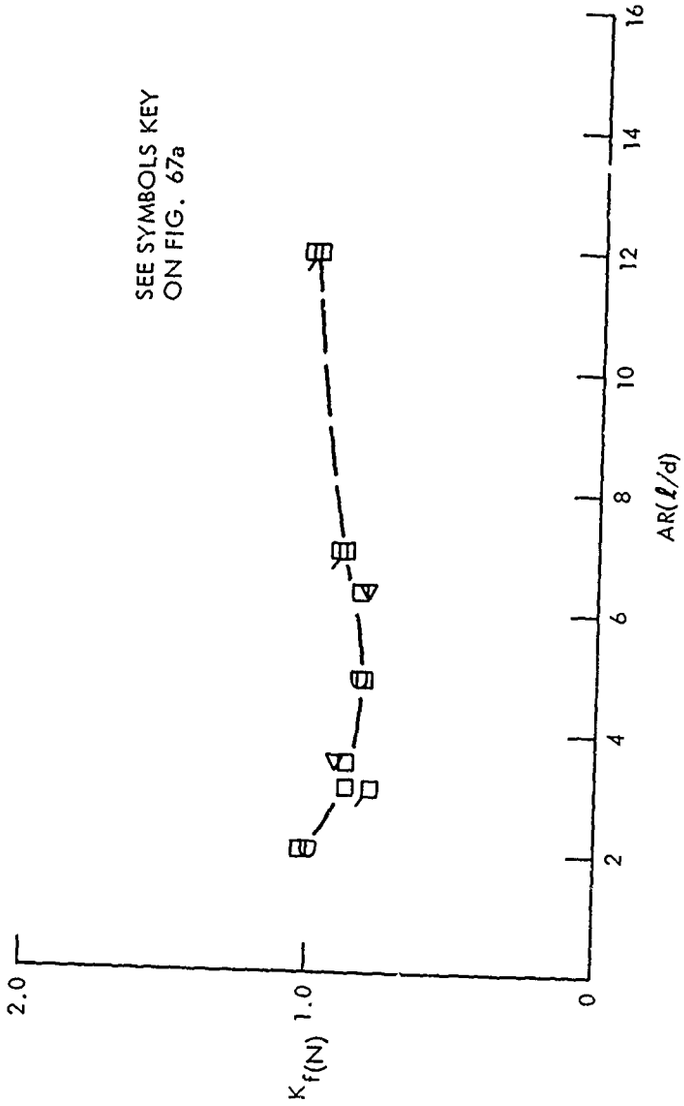

FIG. 67b EFFECT OF NOSE BLUNTNESS ON FIN NORMAL FORCE AT SUBSONIC SPEEDS FOR α= 12° TO 15°

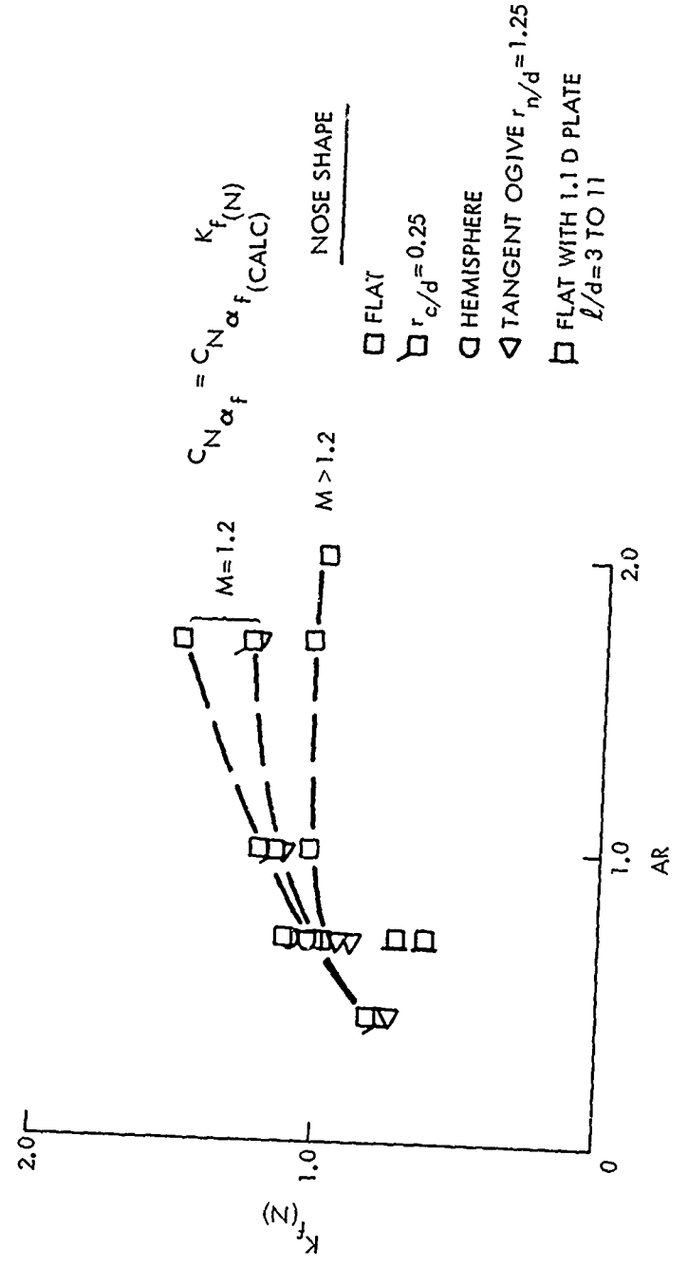

FIG. 68a EFFECT OF NOSE BLUNTNESS ON FIN NORMAL FORCE FOR LOW ASPECT RATIO FINS AT SUPERSONIC SPEEDS $\alpha = 0^{\circ}$

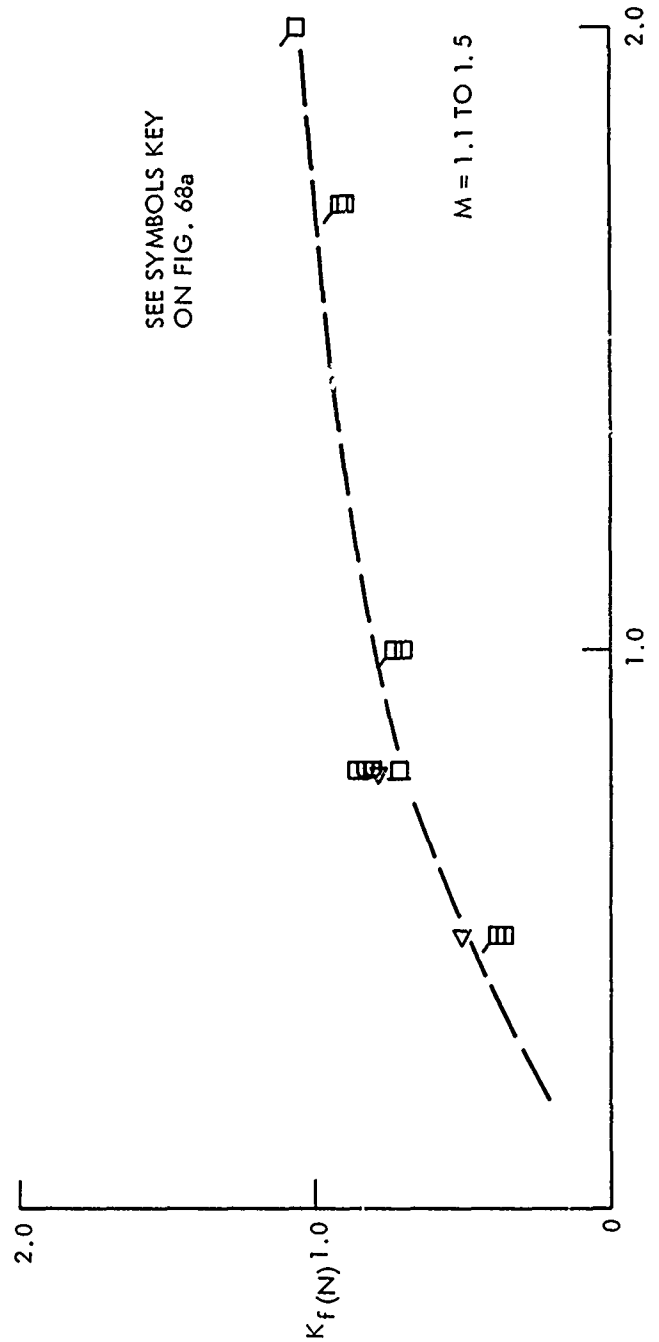

FIG. 68b EFFECT OF NOSE BLUNTNESS AND ASPECT RATIO ON FIN NORMAL FORCE AT SUPERSONIC SPEEDS FOR $\alpha = 12^\circ$ TO 15°

there is a definite effect of fin-aspect ratio on fin effectiveness at higher angles of attack. Nose bluntness and ℓ/d do not have any effect here. Figure 67b shows this effect for α = 12° to 15° over the Mach number range of 1.1 to 1.5. J. E. Fidler (Ref. (13)) pointed out to the author that for angles of attack greater than zero, the usual fin effectiveness factors $K_{f(b)}$ and $K_{b(f)}$ derived by Pitts, Nielsen, and Kaattari of Reference (11) would not suffice at higher angles of attack because there would be an effect of the vortex from the body on the fins not accounted for. These factors of $K_{f(N)}$ at α = 12° to 15° shown on Figures 67b and 68b are probably related to this body vortex effect.

EFFECT OF ADDING FIN-TIP CAPS TO FINS AT SUBSONIC SPEEDS AND SUPERSONIC SPEEDS

Fin-tip caps give added fin normal force without increasing the span. Fin-tip cap normal force may be calculated by treating the tip caps as additional horizontal fins. Use Figure 40 to find $C_{N_{\alpha fe}}$ for the top and bottom tip caps on the vertical tail of a four-finned configuration. The normal force slope ($C_{N_{fe}}$) calculated by Figure 40 is affected by the nose bluntness (r_c/r_d), aspect ratio (AR), and the ratio of the distance the tip cap is above the body surface (y/d). The fin-tip plate factor (K_c) relating all of these effects is plotted on Figure 69. For flat-face configurations (K_c) is approximately half as large as for rounded-and sharp-nosed configurations ($r_c/d \geq 0.5$).

To find the normal force contribution of a fin-tip cap:

(a) find $C_{N_{\alpha we}}$ for one fin-tip cap from Figure 40

(b) find K_c the fin-tip plate factor

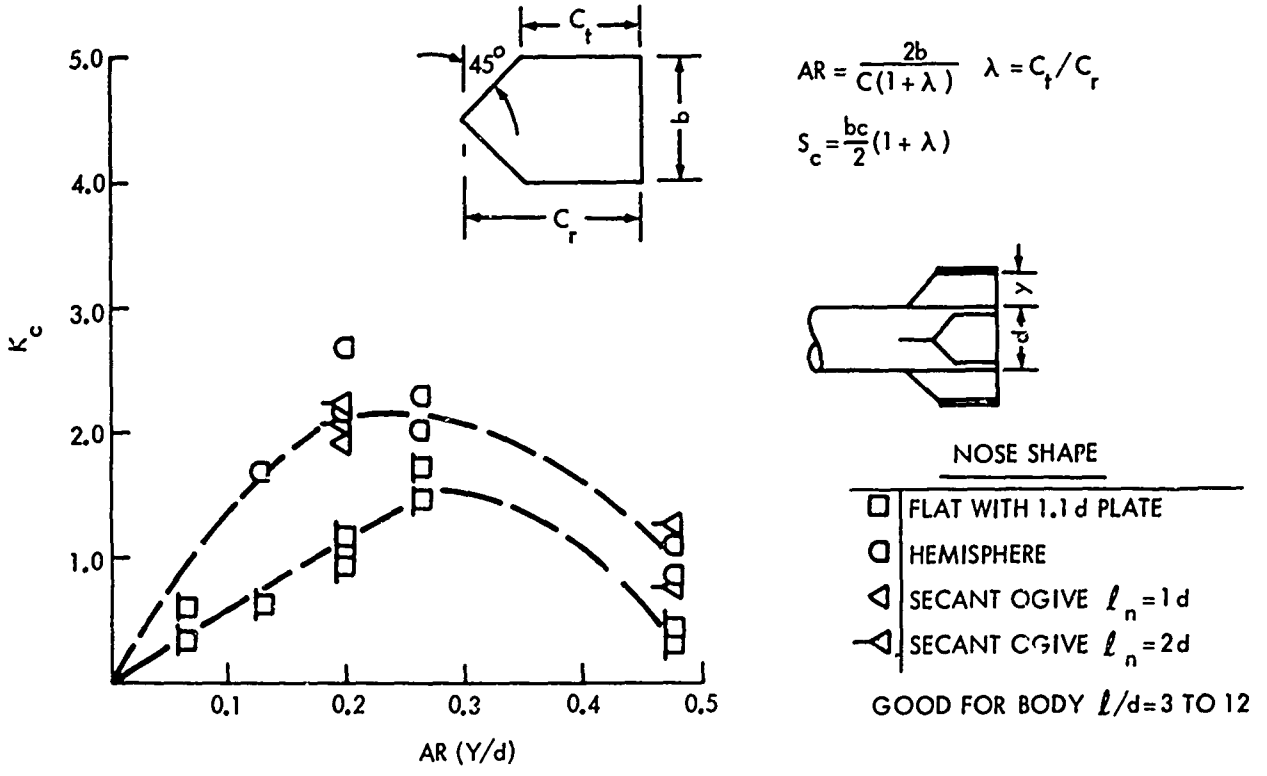

FIG. 69 FIN CAP EFFECTIVENESS FACTOR (K_c) FOR SUBSONIC SPEEDS

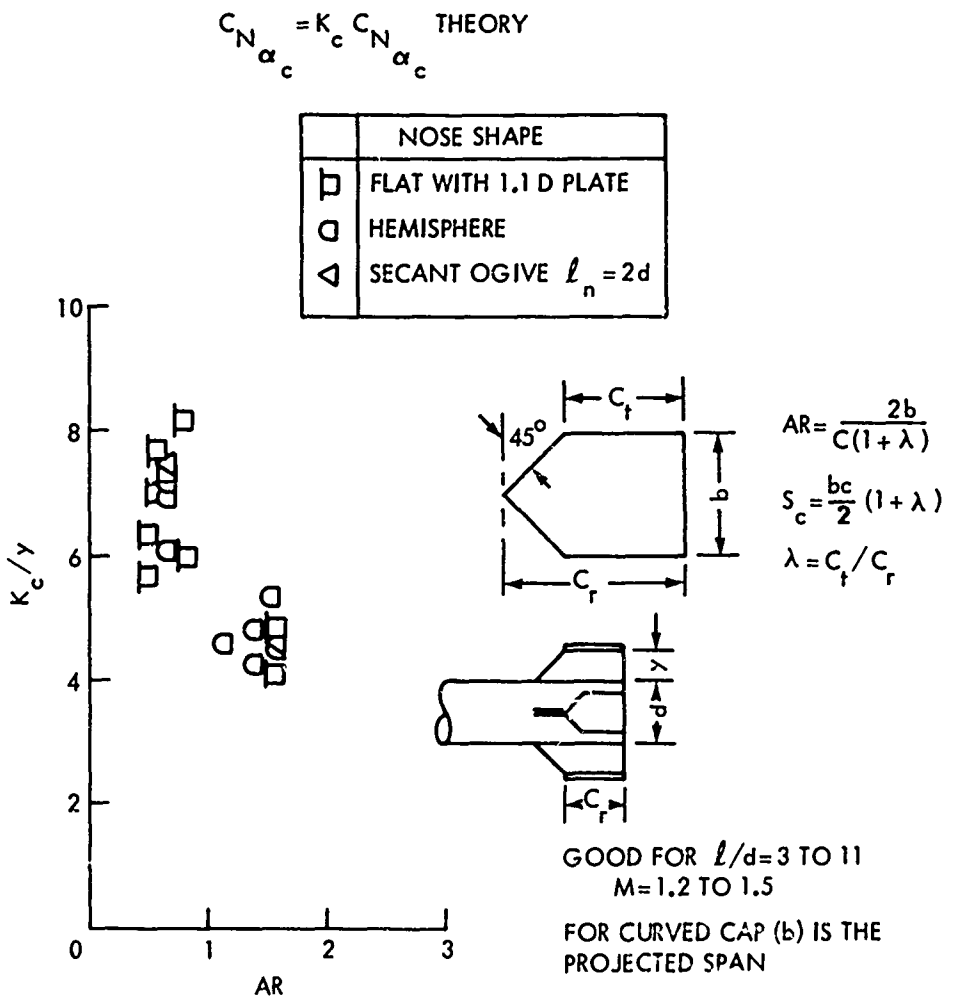

FIG. 70 FIN CAP EFFECTIVENESS FACTOR (K_c) FOR SUPERSONIC SPEEDS

(c) calculate $C_{N_{\alpha f(cap)B}} = 2C_{N_{\alpha fe}} \frac{(S_{fe})}{S_B} K_c$ (39)

(d) add $C_{N_{\alpha f(cap)B}}$ to $C_{N_{\alpha fB}}$

where: $C_{N_{\alpha fB}}$ is found by Equations (20) and (21) for the fins supporting the caps.

The center of pressure of the fin-tip cap may be taken as 0.25 of the mean aerodynamic chord of the cap. Figure 69 was developed from wind-tunnel test results of Reference (6).

The effect of adding fin-tip caps at supersonic speeds is the same as at subsonic speeds. Figure 70 developed from data from Reference (2) gives the effectiveness factor K_c for the fin caps. The points on the figure show a spread. There does not seem to be any effect of nose shape or body length or Mach number for the configurations shown. It is advised that an average value for K_c be used. The only variables are (y), the height of the cap from the body measured in calibers; and (AR) the cap aspect ratio.

To use Figure 70, first find AR, then calculate S_c (using dimensions in calibers) and determine y.

Find K_c/y on the figure and calculate the theoretical fin-cap normal force slope $C_{N_{\alpha fe}}$ using Figure 43 through Figure 49.

Calculate $C_{N_{\alpha f(cap)B}}$ using Equation (30).

CALCULATION OF C_N AND C_m FOR COMPLETE CONFIGURATION

The AMC Handbook (Ref. (2)) gives a good calculation procedure in the form of a table with detailed instructions. The author advises studying this handbook and the AF DATCOM Handbook (Ref. (1)) before proceeding with design calculations.

What have been presented so far are reprints of calculation charts from both handbooks with the addition of modifications to cover the blunt shapes.

Figure 71 shows a sample blunt shape, and the two basic equations for obtaining C_N and C_m. Calculate C_N and x_{cp} for each component. Reference all component coefficients to the same reference area - usually the body cross section area. Then add the components as shown.

Up to about $\alpha = 4°$ to $6°$ C_N for a body is linear with the exception of $\ell/d < 2.0$. Above this crossflow drag must be introduced. Table 1 reviews the component calculations of the report.

Table 2, page 122, lists and analyzes a bibliography of material which has blunt-body information. In the original search for material to include in this report these sources of material were studied. In most cases the configurations are so specialized that they were not adaptable for use in making the curves and charts of the report.

Appendix A demonstrates a computation of C_N and x_{cp} of a typical blunt configuration with a comparison to experimental results. The configuration shown was tested in the NOL Supersonic Tunnel No. 1.

TABLE 1 - COMPREHENSIVE REVIEW OF CALCULATION PROCEDURES FOR FINDING C_N AND X_{CP} OF BLUNT SHAPES

BODY COMPONENT	MACH NO. RANGE	α-RANGE	ℓ/d	NOSE BLUNTNESS	C_N	X_{CP}
NOSE BODY	0.4 TO 1.0	0 TO 6 OR 15° FIG. 7	0.5 TO 11	r_c/r_d - 0 TO 2.5	$C_{N\alpha\ \alpha=0}(\alpha)$ FIG. 2-4	FIG. 9, 10, 11
		6 TO 20°			$C_{N\alpha\ \alpha=0}(\alpha) + \eta C_{D_s} e(A_D/S_{ref}) \sin^2\alpha$ FIGS. 5-8	FIG. 18a, b $\alpha = 10°$
	0.8 TO 1.2	0 - 10°	6 TO 15	0 TO 2.5	$C_N + C_{N\alpha}(\alpha) + C_{N\alpha_2}(\alpha)^2$ FIGS. 12, -13 (a-g)	$X_{CP} = (X_{CP})_{\alpha=0°} + D_1\alpha$ FIGS. 14, 15 (a - g)
	1.2 TO 2.5	0 TO 10°	1 TO 11	0 TO 2.5	$C_{N\alpha\ \alpha=0}(\alpha)$ FIG. 16	FIG. 17 FIG. 18a, b
	1.4 TO 7.0	0 TO 4°	3 TO 17	ℓ_m/d = 3.0 TO 7.0	FIGS. 19, 21	FIGS. 20, 22
	LIMITED TO M_c = 0.8 OR LESS $M_c - M \sin\alpha$	0 TO 90°	3 TO 20	CONE HALF ANGLE <75°	$C_N = 1/2\, C_{N\alpha\ \alpha=0}(\sin 2\alpha) \frac{+ KF \sin\alpha\cos\alpha}{S}\left(\frac{J\cot\alpha}{J}\left[B\right]_o^{X_N} + \left[A\right]_{X_N}^{X_L-E} + H\left[A\right]_{X_L-E}^{X_L}\right)$ FIGS. 23 - 34	$-C_m = 1/2\, C_{m\alpha_{\alpha=0}} \sin 2\alpha + KF\frac{\cos^2\alpha}{S^2}\left(\frac{J}{S}\cot\alpha\left[C\right]_o^{X_N} + \left[B\right]_{X_N}^{X_L-E} + \left[B\right]_{X_L-E}^{X_L}\right)$ FIG. 22 - 34
BOAT TAIL	0.4 TO 0.8	0 TO 6°	3 TO 11	r_c/r = 0 TO 2.5	$\Delta C_{N\alpha} = K_{BT}\left(\frac{S_{bt}}{S_{ref}}\right)\left[1 - \left(\frac{d_{bt}}{d_c}\right)^2\right]$ FIG. 36	FIG. 36
	1.5 TO 5.0	0 TO 6°	3 TO 20	SLENDER	FIG. 37	FIG. 38
CONICAL FLARE AFTERBODY	0.4 TO 5.0	0 TO 6°	3 TO 20	SLENDER	$\Delta C_{N\alpha} = 2\ \frac{S_f}{S_{ref}}\left[1 - \left(\frac{dc}{df}\right)^2\right]$ FIG. 39	60% ℓ_f

TABLE 1 - (CONTINUED)

BODY COMPONENT	MACH NO. RANGE	α-RANGE	ℓ/d	NOSE BLUNTNESS	C_N	X_{CP}
FIN	SUBSONIC	0 TO 6°	—	—	$C_{N_{\alpha\,(fe)}} = AR \left(\frac{2\pi}{2 + \left[(AR)^2 (\beta^2 + \tan \frac{A_c}{2}) + 4 \right]^{1/2}} \right)$ FIG. 40	0.25 mac FIG. 41
					FIN BODY INTERFERENCE $C_{N_{\alpha\,(f_w)}} = C_{N_{\alpha(fe)}} = \frac{S_{fe}}{S_{fw}} \left[K_{f\,(b)} + K_{b(f)} \right]$ FIG. 42 $C_{N_{\alpha\,(fb)}} = C_{N_{\alpha f(w)}} \left(\frac{S_{fw}}{S_b} \right)$	
	TRANSONIC	0 TO 6°	—	—	RECTANGULAR FIG. 43 FIG. 45A-E	FIG. 44
	SUPERSONIC	0 TO 10°			RECTANGULAR FIGS. 46-47 SWEPT FIGS. 48A-C THICKNESS EFFECT FIG. 50	FIG. 46 FIGS. 49A-C
					FIN BODY INTERFERENCE (METHOD SAME AS SUBSONIC) FIG. 42 FOR $K_{f\,(b)}$ FIG. 51 FOR $K_{b\,(f)}$ OR FIGS. 52A-E.	
NONLINEAR FIN FORCE	SUBSONIC TO SUPERSONIC	0 TO 90°	—	—	EQ. 33, 34, 35 FIGS. 55 TO 61	EQ. 36, 37 FIGS. 62-65
FIN-FIN INTERFERENCE	SUBSONIC	0 TO 6°	—	—	C_{N_α} 6 FINS/C_{N_α} 4 FINS = 1.37 C_{N_α} 8 FINS/C_{N_α} 4 FINS = 1.62	
	SUPERSONIC	0 TO 6°	—	—	FIG. 53	

TABLE 1 - (CONTINUED)

BODY COMPONENT	MACH NO. RANGE	α-RANGE	ℓ/d	NOSE BLUNTNESS	C_N	X_{CP}
BOAT TAIL EFFECT ON FINS	SUBSONIC	0 TO 6°	3 TO 10	FLAT TO $r_c/r_d=0.25$	$C_{N\alpha\ F} = K_f(sc)\ (C_{N\alpha\ f})_{bt}$ FIG. 54	0.25 C
RING TAILS	0.8 TO 3.0	0 TO 6°	3 TO 10	—	FIG. 66 A TO F	0.50 C
EFFECT OF NOSE BLUNTNESS ON FIN NORMAL FORCE	SUBSONIC SUPERSONIC	0 TO 6° AND 12° TO 15°	3 TO 11	FLAT TO 2d SECANT OGIVE	$C_{N\alpha fbn} = C_{N\alpha\ fb}\ K_f(N)$ FIG. 67, 68	
FIN TIP CAPS	SUBSONIC SUPERSONIC	0 TO 6°	3 TO 10	FLAT TO 2d SECANT OGIVE	$C_{N\alpha(FIN\ CAP)_B} = C_{N\alpha\ fe}(2)$ $(S_{fe})\ Kc/S_b$ FIG. 69, 70	0.25 C

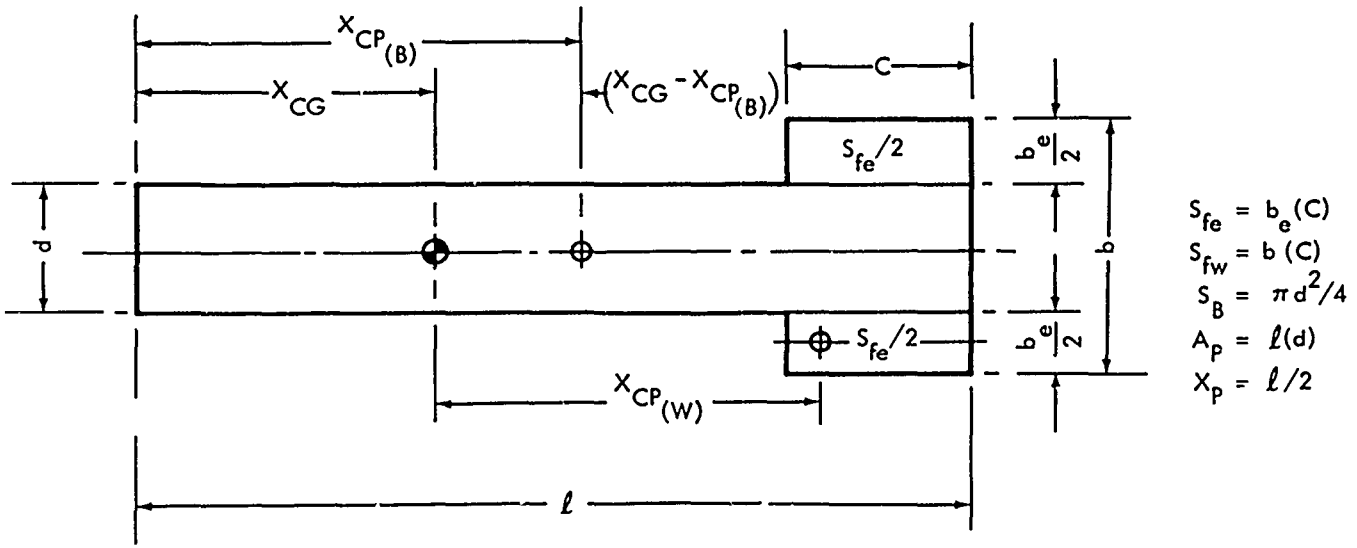

(1) $$C_N = C_{N_{\alpha_{(BODY)}}}(\alpha) + C_{N_{\alpha_{fe}}}(\alpha)\left(K_{fn}\right)\frac{S_{fe}}{S_{fw}}\left[K_{f(b)} + K_{b(f)}\right]\frac{S_{fw}}{S_B} + \eta C_{D_C}\,(AP/S_B)\,\sin^2\alpha$$

(2) $$C_m = C_{N_{\alpha_{(BODY)}}}(\alpha)\left(X_{CG} - X_{CP}\right) + \eta C_{D_C}\,AP/S_{ref}\left(X_{CG} - X_P\right)(\sin^2\alpha)/\ell$$

$$+ C_{N_{\alpha_{fe}}}(\alpha)\,\frac{S_{fe}}{S_{fw}}\left[K_{f(b)} + K_{b(f)}\right]\left(\frac{X_{CP}}{d}(w)\right)\left(\frac{S_{fw}}{S_B}\right) \qquad \alpha \text{ (IN RADIANS)}$$

FIG. 71 SAMPLE BLUNT BODY SHOWING EQUATIONS FOR CALCULATING NORMAL FORCE AND PITCHING MOMENT COEFFICIENTS

REFERENCES

(1) Hoak, D. E., Carlson, J. W., "USAF Stability and Control Handbook," Wright-Patterson Air Force Base, Ohio, Oct 1960

(2) Headquarters, U.S. Army Material Command, "Design of Aerodynamically Stabilized Free Rockets," AMCP 706-280, Jul 1968

(3) Munk, M. M., "The Aerodynamic Forces on Airship Hulls," NACA-TR-184, 1924

(4) Hayes, W. C. and Henderson, W. P., "Some Effects of Bluntness and Fineness Ratio on the Static Longitudinal Aerodynamic Characteristics of Bodies of Revolution at Subsonic Speeds," NASA TN/D-650, Feb 1961

(5) Karpov, B. G., "Wind Tunnel Tests of Mortar Shell Models," BRL Report 1293, Sep 1965

(6) Rogers, R. M. and Butler, C. B., "Aerodynamic Characteristics of Several Bluff Body Configurations at Subsonic and Transonic Mach Numbers," AFATL-TR-72-25, 1972

(7) Potter, J. L., Murphree, W. D. and Shapiro, A., "Normal Force Distributions on Right Circular Cylinders in Subsonic and Supersonic Flows," OML Report No. 2R4F, 1954

(8) Faro, I.D.V.,"Handbook of Supersonic Aerodynamics Section 8, Bodies of Revolution," NAVORD Report 1488, Vol. 3, Oct 1961

REFERENCES (Cont.)

(9) Barth, H., "Data for Determining Normal Force, Moment, and Tangential Force Characteristics of Slender Nose-Cylinder Configurations in the Transonic Velocity Range," Report No. WE 2-97/69, Messerschmitt-Buelkow-Blohm Corp. (Germany) 19 Dec 69

(10) Thomson, K. D., "The Estimation of Viscous Normal Force, Pitching Moment, Side Force, and Yawing Moment on Bodies of Revolution at Incidences up to 90°," WRE Report 782 (WR & D), Dept. of Supply, Australian Defense Scientific Service, Oct 1972

(11) Pitts, W., Nielsen, J. and Kaattari, G., "Lift and Center of Pressure of Wing-Body-Tail Combinations at Subsonic, Transonic and Supersonic Speeds," NACA Report 1307, 1958

(12) Chin, S. S., Missile Configuration Design, McGraw Hill Book Co., Inc., 1961

(13) Fidler, J. E. and Bateman, M. C., "Aerodynamic Methodology (Isolated Fins and Bodies)," OR 12399, U. S. Army Materiel Command, Mar 1973

TABLE 2. ANALYSIS OF CONTENTS OF ITEMS IN BIBLIOGRAPHY

BIBLIOGRAPHY ITEM NO.	MACH NO. RANGE	CONFIGURATION				AERODYNAMIC INFORMATION					
		l/d	NOSE	BODY	TAIL	STATIC STABILITY	DRAG	PITCH DAMPING	ROLL DAMPING	MAGNUS	DATA OR THEORY
1	0.40 TO 1.3	1.76	B	C	S	X	X	X			DATA
2	0.6 TO 1.5	3 TO 11	B,H,O	C	O,S,C	X	X				DATA
3	0.8 TO 1.2	6 TO 15	B,C,H,O	C	O	X					DATA
4	0.75 TO 3.0	3	S	C	R	X	X				DATA
5	SUBSONIC DISPERSION BOMBLETS										DATA AND THEORY
6	0.6 TO 1.3	4 TO 6	B	C	C			X			DATA
7	0.6 TO 1.3	6	B	C	C			X			DATA
8	0.2 TO 1.2	3 TO 11	B,O	C	B,C,S	X	X	X			DATA
9	0.6 TO 1.3	5	B	C	C	X	X				DATA
10	0.6 TO 1.4	3	B,B'	C	R,P	X	X				DATA
11	0.6 TO 0.95	2,4	B,P	R	S,W			X			DATA
12	0.2 TO 4.0	1 TO 4	B,C	B	O	X		X			DATA
13	0.8 TO 2.2	9	O	C	S	X					THEORY
14	SUBSONIC	12	O	C	S	X					THEORY
15	0.7 TO 1.2	3	B,C,BO	C,B	O	X	X				DATA
16	0.25 TO 0.80	0.5 TO 2	B	C	O	X	X				DATA
17	0.7 TO 1.01	2.3	BO	CB	S	X	X				DATA
18	0.6 TO 1.2	2	B	C	F,P		X				DATA
19	0.13	4 TO 8	B,BO	CB	S,R	X	X				DATA
20	1.2 TO 4.0	6,7	BS	CB	SE	X	X				DATA
21	1.3 TO 4.5	5	BICONIC	O	SW	X					DATA
22	1.7 TO 3.7	5	BS	CB	S	X	X				DATA
23	3	9	C,CB	CB	SE	X					DATA
24	0.25	6 TO 8	B,H,O	CB	C	X	X				DATA
25	0.25	5.5	O	CB	C	X	X				DATA

TABLE 2 (CONT'D.)

BIBLI-OGRAPHY ITEM NO.	MACH NO. RANGE	CONFIGURATION				AERODYNAMIC INFORMATION					
		l/d	NOSE	BODY	TAIL	STATIC STABILITY	DRAG	PITCH DAMPING	ROLL DAMPING	MAGNUS	DATA OR THEORY
26	0.74 TO 1.8	1 TO 3	B	R	S	X		X			DATA
27	SUBSONIC TO SUPERSONIC	7 TO 12	O	C	S	X					THEORY
28	0.13 TO 2.86	2,5	B	C	O	PRESSURE DIST.					DATA
29	0.6 TO 1 8	5	O	CB	S	X	X	X			DATA
30	0.2 TO 1.5	3 TO 11	B,O	C	S,O,C,W	X	X				DATA
31	0.9 TO 1.2	9	BO	C	O	X	X	X		X	DATA
32	0.7 TO 2.5	5	BO	CH	O	X	X	X	X	X	DATA
33	0.5 TO 1.1	8	B,S	CB	S	X	X	X			DATA
34	0.5 TO 1.2	4	B,h	C,B	S				X	X	DATA
35	0.3 TO 1.2	4	H	C,B	S	X	X	X			DATA
36	1.7 TO 3.8	4 TO 7	BS	CB	F	X	X				DATA
37	M_c=0 TO 0.7	>3	C,O	C	O,B,F	X					THEORY
38	0.3 TO 1.2	4	B	C	S			X			DATA
39	0.5 TO 1.2	2.5	B	C	F	X		X			DATA
40	0.7 TO 3	3	BH,S	C	S	X		X			DATA

KEY TO CONFIGURATION LETTER SYMBOLS

NOSE
- B - BLUNT
- C - CONE
- O - OGIVE
- P - PYRAMID
- S - SPIKE
- H - HEMISPHERE
- ' - WITH BAND
- " - WITH SPOILERS

BODY
- B - BOATTAIL
- C - CYLINDRICAL
- H - HEMISPHERE BASE
- Q - NO BODY
- R - RECTANGULAR
- ' - WITH BANDS

TAIL
- B - BOX
- C - RECTANGULAR WITH CAPS
- E - END PLATES
- F - FLARE
- O - NO TAIL
- P - PLATE
- R - RING
- S - RECTANGULAR
- W - WRAP AROUND

BIBLIOGRAPHY

1. Anderson, C. F., "Static and Dynamic Stability Characteristics of Several Short Blunt Cylindrical Bomblet Models at Mach Numbers from 0.4 to 1.3," AEDC TR-71-110, May 1971

2. Anderson, C. F. and Henson, J. R., "Aerodynamic Characteristics of Several Bluff Bodies of Revolution at Mach Numbers from 0.6 to 1.5," AEDC TR 71-130, Jul 1971

3. Barth, Messerschmitt-Buelkow-Blohm Corporation, "Data for Determining Normal Force Moment and Tangential Force Characteristics of Slender Nose-Cylinder Configurations in the Transonic Velocity Range," Report No. WE 2-97/69, 19 Dec 1969

4. Bliler, A., Martin, J. D., "Bomb Development Installation and Handling," D2-2075, Boeing Airplane Co. 1957

5. Burgess, F., "Proceedings of Conference on Dynamics and Aerodynamics of Bomblets," AFATL-TR-67-195, Vol. 1, 1967

6. Burt, G. E., Mansfield, A. C., and Caldwell, R. L., "Damping-in-Pitch Characteristics of Some Proposed Configurations for the Modular Weapon System at Mach Numbers 0.6 to 1.3," AEDC TR-71-67, May 1971

7. Burt, G. E., Caldwell, R. L. and Mansfield, A. C., "Effects of Nose-Mounted Spoilers on the Damping-in-Pitch Characteristics of a Bomb Model at Transonic Mach Numbers," AEDC TR-71-120, Jul 1971

BIBLIOGRAPHY (Cont.)

8. Caldwell, R. L., "Static and Dynamic Stability Investigations of Bombs for the Modular Weapon System at Transonic Mach Numbers," AEDC TR-71-65, Apr 1971

9. Caldwell, R. L., "Effects of Nose-Mounted Jet and Cylindrical Spoilers on the Static Stability Characteristic of Hemisphere-Nosed Bomb Model at Transonic Mach Numbers," AEDC TR-71-92, May 1971

10. Clarkson, M. H., Fenter, F. W., Damstrom, E. K., "An Investigation of the Static Stability Characteristics of Finless Bluff Bodies of Revolution at Transonic Speeds," WADD TR 59-781, 1960

11. Durkin, J., "A Forced Oscillation Test of a Square Cross-Section Model at Transonic Speeds," NSRDC TR AL-59, 1970

12. Ericsson, L., "Aerodynamic Effects of Bulbous Bases," TR-4-17-67-3 LMSC, 1967

13. Fidler, J. E. and Bateman, M. C., "Aerodynamic Methodology (Isolated Fins and Bodies),"AD (Not Numbered) U.S. Army Material Command, Mar 1973

14. Flax, A. and Lawrence, H., "The Aerodynamics of Low-Aspect-Ratio Wings and Wing-Body Combinations," CAL-37, Cornell Aero. Lab., 1951

15. Gambucci, B. and Robinson, R., "Force Measurements on Axisymmetric Models with Hammerhead Noses at Transonic Speeds," NASA TMX-1433, 1967

BIBLIOGRAPHY (Cont.)

16. Hayes, W. and Henderson, W., "Some Effects of Nose Bluntness and Fineness Ratio on Static Longitudinal Aerodynamic Characteristics of Bodies of Revolution at Subsonic Speeds," NASA TN D-650, 1961

17. Holland T., "Force Test of a Dragoon Model Configuration in the Sandia Corporation 12 by 12 inch Transonic Wind Tunnel," SCTM 4-60 (51), 1960

18. Judd, J. and Woodbury, G., "Free-Flight Measurements of the Transonic Drag Characteristics of Low-Fineness-Ratio Cylinders Including Stabilizing Plates and Flares," NASA TN D-36, 1960

19. Karpov, B., "Wind Tunnel Tests of Mortar Shell Models," BRL R. 1293, 1965

20. Krieger, R., "The Aerodynamic Design of Fin Stabilized Ammunition," BRL MR 971, 1956

21. Krieger, R. and Hughes, J., "Wind Tunnel Results on the Redstone "Top" Assembly at Mach Numbers from 1.36 to 4.53," BRL MR 973, 1956

22. Krieger, R. and Hughes, J., "Wind Tunnel Tests on the Budd Company T-153 120 mm Heat Spike Nose, Folding Fin Projectile," BRL MR 738, 1953

23. Krieger, R. H., "Wind Tunnel Tests on the T-153 120 mm Heat Projectile," BRL TN 724, 1952

24. Ludke, W. P., "Static Wind-Tunnel Tests of the Quick Strike Mine with Various Nose Configurations," NOLTR 72-133, 1972

BIBLIOGRAPHY (Cont.)

25. Ludke, W. P., "Wind Tunnel Tests of the Quick Strike Test Vehicle," NOLTR 72-144, 1972

26. O'Neill, E. B., "Summary of Some Experimental Aerodynamic Investigations of Blunt Non-Circular Cross-Section Bodies," NSRDC TN-AL-156, Feb 1970

27. Pitts, W., Nielsen, J. and Kaaltari, G., "Lift and Center of Pressure of Wing-Body-Tail Combinations at Subsonic, Transonic and Supersonic Speeds," NACA Report 1307, 1958

28. Potter, J., Shapiro, N., Murphree, W., "Normal Force Distributions on Right Circular Cylinders in Subsonic and Supersonic Flows," OML Report No. 2R4F, 1954

29. Roecker, E. T., "Aerodynamic Properties of a Finned Bomb," BRL MR 1046, 1956

30. Rogers, R. M., Butler, C. B., "Aerodynamic Characteristics of Several Bluff Body Configurations at Subsonic and Transonic Mach Numbers," AFATL-TR-72-25, 1972

31. Roschke, E. J., "The Effect of Nose Truncation on the Aerodynamic Properties of 9-Caliber Long Army-Navy Spinner Rocket Models Near Sonic Velocity," BRL TN 902, 1955

32. Roschke, E. J., "The Drag and Stability Properties of the Hemisphere Base Shell," BRL MR 927, 1955

33. Sabin, C. P., "The Aerodynamic Properties of a Spike-Nosed Shell at Transonic Velocities," BRL MR 1112, 1957

34. Shadow, T. O., "Transonic Roll-Damping and Magnus Characteristics of three Bomblet Munition Models used in the Evaluation of Aerodynamic Dispersion Techniques," AEDC TR 71-33, 1971

BIBLIOGRAPHY (Cont.)

35. Shadow, T. O. and Gomillion, G. R., "Transonic Aerodynamic Characteristics of Bomblet Munition Models Used in the Evaluation of the Roll Through Zero Aerodynamic Dispersion Technique," AFATL-TR-72-138, 1972

36. Sylvester, M. E., and Krieger, R. H., "Wind Tunnel Tests of the T 340E11 90 mm HE Projectile with Varying Spike Nose and Spool-Type-Body Parameters," BRL M/R 1146, 1958

37. Thomson, K. D., "The Estimation of Viscous Normal Force, Pitching Moment, Side Force and Yawing Moment on Bodies of Revolution at Incidences up to 90°," WRE Report 782 (WR & D) Dept. of Supply, Australian Defense Scientific Service, Oct 1972

38. Uselton, B., Carman, J. Shadow, T., "Dynamic Stability Characteristics of Axisymmetric Bomblet Munition Models at Mach Numbers 0.3 to 1.2, AEDC TR 70-270, Dec 1970

39. Walchner, A., Weigand, H. and Kroeger, H., "Dynamic Stabilizer for the Finless Bluff Bomb," WCRR 54-53, 1954

40. Williams, M. L., "Results of Dynamic Stability Tests of the TX-41 Configuration with Nose Probes in the Sandia Laboaratory 12-inch Trisonic Wind Tunnel (Program III-78) SCTM 127-61 (71), 1961

APPENDIX A

CALCULATION OF C_N AND C_m AT M = 0.85 OF TYPICAL BODY-FIN CONFIGURATION WITH COMPARISON TO EXPERIMENT

A. Body-Alone (Figure 1a)

(1) $\alpha = 5°$

$C_N = C_{N_\alpha}(\alpha) + C_{N_{\alpha BT}}(\alpha)$

$C_{N_\alpha} = 2.5/\text{rad}$ (Fig. 2)

$C_{N_{\alpha BT}} = -0.486/\text{rad}$ (Eq. (16))

$C_{N_{\alpha=5°}} = 2.5(5/57.3) - 0.486(5/57.3)$

$C_{N_{\alpha=5°}} = 0.218 - 0.042 = 0.176$

Moments about the nose:

$C_N x_{cp} = C_{N_B} x_{cp_B} + C_{N_{BT}} x_{cp(BT)}$ (Fig. 9)

$0.176\ x_{cp} = +0.218(-1.25) - 0.042(-6.60)$ ($x_{cpBT} = 0.3$)

$x_{cp} = +0.004/0.176 = +0.023$ (from nose)

(2) $\alpha = 10°$

$C_N = C_{N_\alpha}(\alpha) + C_{N_{\alpha 2}}(\alpha)^2$ (Eq. (5))

$C_{N_{\alpha=10°}} = 2.42(0.174) + 2.15(0.030)$ (Fig. 12b, 13b)

$C_{N_{\alpha=10°}} = 0.486$

Effect of Boattail

$C_{N_{\alpha=10°}} = 0.486 - (0.174)(0.486) = 0.402$

$x_{cp} = (x_{cp})_{\alpha=0} + D_1\alpha$ (Fig. 14b, 15b)

$x_{cp} = -1.44 - 5.6(0.174) = 02.41$ (From nose)

Moments about nose:

$C_N x_{cp} = C_{N_B} x_{cpB} + C_{N_{BT}} x_{cp(BT)}$

$0.402\, x_{cp} = -0.486(-2.41) + 0.084(-6.6)$

$x_{cp} = -0.6166/0.402 = -1.534$ (From nose)

(3) $\alpha = 20°, 30°, 40°$

$C_N = 1/2\, C_{N_\alpha} \sin 2\alpha + \Delta C_{N_v} + C_{N_{BT}}$ (Eq. (8))

$$\frac{\Delta C_{N_v} S}{KF \sin\alpha \cos\alpha} = \frac{J}{S} \cot\alpha \,[B]_0^{X_N} + [A]_{X_N}^{X_L-E} + H[A]_{X_L-E}^{X_L-X_{BT}} +$$

$$\frac{2}{\pi} \frac{\sin 2\alpha'}{S} \int_{X_L-X_{BT}}^{X_L} C_{D_C}\left(\frac{d}{d}\right)_{ref} dx \quad \text{(Eq. (9), (14))}$$

(Where $\alpha' = \alpha - 15°$ and $X_{BT} = \ell_{BT} S \tan\alpha'$)

α	K	F	S	J	H	E	X_N	X_L	X_L-E	X_L-X_{BT}
20°	0.56	0.88	0.2	0	0.91	0.125	0.036	0.505	0.380	0.442
30°	0.54	0.75	0.2	0	0.94	0.126	0.058	0.799	0.673	0.699
40°	0.50	0.67	0.2	0	0.96	0.135	1.084	1.161	1.026	1.015

α	B_{XN}	A_{XN}	A_{XL-E}	A_{XL-XBT}	C_{D_C}/F	ΔC_{N_v}	$1/2 C_{N_\alpha} \sin 2\alpha$	$C_{N_{BT}}$	C_N
20°	0	0.010	0.61	0.72	1.22	0.561	0.803	-0.169	1.20
30°	0	0.015	1.20	1.245	1.30	1.137	1.083	-0.252	1.968
40°	0	0.030	2.07	1.98	1.50	1.787 3.413	1.231	-	3.081 4.644

$$C_m = 1/2\ C_{N_\alpha}\ x_{cp} \sin 2\alpha + \Delta C_{m_v} \qquad \text{(Eq. (10))}$$

$$\frac{\Delta C_{m_v} S^2}{KF \cos^2\alpha} = \frac{J}{S} \cot \alpha\ [C]_0^{X_N} + [B]_{X_N}^{X_{L-E}} + H[B]_{X_{L-E}}^{X_{L-BT}} +$$

$$\frac{4}{\pi} \frac{\cos^2\alpha'}{S^2} \int_{X_L - X_{BT}}^{X_L} C_{D_c} \left(\frac{d}{d_{ref}}\right) X dX \qquad \text{(Eq. (11), (15))}$$

[where $X = (\ell - x_{cpBT})S \tan\alpha$]

α	C_{XN}	B_{XN}	B_{XL-E}	$B_{XL-X_{BT}}$	ΔC_{m_v}	$C_{m_{BT}}$	$x_{cp(nose)}$	$C_{m(nose)}$
20°	0	0	0.13	0.185	-2.016	+1.115	-1.587	-1.905
30°	0	0	0.43	0.43	-4.032	+1.66	-1.893	-3.725
40°	0	0.03	1.12	1.07	-6.722 -12.374	-	-2.737 2.996	-8.26 -13.912

B. Tail Fins (Fig. 1a)

Since M = 0.85 is beyond the range of Figure 40 for finding $C_{N_{\alpha(fe)}}$ a curve of $C_{N_{\alpha(fe)}}$ versus M must be constructed.

Find $C_{N_{\alpha(fe)}}$ at M = 0.6 AR = 1.56 (Fig. 40)

$C_{N_{\alpha(fe)}} = 1.59/\text{rad}$ $\frac{\Lambda_c}{2} = 60°$

$(M_{FB})_{\Lambda=0} = 0.89$ (AR = 1.56, t/c = 23%) (Fig. 45a)

$(M_{FB})_{\Lambda} = 0.96$ (Fig. 45b)

$(C_{N_{\alpha(fe)}})_{FB_{\Lambda=0}} = 1.80/\text{rad}$ at $(M_{FB})_{\Lambda}$ (Fig. 40)

Correct $C_{N_{\alpha(fe)_{FB=\Lambda}}} = 1.80\ (0.88) = 1.60/\text{rad}$ (Fig. 45c)

$M_a = (M_{FB})_\Lambda + 0.7 = 1.03$ (Eq. (22))

$C_{N_{\alpha_{(fe)a}}} = (1 - \frac{a}{c})(C_{N_{\alpha_{(fe)}}})_{FB=\Lambda} = 1.12/\text{rad at } M_a$

(Eq. (23) Fig. 45d)

$M_b = (M_{FB})_\Lambda + 0.14 = 1.10$ (Eq. (24) Fig. 45e)

$C_{N_{\alpha_{(fe)b}}} = (1 - \frac{b}{c})(C_{N_{\alpha_{(fe)}}})_{FB=\Lambda} = 1.35 \text{ at } M_b$

From Figure 2a $C_{N_{\alpha_{fe}}} = 1.59$ at M = 0.85

Use Equation (33) to calculate $C_{N_{fe}}$ up to α'

Find α' from Figure 56 for AR = 1.56 λ = 0.7, $\alpha' = 15°$

$f\left(\frac{\pi}{2}\right) = 2.8$ (Fig. 55)

$$C_{N_{fe}} = C_{N_{\alpha_{fe}}}(\alpha) + \left[\frac{16f\left(\frac{\pi}{2}\right)}{\pi^2} - \frac{5C_{N_{\alpha_{fe}}}}{\pi}\right]\alpha^2 + \left[\frac{8C_{N_{\alpha_{fe}}}}{\pi^2} - \frac{32f\left(\frac{\pi}{2}\right)}{\pi^3}\right]\alpha^3$$

$$+ \left[\frac{16f\left(\frac{\pi}{2}\right)}{\pi^4} - \frac{4C_{N_{\alpha_{fe}}}}{\pi^3}\right]\alpha^4 \qquad \text{(Eq. (33))}$$

For $\alpha = 5°$ $C_{N_{fe}} = C_{N_{\alpha_{fe}}} = 1.59\ (5/57.3) = 0.14$

For $\alpha = 10°$ and $15°$

$$C_{N_{fe}} = 1.59\begin{bmatrix}0.174\\0.262\end{bmatrix} + [4.53 - 2.53]\begin{bmatrix}0.030\\0.068\end{bmatrix} + [1.29 - 2.89]\begin{bmatrix}0.005\\0.018\end{bmatrix}$$

$$+ [0.459 - 0.205]\begin{bmatrix}0.001\\0.005\end{bmatrix} = \begin{bmatrix}0.3289,\ \alpha = 10°\\0.5251,\ \alpha = 15°\end{bmatrix}$$

$\alpha = 20°$

$$\frac{\alpha - \alpha'}{30 - \alpha} = \frac{20 - 15}{30 - 15} = 0.33 \qquad \text{(Fig. 57)}$$

$$\frac{\Delta C_N}{\Delta C_{N_m}} = 0.31 \quad \Delta C_{N_m} = 0.35$$

$$\Delta C_N = 0.1085$$

$$C_{N_{fe}} = 0.5249 + 0.1085 = 0.6334$$

$\alpha = 30°$

$$\frac{\alpha - \alpha'}{30 - \alpha} = \frac{30 - 15}{30 - 15} = 1$$

$$\frac{\Delta C_N}{\Delta C_{N_m}} = 0.75 \quad \Delta C_N = 0.262$$

$$C_{N_{fe}} = 0.5249 + 0.262 = 0.7869$$

To calculate $C_{N_{fe}}$ at $\alpha = 40$, first calculate $C_{N_{fe}}$ at $\alpha = 50°$ using Equation (34) and fair the curve between the values at $\alpha = 30°$ and $50°$.

$\alpha = 50°$

$$C_{N_{fe}} = f(30) + 1.738A - 1.652f'(30) \qquad \text{(Eq. (34))}$$
$$+ [4.82f'(30) - 6.6A]\alpha$$
$$+ [7.54A - 4.15f'(30)]\alpha^2$$
$$+ [1.11f'(30) - 2.31A]\alpha^3$$

$f(30) = 0.91$ (Fig. 60a, b)

$f'(30) = 0.70$ (Fig. 61)

$C_{N_c} = 1.1$ (Fig. 59)

$A = C_{N_c} - f(30) = 1.1 - 0.91 = 0.19$ (Eq. (34))

$C_{N_{fe}} = 0.91 + 1.738(0.19) - 1.652(0.70) = +0.084$

$+ [4.82(0.7) - 6.6(0.19)]0.873 = +1.95$

$+ [7.5(0.19) - 4.15(0.70)]0.761 = -1.12$

$+ [1.11(0.70) - 2.31(0.19)]0.664 = 0.22$

1.03

From Figure 2a, $C_{N_{fe}} = 0.93$ at $\alpha = 40°$

C. Total C_N for Body + Fins

$$C_{N_T} = C_{N_B} + C_{N_{vB}} + C_{N_{BT}} + C_{N_{vBT}} + C_{N_{FB}}$$

where: $C_{N_{FB}} = C_{N_{fe}}$ (0.806) for $\alpha = 0°$ to $15°$
$= C_{N_{fe}}$ (1.088) for $\alpha = 16°$ to $90°$ } see Fig. A-1

See Table 1a for values of $C_{N_{FB}}$

D. Center of Pressure of Fins

$$\frac{x_{cp}}{c} = \left(\frac{x_{cp}}{c}\right)_{\alpha=90°} - \left(\frac{\Delta x_{cp}}{c}\right)[1 + F(M)]N \quad \text{(Eq. (36))}$$

$$\left(\frac{x_{cp}}{c}\right)_{\alpha=90°} = -0.58 \text{ for } \lambda = 0.70 \quad \text{(Fig. 63)}$$

Find $\frac{x_{cp}}{c}$ for M = 0.98 for $\alpha = 5°, 10°, 20°, 30°, 40°$ from Figure 63. See Table 1a for values.

$$\left(\frac{\Delta x_{cp}}{c}\right)_{M=0.98} = \left(\frac{x_{cp}}{c}\right)_{\alpha=90} - \left(\frac{x_{cp}}{c}\right)_{M=0.98} \qquad \text{(Eq. (37))}$$

See Table 1a for values.

At M = 0.85 F(M) = 0.20, N = 1 (Fig. 64, 65)

See Table 1a for values of $\frac{\Delta x_{cp}}{c}$ [1 + F(M)]

$$\frac{x_{cp}}{c} = -0.58 - \frac{\Delta x_{cp}}{c}\,[1 + F(M)] \quad \text{see Table 1a}$$

x_{cp} from leading edge of fin is $\frac{x_{cp}}{c}$ (0.87)

x_{cp} from nose of body is $-6.07 + x_{cp}$

$C_{m_{FB}} = (x_{cp} - 6.07)C_{N_{FB}}$

E. Total Pitching Moment Referred to Nose of Body

$C_{mT} = C_{m_{TB}} + C_{m_{TF}}$ see Table 1a for values.

Table A-1

RESULTS OF HANDBOOK CALCULATION OF C_N & C_m FOR

A TYPICAL FREE FALL SHAPE, M = 0.85

α	BODY			
	INVISCID		VISCOUS	
	C_{N_B}	x_{cp_B}	$C_{N_{v_B}}$	$x_{cp_{v_B}}$
5°	0.218, Fig. 2	-1.25, Fig. 10	---	
10°	0.421, Fig. 12b	-2.41, Fig. 14b 15b	0.065, Fig. 13b	-2.41, Fig. 14b 15b
20°	0.803, Eq. (8)	-1.25, Fig. 10	0.539, Eq. (9)	-3.653, Eq. (9) (11)
30°	1.083, Eq. (8)	-1.25, Fig. 10	1.076, Eq. (9)	-3.37, Eq. (9) (11)
40°	1.231, Eq. (8)	-1.25, Fig. 10	$\frac{1.787}{3.413}$ Eq. (9)	$\frac{-3.37}{-3.37}$ Eq. (9) (11)

α	BOATTAIL			
	INVISCID		VISCOUS	
	$C_{N_{BT}}$	$x_{cp_{BT}}$	$C_{N_{vBT}}$	$x_{cp_{vBT}}$
5°	-0.042, Eq. (16)	-6.60, Fig. 36	---	---
10°	-0.084, Eq. (16)	-6.60, Fig. 36	---	---
20°	-0.169, Eq. (16)	-6.60, Fig. 36	0.007	-6.6 (centroid of BT)
30°	-0.252	-6.60, Fig. 36	0.061	-6.6 (centroid of BT)
40°	---	-6.60, Fig. 36	0.162	-6.6 (centroid of BT)

Table A-1 (Cont.)

α	FINS			
		Fig. 63	Eq. (30a)	(a)
	$C_{N_{FB}}$	$\left(\frac{x_{cp}}{c}\right)_{M=0.98}$	$\left(\frac{\Delta x_{cp}}{c}\right)_{M=0.98}$	$\frac{\Delta x_{cp}}{c}$ [1 + F(M)]
5°	0.112	-0.300	0.28	0.34
10°	0.265	-0.37	0.21	0.25
20°	0.693	-0.44	0.14	0.17
30°	0.860	-0.47	0.11	0.13
40°	1.016	-0.50	0.08	0.10

α	FINS			
	$\frac{x_{cp}}{c} = 0.58 - a$	x_{cp}	$-6.075 + x_{cp}$	$C_{m_{FB}}$
5°	-0.24	-0.21	-6.28	-0.70
10°	-0.33	-0.29	-6.36	-1.68
20°	-0.41	-0.36	-6.43	-4.46
30°	-0.45	-0.39	-6.46	-5.56
40°	-0.48	-0.42	-6.49	-6.59

Table A-1 (Cont.)

α	$C_{N_{TB}}$	$C_{m_{TB}}$ (from nose)	$x_{cp_{Body}}$
5°	0.176	+0.004	+0.02
10°	0.402	-0.617	-1.53
20°	1.180	-1.905	-1.61
30°	1.968	-3.725	-1.89
40°	3.180, TURB	-8.629, TURB	-2.74, (turb)
40°	4.806, LAM	-14.109, LAM	-2.99, (lam)

α	C_{N_T}	C_{m_T}
5°	0.289	-0.71
10°	0.686	-2.30
20°	1.873	-6.37
30°	2.828	-9.28
40°	4.202, TURB	-14.19, (turb)
40°	5.828, LAM	-20.70, (lam)

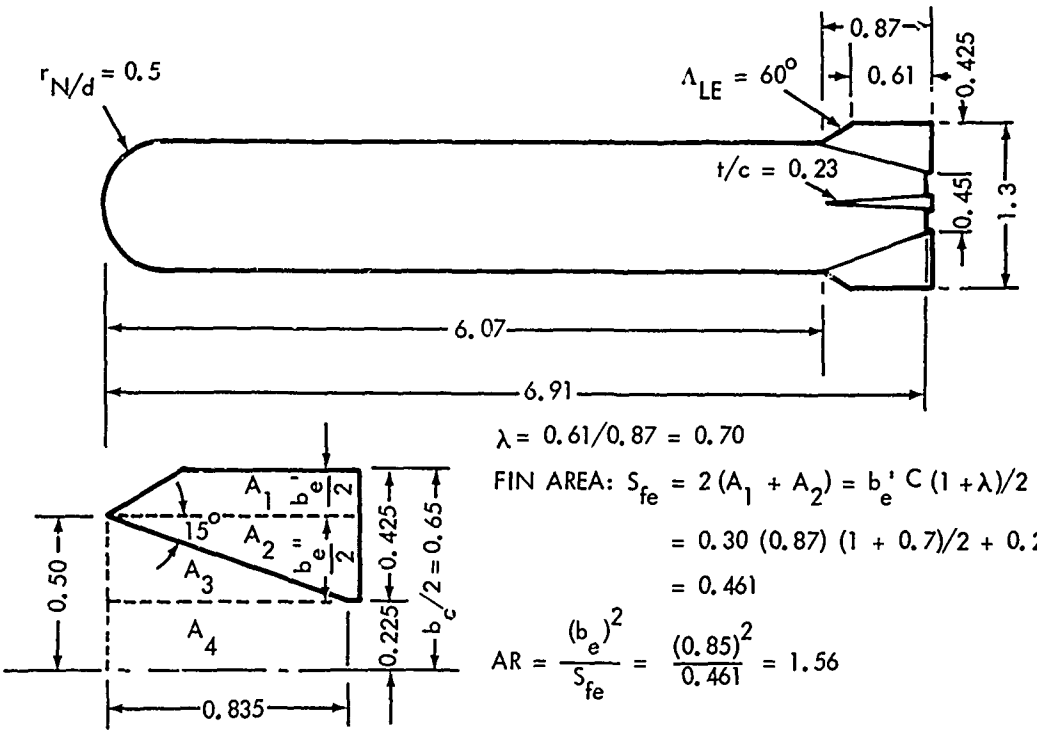

$\lambda = 0.61/0.87 = 0.70$

FIN AREA: $S_{fe} = 2(A_1 + A_2) = b_e' C (1+\lambda)/2 + \frac{b_e''}{2} C$

$= 0.30\ (0.87)\ (1 + 0.7)/2 + 0.275\ (0.87)$

$= 0.461$

$AR = \frac{(b_e)^2}{S_{fe}} = \frac{(0.85)^2}{0.461} = 1.56$

S_W = FIN + BODY AREA = $S_{fe} + (A_3 + A_4)2$

$= 0.461 + 2\ (0.115 + 0.188)$

$S_w = 1.067$

TO FIND WING-BODY AND BODY-WING FACTORS USE d_{BT}/b_e

FIG. 42 $d_{BT}/b_e = 0.450/1.3 = 0.346$ $K_{b(f)} = 0.53$, $K_{f(b)} = 1.32$

TO ACCOUNT FOR BOATTAIL SHADOW EFFECT ON FIN FIND $K_{f(sc)} = 0.5$ (FIG. 54)

$$C_{N_{\alpha_{f_{ref}}}} = C_{N_{\alpha_{fe}}} \left[\frac{S_{fe}}{S_W} \left(K_{f(b)} + K_{b(f)} \right) \left(K_{f(sc)} \frac{A_2}{S_{fe}} + \frac{A_1}{S_{fe}} \right) \left(\frac{S_w}{S_{ref}} \right) \right]$$

$$C_{N_{\alpha_{f_{ref}}}} = C_{N_{\alpha_{fe}}} \left[\frac{0.461}{1.067} \left(1.32 + 0.53 \right) \left(0.5\ \frac{(0.239)}{0.461} + \frac{0.222}{0.461} \right) \frac{1.067}{0.784} \right]$$

$$= 0.806\ C_{N_{\alpha_{fe}}}$$

ABOVE $\alpha = 10^o$ THE SHADOW EFFECT STOPS

THEN: $C_{N_{\alpha_{f_{ref}}}} = 1.088\ C_{N_{\alpha_{fe}}}$

FIG. A-1 TYPICAL FREE FALL SHAPE

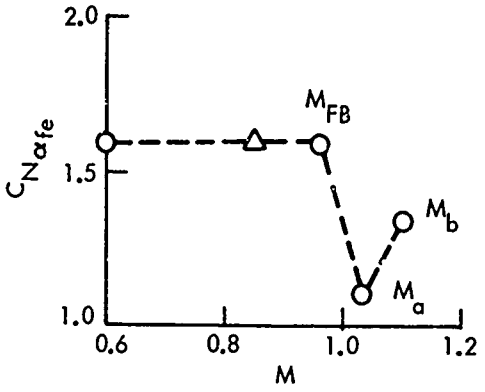

CONSTRUCTION OF FIN NORMAL FORCE CURVE AS A FUNCTION OF MACH NUMBER

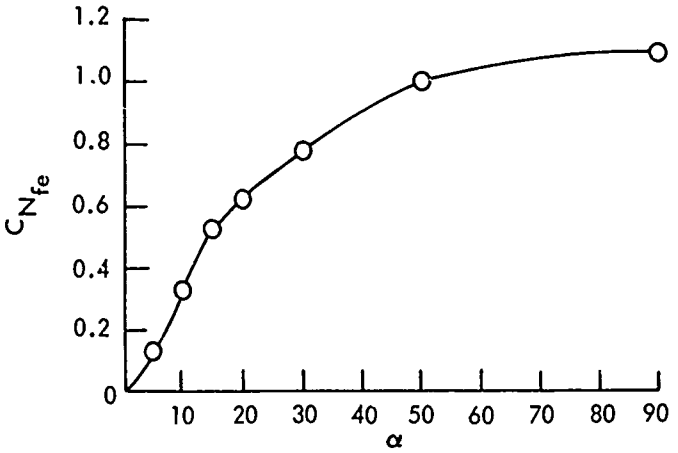

FIN NORMAL FORCE AS A FUNCTION OF α FOR M=0.85

FIG. A-2 DEVELOPMENT OF FIN NORMAL FORCE COEFFICIENT

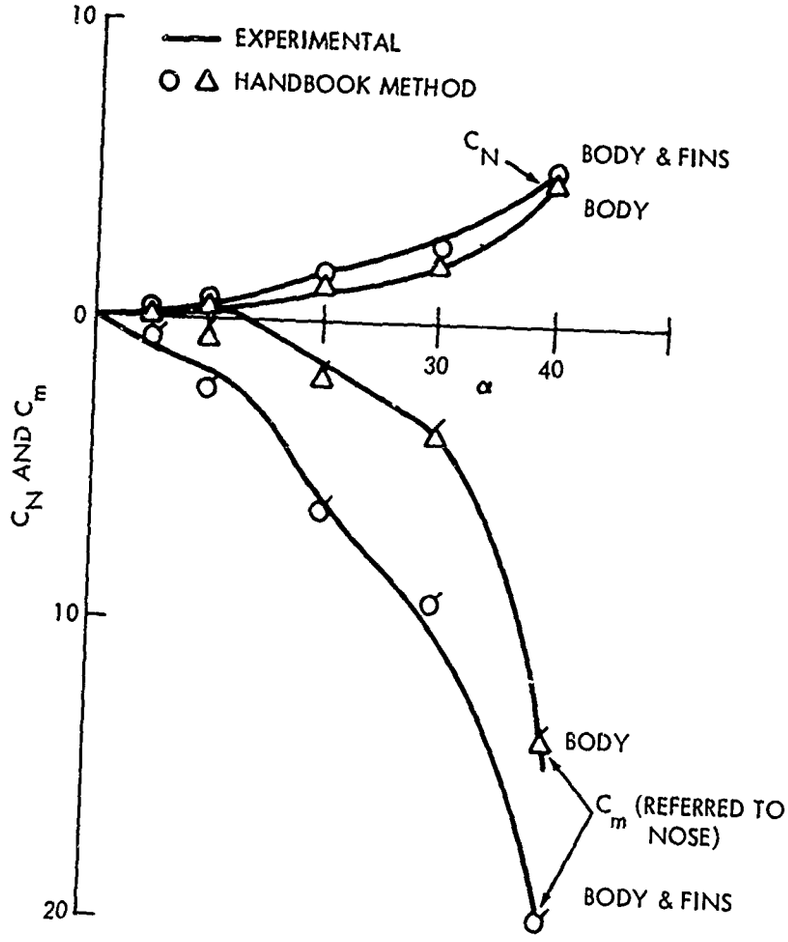

FIG. A-3 NORMAL FORCE AND PITCHING MOMENT COEFFICIENTS FOR A TYPICAL BLUFF FREE FALL SHAPE M= 0.85